

601

GUIDE FOR THERMAL RATING CALCULATIONS OF OVERHEAD LINES

**Working Group
B2.43**

December 2014



GUIDE FOR THERMAL RATING CALCULATIONS OF OVERHEAD LINES

WG B2.43

Members

Javier IGLESIAS, **Convener** (ES), George WATT, **Secretary** (CA)

Dale DOUGLASS (US), Vincent MORGAN (AU), Rob STEPHEN (ZA), Mark BERTINAT (UK), Dzevad MUFTIC (ZA), Ralf PUFFER (DE), Daniel GUERY (FR), Sidnei UEDA (BR), Kresimir BAKIC (SI), Sven HOFFMANN (UK), Tapani SEPPA (US), Franc JAKL (SI), Carlos DO NASCIMENTO (BR), Francesco ZANELATO (IT), Huu-Minh NGUYEN (BE).

Reviewers

Thadeu FURTADO (BR), Stefan STEEVENS (DE), Sergey KOLOSOV (RU), Konstantin KONAKOV (RU), Mark LANCASTER (US)

Copyright © 2012

“Ownership of a CIGRE publication, whether in paper form or on electronic support only infers right of use for personal purposes. Unless explicitly agreed by CIGRE in writing, total or partial reproduction of the publication and/or transfer to a third party is prohibited other than for personal use by CIGRE Individual Members or for use within CIGRE Collective Member organisations. Circulation on any intranet or other company network is forbidden for all persons. As an exception, CIGRE Collective Members only are allowed to reproduce the publication.”

Disclaimer notice

“CIGRE gives no warranty or assurance about the contents of this publication, nor does it accept any responsibility, as to the accuracy or exhaustiveness of the information. All implied warranties and conditions are excluded to the maximum extent permitted by law”.



ISBN : 978-2-85873-302-6

The members of the Working Group B2.43 would like to dedicate this Document to the memory of **Michael Schmale**, who contributed actively, with a lot of enthusiasm and energy, to the work developed during years within this group and the Cigré Study Committee B2.

GUIDE FOR THERMAL RATING CALCULATIONS OF OVERHEAD LINES

CONSIDERATIONS FOR HIGH TEMPERATURES AND CHANGING WEATHER AND LOAD DATA

Table of Contents

EXECUTIVE SUMMARY	4
Section 1. Foreword	6
1.1. Background and objectives	6
1.2. Nomenclature	7
Section 2. Overview and general equations	10
2.1. Steady state heat balance	10
2.2. Transient state.....	10
Section 3. Calculation of heating and cooling	13
3.1. Joule heating calculation.....	13
3.2. Magnetic heating calculation	16
3.3. Solar heating calculation.....	18
3.4. Conductor temperature distribution	21
3.5. Convective cooling calculation.....	24
3.6. Radiative cooling calculation.....	30
Section 4. Thermal models	32
4.1. Numerical models for steady state.....	32
4.2. Numerical models for transient state.....	34
Section 5. Input data and sensitivity studies	38
References	41

Annex A. Analytical calculation of conductor resistance	47
A.1. DC resistance	47
A.2. AC resistance (skin effect)	49
Annex B. Analytical calculation of magnetic heating	53
B.1. Heat gain in the steel core	53
B.2. Heat gain due to redistribution of the current densities.....	56
B.3. Example.....	58
Annex C. Models of convective cooling.....	63
C.1. Perpendicular flow	63
C.2. Wind direction	64
C.3. Natural Convection	65
C.4. Low wind speeds	66
Annex D. Analytical calculations for transient state	69
D.1. Time dependent heating or cooling	70
D.2. Adiabatic heating.....	75
Annex E. Examples of calculation	79
E.1. Steady state thermal rating	79
E.2. Steady state conductor temperature	82
E.3. Temperature tracking calculation	84
E.4. Temperature tracking calculation. Comparison with steady state ...	91

EXECUTIVE SUMMARY

The present guide provides a general method for calculating the thermal rating of overhead lines. It is intended for updating and expanding the Cigré Technical Brochure 207 [1], which only covered the thermal behaviour of overhead conductors at low current densities (<1.5 A/mm²) and low temperatures ($<100^{\circ}\text{C}$), and did not consider variations in weather conditions or current with time. In the recent years, various modeling improvements have been developed that take account of these time variations and also of higher currents and higher temperatures, and these have been incorporated into the overall thermal model.

For example, a more accurate model for the calculation of the resistance of the steel-cored conductors operating at high ac current densities has been developed [16], and more reliable data on the radial and axial temperature distributions within the conductors are available thanks to various researches.

Convective cooling is a major issue for line ratings, particularly when the conductors are operating at high temperatures. An improvement in the convection model included in the TB 207 [1] was necessary for low wind speeds due to some inconsistencies therein and the need for a better assessment of wind. Also a more flexible solar radiation model had to be incorporated in order to better understand its effects and variations. These are key factors for dynamic rating systems and need to be carefully treated if the variation of conductor temperature with time is to be accurately calculated.



Figure 1: Control centre and transmission line

In this document, numerical and analytical models for both steady and transient states are described. In particular, the use of proper real-time values for the ambient parameters and line current, with the knowledge of the conductor properties, can be combined into suitable

algorithms to track the conductor temperature with time. These temperature-tracking algorithms may provide the tools for maximizing the ratings of the overhead lines without exceeding their design temperatures.

The document also gives examples of typical input parameters used in the thermal model: wind speed, wind direction, ambient temperature, solar radiation, conductor resistance, etc. However, it does not recommend suitably conservative weather conditions for line ratings, deferring this to the Cigré Technical Brochure 299 [5]. The variation of weather conditions along the line and with time is of great importance for the conductor thermal behaviour. Modeling the variation of conductor temperature along the line and radially within the conductor is emphasized.

Several example calculations are included to help the user in the application of the thermal method to their overhead lines. Also, in the annexes, certain analytical approaches for thermal rating calculations are included (conductor resistance, magnetic effects or time dependent heating models).

Section 1. Foreword

1.1. Background and objectives

There is a general need in the world for maximizing the use of electrical infrastructures, allowing them to operate at higher current densities and temperatures to increase the line's maximum power flow. In thermally-limited overhead lines, the maximum power that can be transmitted is limited by the maximum allowable temperature of the conductor, which should not be exceeded if excessive sags (to maintain the safety clearances) and possible thermal damage to the conductor and its fittings are to be avoided.

At the same time, changes in the electrical systems and the increasing need to integrate renewable, highly variable sources of power generation such as wind and solar, are forcing grid owners to control more accurately the behaviour of their lines in a changing environment. Hence the increasing use of real-time monitoring systems [64] to optimize the grid within its thermal limits.

The objective of this Technical Brochure is to provide the tools for calculating the thermal rating of overhead lines, including those lines operated at high current densities and temperatures, and including dynamic rating calculation methods to take into account the continuously changing weather conditions. TB 207 [1] was intended for thermal rating calculations at low current densities and moderate temperatures for constant weather conditions. This brochure takes into account improvements in the calculation of the ac resistance of stranded conductors, includes a more realistic estimation of the axial and radial temperature distributions within the conductor, presents a more coherent convection model for low wind speeds, and has a more flexible solar radiation model. These improvements allow a more accurate estimation of the sag of bare overhead conductors when running at high temperatures [2]. This is particularly the case for the high temperature conductors now available on the market [3], which have different constructions and different materials, both of which need to be taken into account for a proper design and a proper use of the dynamic rating systems.

A more accurate model of a line's thermal behaviour also provides a better basis for probabilistic methods of predicting thermal line ratings in particular circumstances, which is of great importance with respect to integrating renewable power generation into the grid.

This Technical Brochure is focused on static and dynamic thermal rating calculations, both for ac and dc operation, particularly at high temperatures and current densities. Other thermal

aspects, such as thermal methods for de-icing of overhead lines, are not within the scope of the document, and are dealt with in other documents [65].

This document does not recommend proper weather values or conditions to be used for line ratings [5], nor the temperature limits for safe operation of the conductors and accessories.

Note that in some cases the maximum capacity of an overhead line may not be determined solely by its maximum operating temperature and/or maximum sag. Other limiting factors may include other mechanical effects, system stability problems, other regulatory aspects (electromagnetic fields, for example), electric loss-limitation, the effects of underground cables in series with the overhead line, etc.

Also, some countries may have specific codes or regulations that could differ from the methods or models described in this document. For example, aspects related to dynamic rating methods, assumptions on weather parameters, or statistical approaches, may not be permitted in some regulations.

1.2. Nomenclature

List of symbols:

Symbol	Description	Units
A	cross-sectional area; constant	m ² ; dimensionless
B	magnetic induction; constant	T; dimensionless
C	constant	dimensionless
c	specific heat capacity	J · kg ⁻¹ · K ⁻¹
D	diameter of circle circumscribing the conductor	m
D_1	diameter of steel core	m
D_z	mean diameter of layer z	m
d	diameter of wire in outer layer	m
d_a	diameter of non-ferrous wire	m
d_s	diameter of steel wire	m
E	electric field	V · m ⁻¹
F	albedo (reflectance) of surface	dimensionless
\mathcal{F}	transfer factor or portion of heat radiated from one body to another	dimensionless
f	frequency	Hz
g	acceleration due to gravity, 9.807	m · s ⁻²
GMR	geometric mean radius	m
Gr	Grashof number, $Gr = D^3 \cdot (T_s - T_a) \cdot g / [(T_f + 273) \cdot \nu_f^2]$	dimensionless
h_c	convection heat transfer coefficient	W · m ⁻² · K ⁻¹
H	magnetic field strength	A · m ⁻¹
H_s	solar altitude	deg

I	effective current	A
I_B	intensity of direct solar radiation on surface normal to solar beam	$W \cdot m^{-2}$
I_d	intensity of diffuse solar radiation on horizontal surface	$W \cdot m^{-2}$
I_T	global solar radiation	$W \cdot m^{-2}$
k_{sk}	skin effect factor	dimensionless
l_z	lay length of the wires in layer z	m
m	mass per unit length; constant	$kg \cdot m^{-1}$; dimensionless
n	constant	dimensionless
N^*	day of the year (1 st January=1)	dimensionless
N_S	clearness ratio	dimensionless
Nu	Nusselt number, $Nu = h_c \cdot D / \lambda_f$	dimensionless
P	power exchange per unit length	$W \cdot m^{-1}$
Pr	Prandtl number, $Pr = c_f \cdot \mu_f / \lambda_f$	dimensionless
Q	power transferred per unit volume	$W \cdot m^{-3}$
R	resistance per unit length	$\Omega \cdot m^{-1}$
Re	Reynolds number, $Re = V \cdot D / \nu_f$	dimensionless
R_s	conductor roughness, $R_s = d / [2 \cdot (D - d)]$	dimensionless
r	radius	m
t	time interval	s
T	temperature	$^{\circ}C$
T_1	initial temperature	$^{\circ}C$
T_2	final temperature	$^{\circ}C$
V	speed	$m \cdot s^{-1}$
y	height above sea level	m
z	axial length; layer number	m; dimensionless
Z	hour angle of sun (positive before noon)	deg

Table 1: Nomenclature

Greek symbols:

Symbol	Description	Units
α	linear temperature coefficient of resistance	K^{-1}
α_s	solar absorptivity of conductor surface	dimensionless
β	temperature coefficient of specific heat capacity; inclination	K^{-1} ; deg
δ	wind angle of attack; skin depth	deg; m
δ_s	declination	deg
ε	solar emissivity of surface	dimensionless
γ	mass density	$kg \cdot m^{-3}$
γ_r	relative air density, $\gamma_r = \gamma / \gamma_0$ (=1 at sea level)	dimensionless
γ_0	air density at sea level 20°C, 1.2041	$kg \cdot m^{-3}$
γ_c	azimuth of conductor (positive from south through west)	deg
γ_s	azimuth of sun (positive from south through west)	deg

ζ	quadratic temperature coefficient of resistance	K^{-2}
η	angle of incidence of solar beam relative to axis of conductor	deg
λ	effective radial thermal conductivity, air thermal conductivity	$W \cdot m^{-1} \cdot K^{-1}$
μ	dynamic viscosity	$kg \cdot m^{-1} \cdot s^{-1}$
μ_r	relative permeability	dimensionless
μ_0	permeability of free space, $\mu_0 = 4 \cdot \pi \cdot 10^{-7}$	$H \cdot m^{-1}$
ν	kinematic viscosity, $\nu = \mu/\gamma$	$m^2 \cdot s^{-1}$
ρ	resistivity	$\Omega \cdot m$
σ_B	Stefan–Boltzmann constant, $5.6697 \cdot 10^{-8}$	$W \cdot m^{-2} \cdot K^{-4}$
θ	temperature rise above ambient	K
τ	thermal time constant	s
φ	Latitude (north positive); azimuthal angle	deg

Table 2: Greek symbols

Subscripts:

Symbol	Description
a	ambient; non-ferrous (aluminum)
ac	alternating current
ad	adiabatic
av	mean value
c	core; convection
dc	direct current
f	film at surface
h	heating
i	ionization, corona
in	inner
J	Joule
M	magnetic
m	asymptotic value
n	natural
ou	outer
R	real
r	radiation; relative
s	steel; surface
S	solar
T	total
th	thermal
w	mass transfer, evaporation
z	layer number

Table 3: Subscripts

Section 2. Overview and general equations

2.1. Steady state heat balance

The thermal state of overhead conductors depends on prevailing ambient weather parameters such as wind speed and direction, ambient temperature or solar radiation, and on the electrical current flowing through it. Assuming that all these parameters remain fairly constant over time, the conductor can be considered in a “steady state” with both the current and temperature constant. In this situation, the heat supplied primarily by Joule losses and solar radiation is equal to the heat dissipated primarily by convection and radiation to the surrounding atmosphere. Including secondary sources of heating by corona losses and magnetic core losses in steel core conductors and intermittent heat loss by evaporation, the heat balance equation can then be written as:

$$\begin{aligned} \text{Heat gain} &= \text{Heat loss} \\ P_J + P_S + P_M + P_i &= P_c + P_r + P_w \end{aligned} \quad (1)$$

where, P_J is the Joule heating, P_S the solar heating, P_M the magnetic heating, P_i the corona heating, P_c the convective cooling, P_r the radiative cooling and P_w the evaporative cooling.

The corona heating can be significant at times of high humidity and high wind speeds, but it is normally irrelevant for rating purposes due to the fact that convective effects at that times are much more important. The heat loss due to evaporation can have a major effect on the temperature of a conductor, but in most thermal rating calculations it is ignored for being rare that the entire line will be wet and the difficulty of assessment [32]. Safe values without considering this effect are preferred, and therefore:

$$P_J + P_S + P_M = P_c + P_r \quad (2)$$

Note that the magnetic heating, P_M , is often included in the Joule heating term by increasing the effective conductor resistance. This simplification gives the more general equation:

$$P_J + P_S = P_c + P_r \quad (3)$$

This equation is almost always accurate enough and easier to use, although in this brochure Joule heating and magnetic heating are generally treated separately.

2.2. Transient state

In general, both ambient conditions and the load of the line vary with time. In this case, the conductor is not always in thermal equilibrium, but in a state of continuous change, and the

general heat equation can be expressed as:

$$\text{Heat stored in conductor} = \text{Heat gain} - \text{Heat loss}$$

The heat stored in the conductor results in a temperature variation over a specified period of time that depends upon the material properties, etc. The heat gain and heat loss are computed as in the steady state case, taking into account their possible time-dependent characteristics.

Particular cases of transient states can be studied. One that has been widely studied is a step change in current. Assuming the ambient conditions remain constant, the time for the conductor to reach a certain temperature after a change in current can be calculated and used to anticipate emergency ratings [1, 4]. By also considering changes in weather parameters (wind speed and direction, ambient temperature, solar radiation), the behaviour of conductor temperature with time, or the time dependent heating or cooling, can be studied. By measuring these weather parameters along the line, and the current variation with time, it is thus possible to track the temperature of the conductor over a period of time for use in dynamic line rating methods.

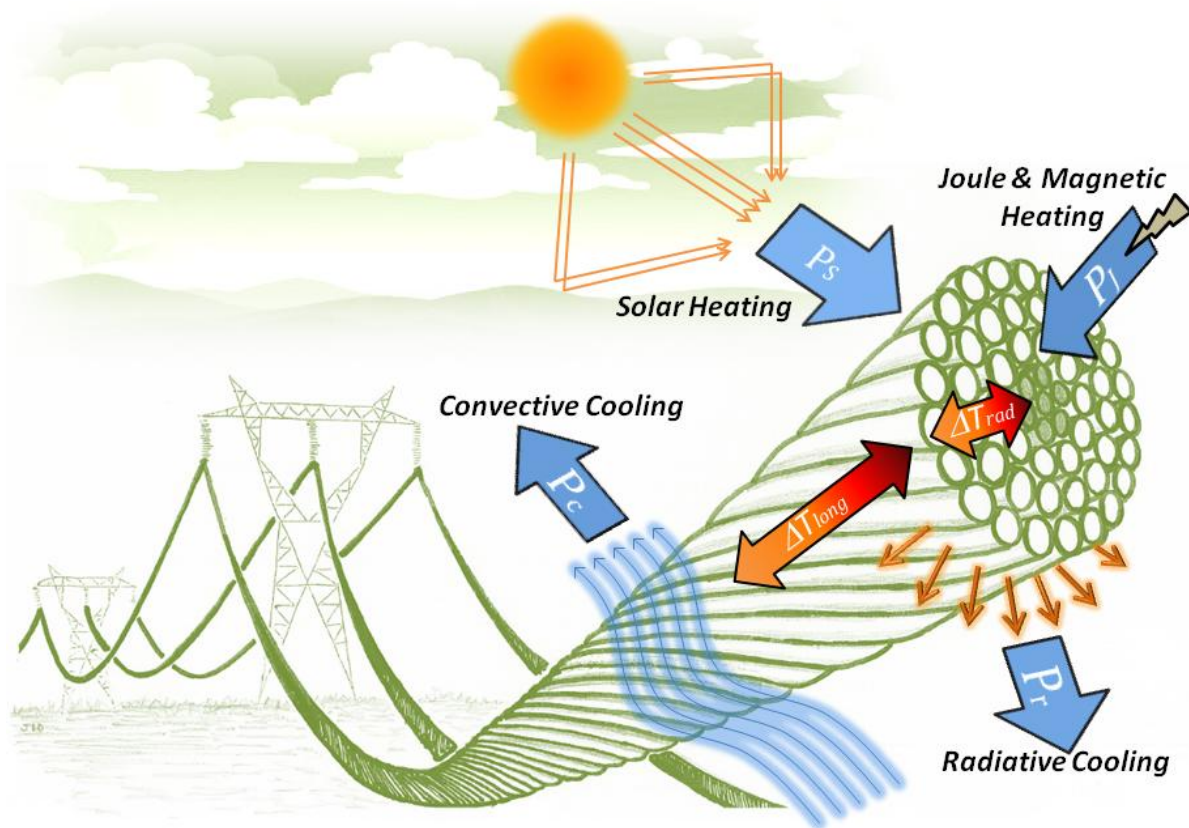


Figure 2: Overhead conductor heating and cooling

As mentioned above, precipitation can have a significant effect on conductor temperature (the conductors cool dramatically with rain), and its effect can be seen with dynamic rating systems. However, it is very difficult to assess along the line and to separate its effects from the wind effects, so it's therefore usually ignored.

Another special case is called the adiabatic state. This is used to model the temperature of a conductor under short-circuit conditions. Since the duration of the fault is very short, it is assumed that there is no cooling, so the heat equation can be written as:

$$\text{Heat stored in conductor} = \text{Heat gained}$$

The heat gained due to the large current flowing through the conductor results in a rapid temperature rise that must be controlled in order to avoid damages to the conductor.

Section 3. Calculation of heating and cooling

3.1. Joule heating calculation

Joule heating refers to the energy generated by current flow through the conductor. It takes into account the pure direct current resistance and the “skin effect” (the increase of current density towards the surface of the conductor) when alternating currents (ac) are used. The Joule heating, as defined in this document, does not include the magnetic effects produced by ac currents due to cyclic magnetic flux, which may cause a non-negligible heating at high current densities in certain conductors with a ferrous core. This magnetic heating is described in Section 3.2. However, the magnetic heating is often included in the Joule heating term by increasing the effective conductor resistance. This avoids the complexity of the calculations needed to determine accurately the magnetic heating effect. The combined ac resistance may be derived for the relevant temperature from available empirical values [49, 56].

Direct current

The Joule heat gain per unit length for conductors carrying direct current is found from:

$$P_J = I^2 \cdot R_{dc} \quad (4)$$

where I is the total direct current (A) and R_{dc} the direct current resistance per unit length (Ω/m), which depends on the resistivity of the materials ρ ($\Omega \cdot \text{m}$) at the temperature considered, the cross-sectional area A (m^2) and the conductor mean temperature T_{av} ($^{\circ}\text{C}$). The resistivity of a material at any temperature T_{av} can be expressed as:

$$\rho = \rho_{20} \cdot [1 + \alpha_{20} \cdot (T_{av} - 20) + \zeta_{20} \cdot (T_{av} - 20)^2] \quad (5)$$

where ρ_{20} , α_{20} and ζ_{20} are the resistivity and its linear and quadratic temperature coefficients ($1/\text{K}$ and $1/\text{K}^2$) at 20°C , respectively. The quadratic term only becomes significant at temperatures higher than about 130°C . Analytical values of R_{dc} for various types of conductors can be obtained as described in Annex A, where typical data for ρ_{20} , α_{20} and ζ_{20} are given in Table 6. Alternatively, empirical values of R_{dc} at different average temperatures may be given by conductor manufacturers and may also be available in the literature. The value of R_{dc} for the desired temperature can be obtained by means of linear interpolation. However, it is important to remember that the variation of the resistance with temperature is not linear, and care must be taken to avoid significant errors [54]. For example, a “Drake” ACSR conductor has an increase of 80% in resistance when changing from 25°C to 250°C (note it is not common to operate ACSR conductors at this temperature). Other conductors may show greater differences.

Alternating current. The skin effect

With alternating current, the resistance of a conductor increases due to the migration of the current towards the surface of the conductor, a phenomenon known as “skin effect” [7, 8]. In this case the Joule heat gain is given by:

$$P_J = k_{sk} \cdot I^2 \cdot R_{dc} \quad (6)$$

where k_{sk} is the skin effect factor. The direct current resistance per unit length R_{dc} can be obtained as described in the previous section for the desired temperature. The skin effect factor increases with increasing conductor diameter and with increasing frequency. It is usually less than 1.02 for the normal range of conductor diameters and with commercial frequencies [10], but could be as much as 1.08 for larger conductors (diameters greater than 45 mm). Analytical values for the skin effect factor can be calculated using Bessel functions [9], although it is quicker, but less accurate, to use a graphical method [10]. In Annex A, simplified Bessel-function equations are given for calculating the skin effect for the normal range of conductors used in overhead lines at power frequency. For a practical application, the approximation of a stranded conductor as a solid wire or tube, as given in Annex A, has proved to be adequate. Graphical expressions and values for different conductor sizes are available [7, 10, 49] in order to check approximate calculations.

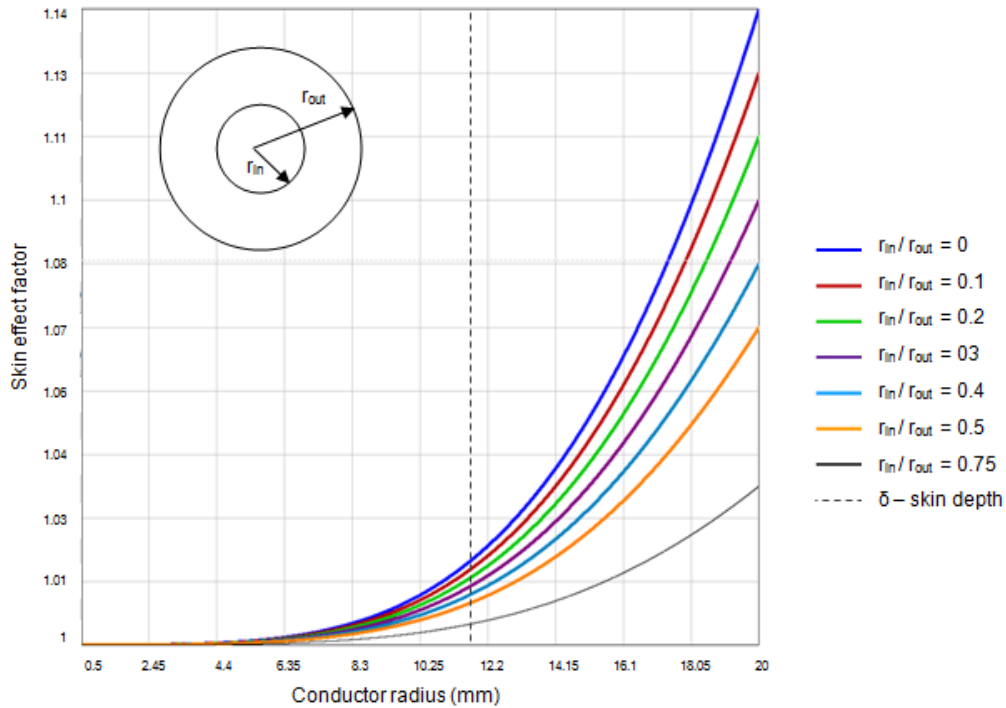


Figure 3: Example of graph for skin effect factor versus outer conductor radius for different r_{in}/r_{out} ratios and certain conditions [7, 10].

The skin depth, δ , or depth of propagation, is defined as the depth at which the current density is $1/e$ or $\approx 37\%$ of its value at the surface. It is a function of the frequency, the relative permeability and the resistivity of the conductor material (see Annex A). As seen in the previous section, the resistivity increases with the temperature, making the skin depth also increases with the temperature. Therefore, the skin effect factor is lower at higher temperatures.

Cigré Technical Brochure 345 [16] provides detailed numerical methods for calculating the skin effect and the magnetic effects (which are discussed below). However, empirical values of ac resistance for specific conductors at particular temperatures are often available from manufacturers or handbooks, and a good approximation for the desired temperature can often be obtained by linear interpolation. Note however that these available values may include magnetic heating effects produced in ferrous conductors due to the alternating current. For example, the US Aluminum Association Handbook [56] includes the skin and magnetic effects in the R_{ac} values given for one-layer ACSR conductors. For three-layer ACSR conductors, a correction factor is proposed for the magnetic effect, depending on the current density. Hence, the user must be aware of the effects considered for each case.

The proximity effect in overhead conductors is usually neglected because the separation distance between the phase conductors or sub-conductors in a bundle is generally large enough that the effect is minimal.

3.2. Magnetic heating calculation

In the case of a steel-cored conductor, such as aluminum-conductor steel-reinforced (ACSR), the axial alternating magnetic flux produced by the spiraling conductor layers causes heating in the steel core, P_{core} , and heating due to redistribution of the current densities in the layers of the non-ferrous wires, P_{redis} , known as the transformer effect. These magnetic effects may be considerable for certain conductors, although for the majority of the cases in transmission lines they can be considered negligible. The total magnetic heat gain per unit length is the sum of both power losses:

$$P_M = P_{core} + P_{redis} \quad (7)$$

A simplified method to calculate the heating in the steel core, P_{core} , and that due to redistribution of the current densities P_{redis} is described in Annex B. A detailed description of the iterative calculation methods can be found in [16]. The magnetic effects are only relevant for steel-cored conductors with one or three aluminum layers and high current densities. With an even number of aluminum layers these effects cancel out. For example, for a single-aluminum-layer steel-cored conductor with a high current density, the magnetic effect could increase the effective resistance by up to 20%. For a 3-aluminum-layer steel-cored conductor, the increase can be up to 5% [16].

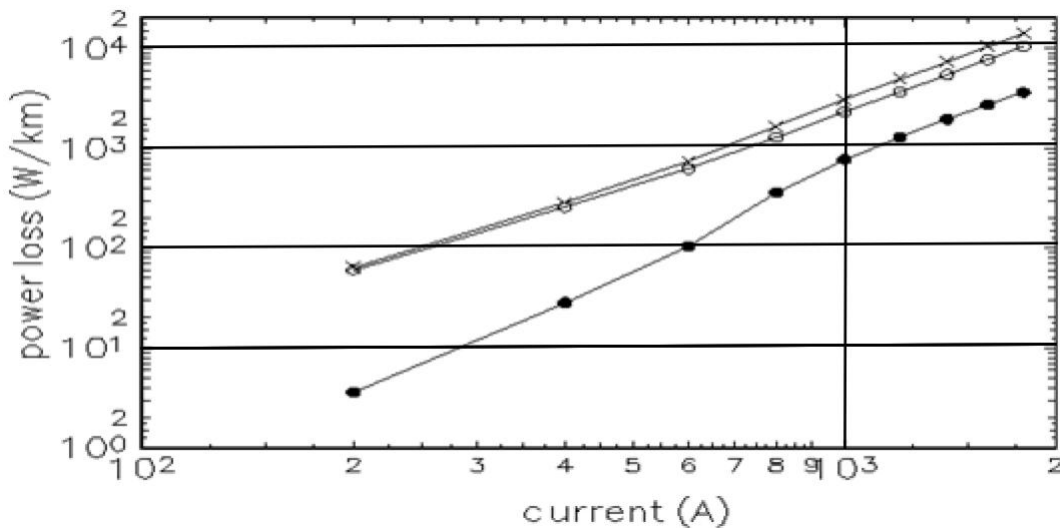


Figure 4: Example of variation of the power loss with current for a “Grackle” Conductor at 25°C, 60 Hz and 290 MPa core stress [13]. (●) core loss, (○) loss due to redistribution of current density, (x) total loss.

It is common to include these magnetic effects in the published effective ac resistance values of the conductor for the different temperatures [49, 56], as mentioned before. When such is adopted, the magnetic heating calculations will not be required, but the user must be aware of the effects considered in the effective resistance value that is used.

It is worth noting that the steel core is considered a mechanical reinforcement for the aluminum wire layers and conductor manufacturers typically make no attempt to control the magnetic properties of steel core wires. Nor do the IEC and ASTM standards for steel core wires have any requirements regarding magnetic properties. As a result, the steel core magnetic properties are likely to vary.

3.3. Solar heating calculation

The solar heat gain per unit length by a conductor, P_S (W/m), is directly proportional to the outer diameter of the conductor, D (m), the absorptivity of the surface of the conductor, α_S , and the global radiation intensity I_T (W/m²) [23]:

$$P_S = \alpha_S \cdot I_T \cdot D \quad (8)$$

The value of α_S varies from around 0.2 for a bright new conductor to around 0.9 for a weathered conductor in an industrial environment [17, 5]. A new conductor in a heavy industrial environment weathers to around $\alpha_S = 0.5$ after about one month's exposure, and to around $\alpha_S = 0.9$ after about one year. The rate of weathering is slower in rural areas. It is not easy to measure the absorptivity accurately. The recommended methods are either determining the emissivity of the conductor, by measuring samples and then estimating absorptivity to be slightly higher than this value (0.1 – 0.2 higher), or using a default absorptivity of no less than 0.8 [5]. Conductor surface treatments may provide different values.

Devices for measuring global radiation intensity I_T are relatively inexpensive and reliable, and can be easily used for line monitoring systems [64], as they can provide measurements of the mean global radiation intensity for a period of time for the dynamic thermal rating calculations (see Section 4). But there are some considerations that have to be noted. The global radiation received by the conductor is not necessarily the same at all points along the line. It depends on the location, and important differences may arise due to different orientation, sheltered areas, reflectance from ground, etc. The variability with time is also not the same at all points along the line.

For planning or design, it is common to consider a “worst-case” situation, for which the maximum expected value of the global radiation I_T can be anticipated. Care must be taken in anticipating the right values, and their coincidence with other ambient parameters [5]. A value can be estimated for a given location and orientation of the line, and for a specific time and day of the year, from the relative position of the sun (see the formulae below).

The global radiation intensity, I_T , is a combination of the direct solar radiation on a surface normal to the Sun's beam, I_B , the diffuse sky radiation to a horizontal surface, I_d , and the incident radiation reflected from the ground or albedo, F . The formula for the total solar power received per unit length of the conductor P_S (W/m) is given by [19, 23, 29]:

$$P_S = \alpha_S \cdot D \cdot \left[I_B \cdot \left(\sin(\eta) + \frac{\pi}{2} \cdot F \cdot \sin(H_S) \right) + I_d \cdot \left(1 + \frac{\pi}{2} \cdot F \right) \right] \quad (9)$$

where:

α_s = absorptivity of conductor surface (see the text above)

D = diameter of the conductor (m)

I_B = direct (beam) solar radiation intensity (W/m²). An equation to calculate the direct solar radiation at sea level, $I_{B(0)}$, is [66]:

$$I_{B(0)} = N_s \cdot \frac{1280 \cdot \sin(H_s)}{\sin(H_s) + 0.314} \quad (10)$$

where N_s is a clearness ratio, having the value of 1.0 for the standard atmosphere, 0.8 to 1.2 for clear skies with decreasing amounts of dust and aerosols, 0.5 for an industrial atmosphere and less than 0.5 for a cloudy or overcast sky. With thick cloud, $N_s = 0$. The direct beam radiation I_B increases with increasing height above sea level, y , according to the following equation [67]:

$$I_{B(y)} = I_{B(0)} \cdot \left[1 + 1.4 \cdot 10^{-4} \cdot y \cdot \left(\frac{1367}{I_{B(0)}} - 1 \right) \right] \quad (11)$$

H_s is the solar altitude, given by:

$$H_s = \arcsin(\sin(\varphi) \cdot \sin(\delta_s) + \cos(\varphi) \cdot \cos(\delta_s) \cdot \cos(Z)) \quad (12)$$

where:

φ = latitude

$$\delta_s = \text{declination} = 23.3 \cdot \sin \left[\frac{2 \cdot \pi \cdot (284 + N^*)}{365} \right]$$

The declination of the sun can be defined as the angle between the equator and a line drawn from the centre of the earth to the centre of the sun.

N^* = day of year (1st January = 1)

Z = hour angle of the Sun = $15 \cdot (12 - \text{Time})$, in degrees, with *Time* given in hours, from 0 to 24. The solar hour angle Z decreases by 15 degrees for every hour from zero at solar noon. To obtain solar time, add 4 minutes per degree of longitude east of standard time, or subtract 4 minutes per degree west of standard time. There is also a small time correction, not exceeding 16 minutes, for perturbations in the earth's rotation.

I_d is the diffuse solar radiation intensity (W/m^2). There is a correlation between direct radiation I_B and diffuse radiation I_d , as clouds cause both a reduction in I_B and an increase in I_d . An equation to calculate the diffuse radiation for all skies is [68]:

$$I_d = (430.5 - 0.3288 \cdot I_B) \cdot \sin(H_S) \quad (13)$$

η is the angle of solar beam with respect to the axis of the conductor. This angle is given by:

$$\eta = \arccos[\cos(H_S) \cdot \cos(\gamma_S - \gamma_c)] \quad (14)$$

where:

γ_c = azimuth of the conductor

$$\gamma_S = \text{azimuth of the Sun} = \arcsin\left[\frac{\cos(\delta_S) \cdot \sin(Z)}{\cos(H_S)}\right]$$

F is the albedo or reflectance of the ground. The albedo (F) is approximately 0.05 for a water surface ($H_S > 30^\circ$), 0.1 for forests, 0.15 for urban areas, 0.2 for soil, grass and crops, 0.3 for sand, 0.4 to 0.6 for ice and 0.6 to 0.8 for snow. The albedo tends to increase as the solar altitude H_S increases.

The residual gain at night can be considered negligible.

3.4. Conductor temperature distribution

At high current densities (greater than 2 or 3 A/mm²), the radial and axial variations in temperature must be considered if the temperature and sag of the conductor are to be properly evaluated. Sag depends, to a large extent, on the core temperature, T_c , whilst convection and radiation depend on the surface temperature T_s , and resistive heating depends on the average temperature, T_{av} . It is important be able to correctly predict the maximum core and surface temperatures for every span because sag and possible annealing effects may be more of a problem for certain spans of the line, such as those in sheltered sections.

For any conductor, the heat generated in the core has to be transferred to the outer surface of the conductor, resulting in a radial temperature drop. For multi-layered stranded conductors, this radial temperature drop can be substantial, particularly during high temperature operation [76]. For example, in a 3-layer 54/7 Zebra ACSR conductor, approximately 22% of the Joule and magnetic heating occurs in the innermost layer of aluminum strands and 33% in the middle layer. Thus more than half of the Joule and magnetic heat must be conducted to the outermost layer of aluminum strands before reaching the surrounding atmosphere.

Also, experimental and analytical studies show that the conductor temperature along a typical line carrying 4 A/mm² can vary between 135°C and 230°C simply due to variation in wind speed (1 to 2 m/s) and direction (20° to 90°) along the line, with almost no axial equalization of temperature [57].

Radial temperature variation

The heat generated in the internal layers of the conductor is transported to the outermost layer by means of conduction, convection and radiation. This heat transfer depends on a number of variables which are very difficult to assess: strand contact area, contact pressure between layers, degree of corrosion of the strands, air voids (interstices), air gaps between strands...

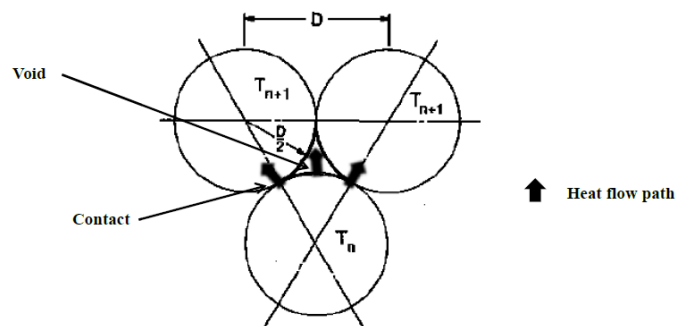


Figure 5: Example of voids between strands in adjacent layers. Model of heat flow from the core to the surface [18, 22]

Several analytical approaches are proposed to calculate the radial temperature distribution in stranded conductors. A complex method is given in [18]. However, assuming that the internal heat generation is uniform, a simplified equation to calculate the radial temperature difference [19] of a cylindrical conductor can be written as follows:

$$T_c - T_s = \frac{P_T}{2 \cdot \pi \cdot \lambda} \cdot \left[\frac{1}{2} - \frac{D_1^2}{D^2 - D_1^2} \cdot \left(\ln \frac{D}{D_1} \right) \right] \quad (15)$$

where:

λ = effective radial thermal conductivity (W/m·K)

P_T = total heat gain per unit length (W/m)

D = overall diameter of conductor (m)

D_1 = internal diameter of a tubular conductor or diameter of a steel core if present (m)

Eq. 15 applies to hollow core mono-metallic conductors or steel-cored conductors. For full-body mono-metallic conductors, $D_1 = 0$, and eq. 15 reduces to eq. 16:

$$T_c - T_s = \frac{P_T}{4 \cdot \pi \cdot \lambda} \quad (16)$$

For these simplified equations, the effective radial thermal conductivity λ is the key factor that determines the temperature gradient. There have been several experiments that measure temperatures on both mono-metallic and steel-cored conductors [20, 21], indicating that it can lie in the range from 0.5 W/m·K to 7 W/m·K. Other conductor constructions, greased conductors, gapped conductors, etc., may produce different values.

It has been found [22, 57] that the longitudinal mechanical tension on the aluminum strands is a major factor in determining this value. This is because of its influence on the pressure between strands, and therefore the metal to metal contact and air interstices. Some authors suggest [57] that values of the order of 0.7 W/m·K for conductors with no tension on aluminum strands (for example conductors operating above knee-point temperature, where aluminum strands bear very little or no tension), and of 1.5 W/m·K for conductors with aluminum strands under a tension of at least 40 N per aluminum strand (conductors operating below knee-point temperature) be used.

Longitudinal temperature variation

Very little of the heat generated within the conductor is transmitted axially. As shown in fig. 6, even when the temperature varies greatly due to varying wind cooling there is very poor temperature equalization along the conductor. Therefore, at high current densities, there can be a substantial variation in conductor temperatures along an overhead line due to variations in the local weather conditions, with almost no axial equalization. The temperature measured at a single location along a line section may thus be quite different from the average conductor temperature in that line section. Differences of 50°C in conductor temperature have been reported within a single partially sheltered span at very high current densities [54].

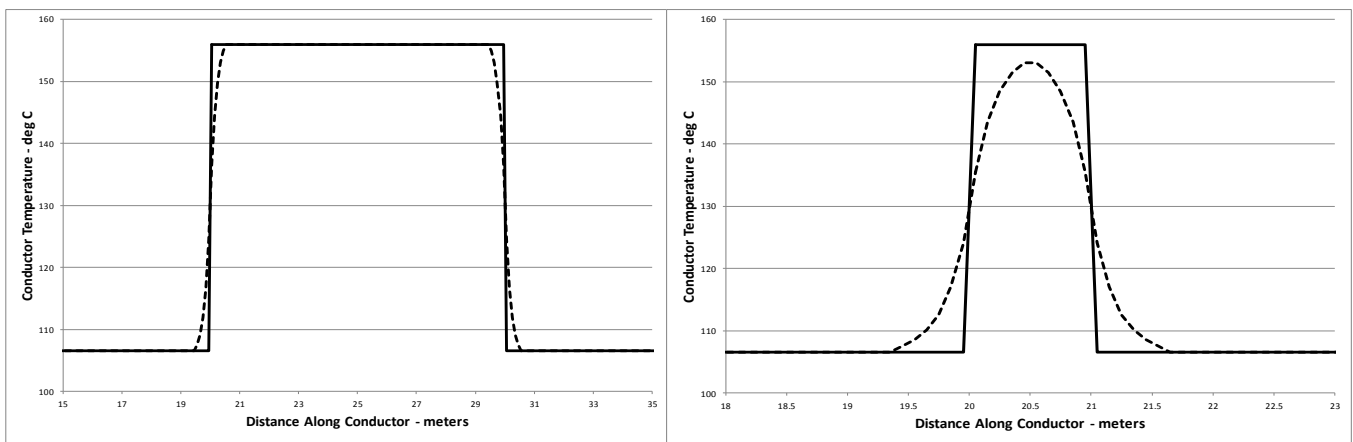


Figure 6: Calculated temperature distribution for two sheltered sections of conductor (10 meter long on the left and 1 meter long on the right). Wind speed is 1.6 m/s at all points outside the section where it is only 0.6 m/s [57].

Mathematical determinations of the axial heat transfer [20, 29, 57] confirm this important temperature variability along the overhead lines, although the order of magnitude of the effective axial thermal conductivity is around hundred times higher than the effective radial thermal conductivity, because the thermal conduction propagates through aluminum strands (see values of thermal conductivity in Table 6, Annex A).

3.5. Convective cooling calculation

Convection is almost always the most important factor for cooling overhead conductors, even for still air conditions (zero wind speed). Conductor temperatures can only be high when convective cooling is low. Hence, for thermal rating purposes, the focus is on situations where wind speed is low or zero. Two types of convection are considered: natural convection, which occurs when wind speed is zero; and forced convection which depends on wind speed and direction relative to the line. At moderate-to-high wind speeds, forced convection dominates and natural convection can be ignored. At low wind speeds, natural convection may have a significant effect, becoming the dominant convection mechanism at very low wind speeds.

Wind variability, even within a single span, makes it very difficult to assess the thermal behaviour of overhead lines, particularly at low wind speeds and high current densities. As noted previously, the axial differences in conductor temperature can be very significant, mainly due to wind variability [54]. Therefore, even though the equations to model the local heat transfer are accurate, the behaviour of the whole line section or a single span may be different. So, for thermal rating purposes, it is necessary to consider this variability and model the wind properly. It is not simple, and some approaches based on statistical analysis are under development to consider this problem. For example, the concept of “effective wind speed” has been introduced as the perpendicular, laminar wind speed which produces the same cooling effect along an entire section.

The heat transfer from a bare stranded overhead conductor to a surrounding atmosphere is dependent on the coefficient of convective heat transfer, h_c (W/K·m²). In order to obtain empirical values that can be used in practical situations, the convective heat loss can be expressed as a function of the dimensionless Nusselt number (see nomenclature) as follows:

$$P_c = \pi \cdot \lambda_f \cdot (T_s - T_a) \cdot Nu \quad (17)$$

where λ_f is the thermal conductivity of the air (W/K·m) at T_f , the temperature of the film of air in contact with the surface, and T_s and T_a are the temperatures of the conductor surface and the air respectively. For film temperatures up to 300 °C the thermal conductivity of the air can be expressed as [54]:

$$\lambda_f = 2.368 \cdot 10^{-2} + 7.23 \cdot 10^{-5} \cdot T_f - 2.763 \cdot 10^{-8} \cdot T_f^2 \quad (18)$$

where the film temperature is assumed to be $T_f = 0.5 \cdot (T_s + T_a)$

Depending on the situation (natural or forced convection), different correlations have been proposed by many authors ([25], [26], [30], [33],...) in order to obtain the Nusselt number (i.e.

the convective heat loss). The following sub-sections show some of these correlations, which are compared in Annex C. However, as mentioned before, the variability of wind speed and direction, both in time and in space, as well as the turbulence regime, is very high. So it is important to choose the appropriate values that yield the correct conductor temperatures within the frame considered.

Forced convection

a) Perpendicular flow

For a cylinder or a round, bare stranded conductor, with perpendicular air flow, it has been shown by multiple researchers that there is a correlation between the dimensionless Nusselt number and Reynolds number, $Re = V \cdot D / \nu_f$, where V is the wind speed (m/s), D is the diameter of the conductor (m), ν_f is the kinematic viscosity (m²/s) of the air at the film temperature T_f . The kinematic viscosity of the air, ν_f , depends on the elevation of the conductor above sea level and can be expressed as $\nu_f = \mu_f / \gamma$, being μ_f the dynamic viscosity of the air at the film temperature and γ the density (kg/m³) of the air at the elevation of the conductor. An expression for μ_f valid for T_f up to 300°C is:

$$\mu_f = (17.239 + 4.635 \cdot 10^{-2} \cdot T_f - 2.03 \cdot 10^{-5} \cdot T_f^2) \cdot 10^{-6} \quad (19)$$

A formula for calculating the density of air at given film temperature and elevation can be expressed as [4]:

$$\gamma = \frac{1.293 - 1.525 \cdot 10^{-4} \cdot y + 6.379 \cdot 10^{-9} \cdot y^2}{1 + 0.00367 \cdot T_f} \quad (20)$$

Among the correlations proposed, it is highlighted the following equation given by Morgan [25], which has been used as benchmarks in many papers by other authors and is based on hundreds of experimental results:

$$Nu_{90} = B \cdot Re^n \quad (21)$$

where the coefficients B and n are as given in Table 4. They depend on the Reynolds number and the roughness R_s of the surface of the conductor, $R_s = d / [2 \cdot (D - d)]$, where d is the diameter of the wires in the outermost layer, and D is the overall diameter. This conductor diameter D should be the overall diameter, in spite of the fact that a stranded conductor may have a surface area 40–45% greater than that of a smooth conductor having the same diameter [25]. This is because the boundary layer detaches from each outer wire and re-attaches at the next wire, thus forming stagnant zones at the interstices between adjacent wires.

Smooth Conductors			Stranded Conductors, $R_s \leq 0.05$			Stranded Conductors, $R_s > 0.05$		
Re	B	n	Re	B	n	Re	B	n
35 – 5,000	0.583	0.471	100 – 2,650	0.641	0.471	100 – 2,650	0.641	0.471
5,000 – 50,000	0.148	0.633	2,650 – 50,000	0.178	0.633	2,650 – 50,000	0.048	0.800
50,000 – 200,000	0.0208	0.814						

Table 4: Coefficients for calculating forced convective heat transfer from conductors with steady crossflow of air [19, 23, 25], see eq. 21. Note that wind speed varies with the height above sea level.

It can be seen from Table 4 that the roughness of the conductor is not relevant for low winds ($Re < 2,650$), but can increase the Nu number, and thus the cooling, by up to 60% at higher winds (Re of 50,000). Other Nusselt number–Reynolds number correlations have been proposed [26–28]. Some of the most important are described and compared in Annex C.

b) Wind direction

The above equations are only valid for an air flow perpendicular to the conductor. However, the wind direction plays an important role in the effectiveness of the forced convective cooling [31]. Again, several relationships have been proposed to fit the available experimental data for the variation of the Nusselt number with the angle of attack δ of the wind with respect to the axis of the conductor.

Some of the proposals to consider this variation of the Nusselt number are compared in Annex C. The following equations proposed by Morgan [29, 32] are reproduced here, where δ is the angle between wind and line direction:

$$\begin{aligned} \frac{Nu_\delta}{Nu_{90}} &= (\sin^2(\delta) + 0.0169 \cdot \cos^2(\delta))^{0.225}; \text{ for smooth conductors} \\ \frac{Nu_\delta}{Nu_{90}} &= 0.42 + 0.68 \cdot (\sin(\delta))^{1.08}; \text{ for stranded conductors with } \delta \leq 24^\circ \\ \frac{Nu_\delta}{Nu_{90}} &= 0.42 + 0.58 \cdot (\sin(\delta))^{0.90} \text{ for stranded conductors with } \delta > 24^\circ \end{aligned} \quad (22)$$

These equations are valid for $Re < 4,000$.

It can be seen from the equations above that the cooling produced by a parallel wind flow is only around 40% of that produced by a perpendicular wind. But the variability in wind direction

is often very high, particularly at low wind speeds. For dynamic line rating purposes, the concept of “effective wind speed” has been developed, as stated before, to deal with this wind variability.

It also should be noted that usually the inclination of a conductor to the horizontal has no significant effect on the forced convective heat loss, provided that the air flow is transverse to the axis of the conductor.

c) Turbulence

Turbulence has a considerable effect on convection cooling of the conductor, especially for high winds. However, it is very difficult to assess in a real overhead line, due to its variability in space and time [54]. Outdoors, the turbulence intensity, defined as the ratio of the standard deviation to the mean speed, can be over 0.3, which is much higher than values obtained in wind-tunnel tests. Also, the scale of outdoor turbulence tends to be much larger than that obtained with grids in a wind tunnel [29], so it is not easy to translate the results of the heat transfer augmentation obtained in turbulent flow in a wind tunnel to outdoor conditions. At Reynolds numbers less than a critical value, turbulence has no effect on the local or overall heat transfer. Above a critical value of Re , turbulence causes earlier transition to a turbulent regime in the boundary layer on a cylinder [59]. Therefore, the user must be aware that considerable errors can be introduced when performing dynamic rating calculations, especially for relatively high winds, due to the impossibility to assess the wind regime (variability, influence of obstacles, influence of bundled conductors...).

Natural convection

In the case of zero wind, it has been found from different researches that the Nusselt number, Nu_{nat} , depends on the product of the dimensionless Grashof and Prandtl numbers (see nomenclature):

$$Nu_{nat} = A \cdot (Gr \cdot Pr)^m \quad (23)$$

As with the Reynolds number (see Forced Convection Section) the conductor diameter D of both smooth and stranded conductors should be the overall diameter. Values of the coefficients A and m proposed by Morgan for various ranges of $Gr \cdot Pr$ are given in Table 5 [19]. These values are based on the results of hundreds of experimental measurements, and have been used as benchmarks. Other correlations may be found in [35–37] and are compared in Annex C.

Range of $Gr \cdot Pr$		A	m
from	to		
10^{-1}	10^2	1.02	0.148
10^2	10^4	0.850	0.188
10^4	10^7	0.480	0.250
10^7	10^{12}	0.125	0.333

Table 5: Coefficients for calculating natural convective heat transfer [19].

See eq. 23.

Inclination of a conductor to the horizontal, β , reduces the natural convective heat loss. The ratio Nu_β/Nu_0 can be found from [29]:

$$\begin{aligned} \frac{Nu_\beta}{Nu_0} &= 1 - 1.58 \cdot 10^{-4} \cdot \beta^{1.5}; \text{ for } \mathbf{smooth\ conductors}, \beta < 60^\circ \\ \frac{Nu_\beta}{Nu_0} &= 1 - 1.76 \cdot 10^{-6} \cdot \beta^{2.5}; \text{ for } \mathbf{stranded\ conductors}, \beta < 80^\circ \end{aligned} \quad (24)$$

Low wind speeds

When the wind speed is low, the physics of the heat transfer can be more complicated due to buoyancy effects that may occur in the air surrounding the conductor. Different models have been proposed by some authors to consider these effects, and provide a smooth transition between forced and natural convection. However, it is very complicated to contrast and use these models in real situations due to the great variability of the wind speed and direction, both in time and space [54, 61].

Some of the convection models for low wind speeds are described in Annex C, but their practical application for dynamic thermal ratings would need an accurate assessment of the wind speed and direction all along the line at any time, which is not possible in practice for normal situations. Therefore, there is a need to develop approaches to provide the proper adjustments of the local weather measurements that can be used for dynamic thermal ratings of a whole line (see Section 5).

It is usually recommended that, in all cases, the higher of the natural and forced convection values as determined from eq. 17 to 24 be used, which is a conservative approach. Thus for the example shown in fig. 7, cooling should be assumed to follow the appropriate solid

coloured curve down to where it meets the natural cooling line. Below this point the natural convection value should be used.

Convective cooling at low wind speeds for various attack angles (Drake example)

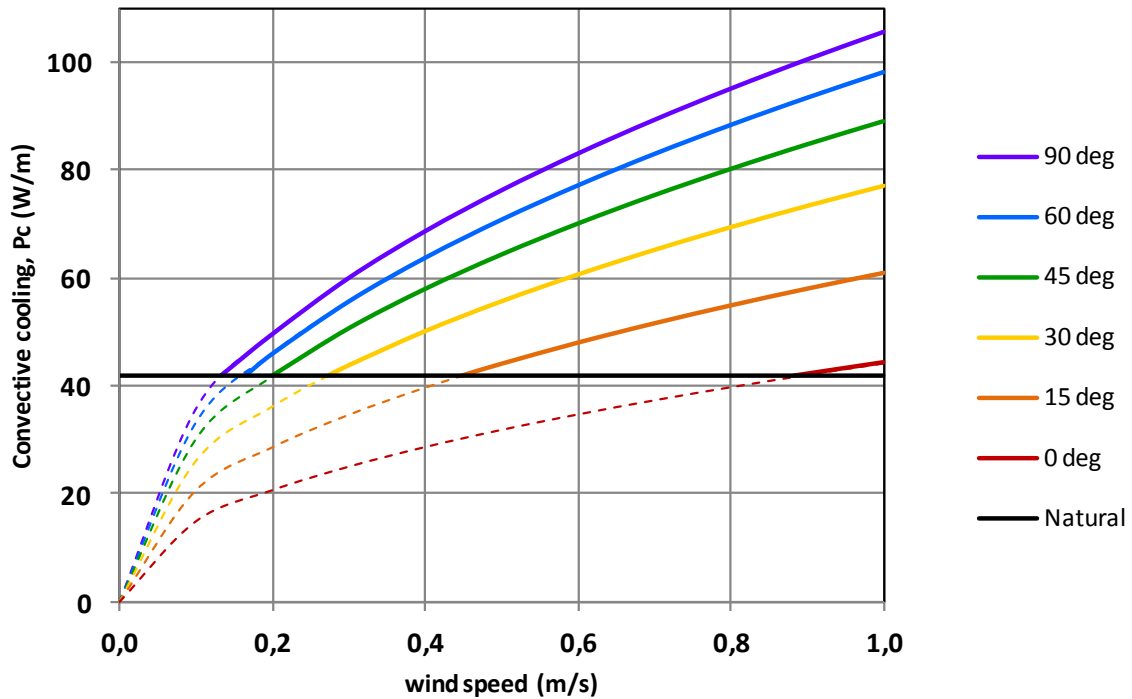


Figure 7: Convective cooling at low wind speeds and various attack angles. Example for “Drake” ACSR conductor at 100°C, ambient 40°C.

3.6. Radiative cooling calculation

The net radiative heat loss from a conductor is the total radiative energy transmitted from its surface. It can be divided into two components [74]: the heat radiated to the ground and surroundings, and the heat radiated directly to the sky. Applying the Stefan–Boltzmann law, the heat loss from the conductor due to radiation can be expressed as [26, 75]:

$$P_r = \pi \cdot D \cdot \sigma_B \cdot \mathcal{F}_{c-g} \cdot \varepsilon_s \cdot \left[(T_s + 273)^4 - (T_g + 273)^4 \right] + \pi \cdot D \cdot \sigma_B \cdot \mathcal{F}_{c-sky} \cdot \varepsilon_s \cdot \left[(T_s + 273)^4 - (T_{sky} + 273)^4 \right] \quad (25)$$

where D is the outer diameter of the conductor (m), σ_B is the Stefan–Boltzmann constant (see Nomenclature), ε_s is the emissivity of the conductor surface, T_s is the temperature of the conductor surface, T_g is the temperature of the ground beneath the conductor, T_{sky} is the temperature of the sky above the conductor, \mathcal{F}_{c-g} is the fraction of radiated energy from the conductor that reaches the ground and surroundings, and \mathcal{F}_{c-sky} is the fraction of radiated energy from the conductor that goes to the sky.

It is often sufficiently accurate, for rating purposes, to set both, T_g and T_{sky} , equal to the ambient temperature, T_a . The ambient temperature is much easier to estimate or measure. So, rearranging the previous equation:

$$P_r = \pi \cdot D \cdot \sigma_B \cdot \varepsilon_s \cdot (\mathcal{F}_{c-g} + \mathcal{F}_{c-sky}) \cdot \left[(T_s + 273)^4 - (T_a + 273)^4 \right] \quad (26)$$

The summation of the radiated energy portion from the conductor to the ground, \mathcal{F}_{c-g} , and the radiated energy portion from the conductor to the sky, \mathcal{F}_{c-sky} , is the total radiated energy leaving the conductor surface, which is equal to one. So the previous equation can be written as:

$$P_r = \pi \cdot D \cdot \sigma_B \cdot \varepsilon_s \cdot \left[(T_s + 273)^4 - (T_a + 273)^4 \right] \quad (27)$$

Emissivities of energized conductors increase rapidly with age from about 0.2 – 0.3 when new to about 0.8 – 0.9 within one or two years of high voltage operation in industrial or heavy agricultural environments [5]. Actual emissivities can be determined by measurements on conductor samples, but it is generally recommended that for weathered conductors, a value of 0.8 or 0.9 be used. It is possible to find conductors with surface treatments that may present different values.



Figure 8: Light reflected by new installed overhead conductors.

From the above formulae, it can be seen that radiative cooling is much more important at high conductor temperatures. For example, a “Drake” ACSR conductor (28.1 mm diameter) operating at 150°C, and an ambient temperature of 35°C, radiates more than ten times the heat radiated when operating at 50°C. However, the heat loss from the conductor by radiation is usually much lower than the heat loss by convection and, therefore, its impact on the thermal ratings is limited (see Section 5). It has to be noted that it is not common to operate regular ACSR conductors at such a high temperature because it may cause a possible loss of mechanical properties.

Section 4. Thermal models

4.1. Numerical models for steady state

At the planning or design stages, thermal equilibrium of the conductor is assumed in order to estimate the maximum allowable line ratings. The steady state equations are used to calculate the current for a given maximum temperature of the conductor under accepted “worst-case” weather conditions (see Section 5). This is the so-called steady state thermal rating.

Alternatively, when redesigning, verifying or uprating lines, the steady state equations can be used to determine the maximum temperature of the conductor for a given desired current under the same “worst-case” weather conditions, assuming the thermal equilibrium of the conductor. This is the so-called steady state conductor temperature.

Steady state thermal rating

A numerical model to calculate the line thermal rating, I , for a maximum conductor temperature, T_{av} , and fixed (expected) weather conditions can be outlined as follows:

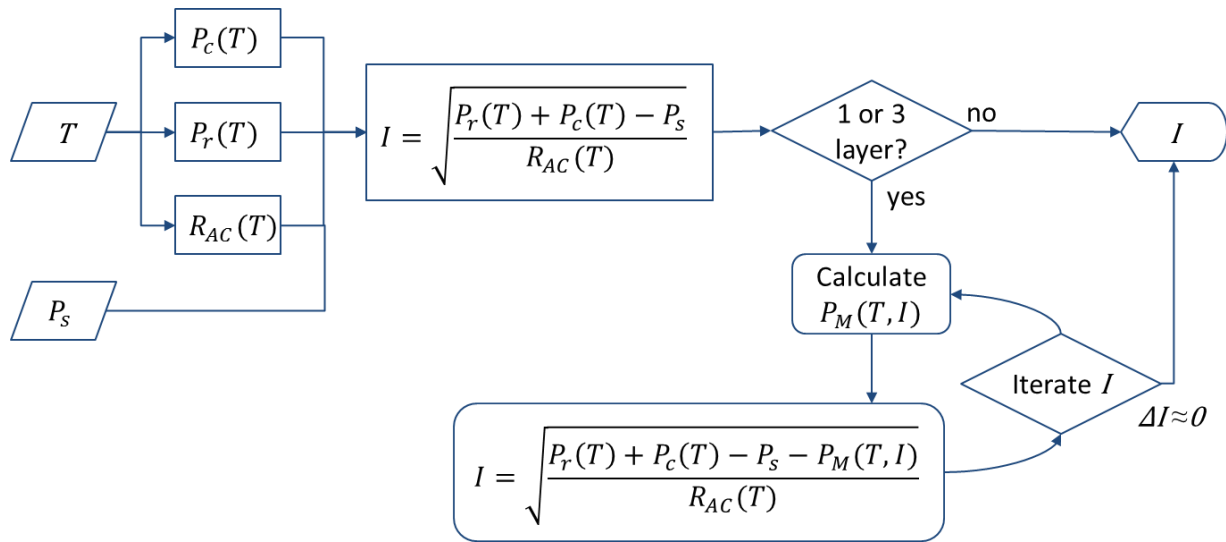


Figure 9: Flow chart for the steady state current calculation algorithm.

Given constant weather parameters (wind speed, wind direction, ambient temperature and solar radiation), the first step is to calculate P_c , P_r and the electrical resistance, R_{ac} , for the known conductor temperature. The current I can be calculated by rearranging the heat balance equation (eq. 2) and neglecting the magnetic losses or incorporating them into the conductor resistance, R_{ac} :

$$I = \sqrt{\frac{P_c(T) + P_r(T) - P_s}{R_{ac}(T)}} \quad (28)$$

In those cases where magnetic losses can be significant (1 or 3 layers with ferromagnetic core and high current densities), it may be necessary to calculate the line rating in an iterative way, adjusting for both conductor temperature and conductor current density. An example can be followed in Annex E.

It also may be necessary to check the radial temperature difference between the core and the conductor surface (see Section 3.4). If the difference is considerable, it may be necessary to reduce the ratings in order to avoid possible damages in the conductor. This is likely to happen at high current densities.

Steady state conductor temperature

In order to verify the conductor temperature T_{av} for a fixed current I and fixed (expected) weather conditions, it is possible to solve the following equation for T :

$$P_J(T, I) + P_M(T, I) + P_S - P_c(T) - P_r(T) = 0 \quad (29)$$

An iterative procedure is necessary, with the temperature T being adjusted each time round (see fig. 10). For the initial step, a first guess of the conductor temperature T is needed. If there are 1 or 3 layer and a ferromagnetic core with high current density, the magnetic losses P_M may have also to be calculated.

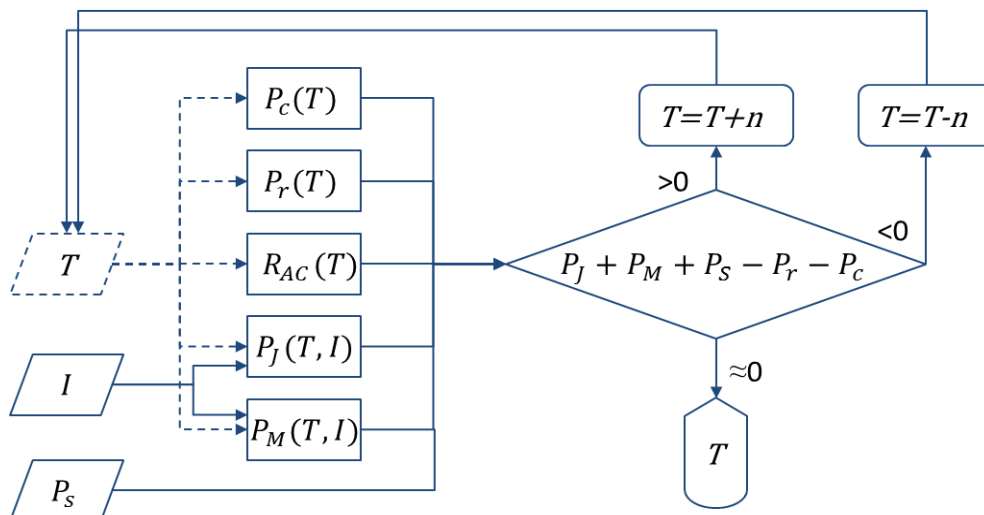


Figure 10: Flow chart for the steady state temperature calculation algorithm.

4.2. Numerical models for transient state

In many cases, it is necessary to determine the temperature of bare overhead line conductors more accurately in a continuously changing environment, to avoid violations of safety distances or possible damage to the materials due to high temperatures. In this regard, methods of monitoring overhead lines have undergone an important development [64]. These methods need to properly relate the changes of the different parameters and variables of an overhead line with time.

The change in temperature of an overhead conductor can be expressed by the following general equation (see Annex D for the details):

$$m \cdot c \cdot \frac{dT_{av}}{dt} = P_J + P_M + P_S - P_c - P_r \quad (30)$$

where m is the mass per unit length of the conductor ($\text{kg} \cdot \text{m}^{-1}$) and c the specific heat capacity of the conductor ($\text{J} \cdot \text{kg}^{-1} \cdot \text{K}^{-1}$). For non-ferrous conductors, $P_M = 0$, and for steel-cored conductors,

$$m \cdot c = m_a \cdot c_a + m_s \cdot c_s \quad (31)$$

where the subscripts a and s refer to the non-ferrous and ferrous sections of the conductor, respectively. Values for the mass density and the specific heat capacity of various conductor materials are given in Table 6. The mass density can be assumed constant up to 100°C , whereas the specific heat capacity varies significantly and can be assumed to rise linearly with temperature, for a moderate temperature rise, see eq. 32.

$$c(T) = c_{20} \cdot [1 + \beta_{20} \cdot (T - 20)] \quad (32)$$

Values for the specific heat capacity c_{20} and its temperature coefficient β_{20} at 20°C for various conductor materials are given in Table 6.

The Joule heat gain P_J varies quite linearly with T_{av} , (the skin effect factor k_{sk} has also a small non-linear dependency of the conductor temperature, as explained in Annex A), but is independent of any other ambient parameter. The magnetic heat gain P_M is zero for non-ferrous conductors, and can be usually neglected except for one or three aluminum layer steel-cored conductors subjected to high current densities. In these cases, it is dependent on the temperature of the conductor, the current and the tensile stress, and also independent of ambient conditions. The solar heat gain P_S depends basically on the global radiation intensity, whatever the current and conductor temperature. The radiative heat loss P_r is very non-linear

with the surface temperature T_s (forth power) and depends on the ambient temperature. The convective heat loss varies with the surface and ambient temperatures, T_s and T_a , and in forced convection with the wind speed and direction. In other words, the changes in the temperature of the conductor are motivated by the changes in the current through it, and the changes in the ambient parameters: wind speed and direction, ambient temperature and global radiation.

Time dependent heating or cooling. Temperature tracking algorithm

For planning emergency ratings, and for obtaining typical conductor time constants, there has been much study of step changes in current [1]. In such studies, the conductor temperature behaviour is evaluated after a sudden increase or decrease in current, keeping the ambient parameters constant (see fig. 11).

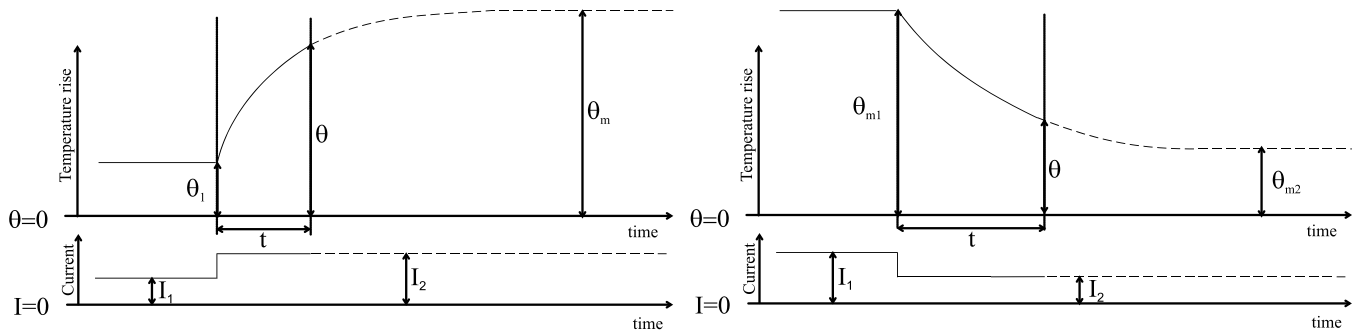


Figure 11: Variation of the conductor temperature with time following a step increase/decrease in current and considering the ambient parameters remain constant.

This is a particular case of a more general situation, where the possible changes of all the weather parameters (wind speed, wind direction, ambient temperature and global radiation) have to be considered. An analytical process to obtain the conductor temperature change produced by the increase/decrease of the different weather parameters and current can be followed in Annex D.

For dynamic ratings, the use of numerical methods is needed. A continuous on-line evaluation of conductor temperature is possible by computing the power terms of eq. 30 at a specific time interval, on the basis of the effective weather data obtained by means of real-time monitoring systems and the current flowing through the conductor. Such systems can provide values every 10–15 minutes, and measurements of current are usually also available for this interval of time. A simple numerical approach can be used: it can be assumed that these ambient conditions and current values are constant during this 10–15 minutes interval. Dividing this time interval into sufficiently small increments of time, and knowing or assuming

the initial value of T_{av} , the increment of conductor temperature T_{av} for every small increment of time can be obtained by solving eq. 30 like a simple linear equation. Repeating these calculations for all the small increments of time, we can obtain the final temperature T_{av} of the 10–15 minutes interval. This final value will be the starting value for the following 10–15 minutes interval, with new ambient and current values obtained from measurements. The resulting estimated conductor temperature can be plotted as a function of time. Note that the incremental intervals must be small compared with the conductor thermal time constant.

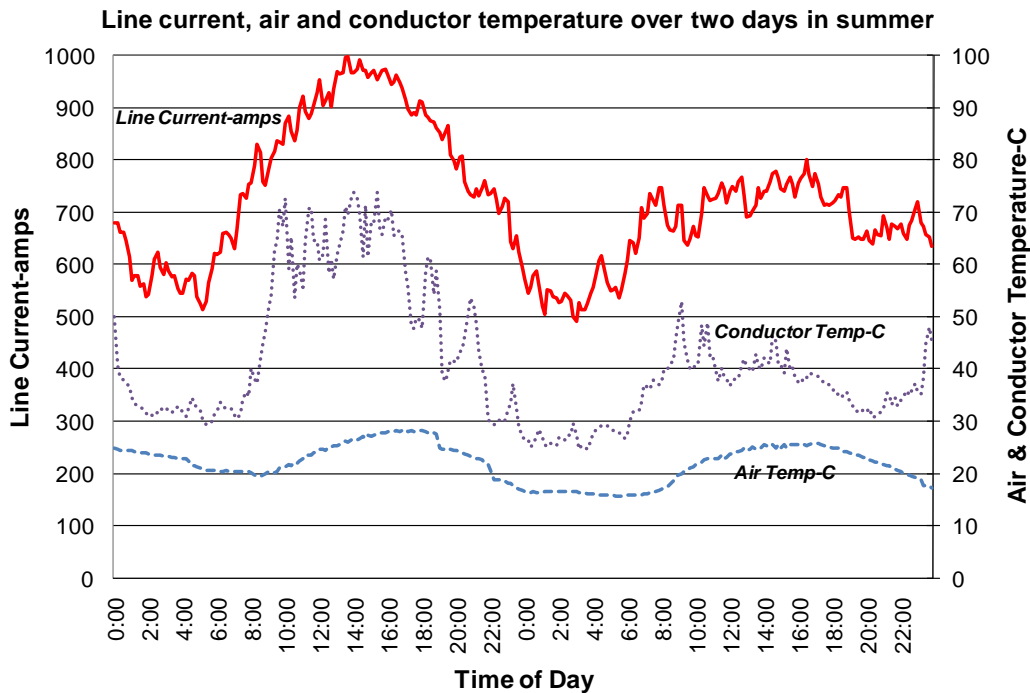


Figure 12: Example of conductor temperature calculated for specific time intervals, given time-varying current and weather conditions [4].

The examples in Annex E illustrate this method with real cases. It should be noted that, in real applications, the input data often have more importance than the calculation methods (see Section 5). The use of proper weather measurements is the key factor and each particular case must be studied in detail to take into account the differences along the line and during time. If the conductors are running at high temperatures, the relationship between the surface and core temperature also has to be considered [77], because the errors can be considerable (see Section 3.4).

Some dynamic rating systems compare the calculated temperature with a real-time measured temperature (or derived from other measured parameters) for every time step, allowing the

adjustment of parameters in order to minimize errors or improve numerical results when predicting line needs for each particular case.

Weather and line current are typically averaged over time intervals of 5 to 15 minutes in making such calculations. The determination of average effective wind speed for an overhead conductor over such intervals can be challenging if the wind speed and direction change rapidly.

With modern computers, there is no difficulty in keeping the numerical calculation interval much shorter than the data averaging interval. Test calculations can be run to determine the most accurate time interval for numerical calculations but a calculation every minute is typically adequate to produce accurate results.

Adiabatic state. Fault current rating

Another particular case of the general model for transient state is the so-called adiabatic state or fault rating calculation. In effect, in this case, a large current flows through the conductor in a short interval of time (fault current). It is assumed that the ambient conditions do not modify the conductor temperature during this time, and therefore the increment of the conductor temperature is due only to the current. The general eq. 30 for transient state can therefore be simplified in the following way:

$$m \cdot c \cdot \frac{dT_{av}}{dt} = P_J \quad (33)$$

The equations to evaluate the conductor temperature in a fault current situation are detailed in Annex D, as well as values of permissible short-time withstand current for a given conductor.

For adiabatic “fault current” calculations with bare overhead conductors, the calculation time interval should be kept short, possibly 1 to 10 seconds to assure adequate accuracy.

Section 5. Input data and sensitivity studies

The use of proper input data for the thermal rating calculations of overhead lines is critical. Not only the weather parameters (wind speed, wind direction, ambient temperature and global radiation), but also the conductor parameters (resistance, emissivity, absorptivity) and geometry (solar angles, height) have to be considered. In many cases, considerable engineering judgment is needed to apply the appropriate values to the model in order to get reliable results. For example, the accurate specification of wind speed and direction to determine the convective cooling of a conductor along the line may require a specific study.

For steady state situations, fixed weather and conductor parameters are assumed in order to calculate the maximum expected ratings or conductor temperatures. These parameters have to be selected carefully, with safe assumptions, and taking into consideration that some of the most important are highly correlated. The Cigré Technical Brochure 299 [5] is a guide to selection of appropriate values both for steady state and transient state situations. Some correlations between pairs of parameters can be found in [29].

For dynamic rating applications, the steady state model cannot be used as the heat capacity of the conductor has to be considered. Otherwise, sudden variations of the current or the weather conditions would lead to unrealistically large temperature variations (see Annex E). Generally, these dynamic applications require a more accurate determination of the conductor temperature, as they are used to operate the line close to its thermal limit. So the input parameters for the calculations are of great importance and have to be reliable. There is a great variability of the weather parameters along the line and with time (especially the wind speed and direction), so the way of getting these data and their use need careful consideration [64]. Some new methods, like probabilistic approaches, may need to be developed in order to adjust the local weather measurements and apply them to the whole system, as “effective weather parameters” for a section or a line, for example.

One of the most important uncertainties introduced in the dynamic rating calculations is the consideration of the different ambient parameter values for a period of time. Usually, the meteorological stations provide average values for 10–20 minutes intervals, which can introduce considerable errors, particularly with the wind.

In general, most of the heat supplied to overhead conductors is caused by the current (Joule heating), and convection is the most important source of cooling. Sensitivity studies of the effect of the different variables on the steady state rating of an ACSR conductor can be found in [48]. Also, probability density functions for the main weather parameters are given in [29,

69, 70]. The following figure shows examples of conductor heating and cooling percentage variation with the wind speed.

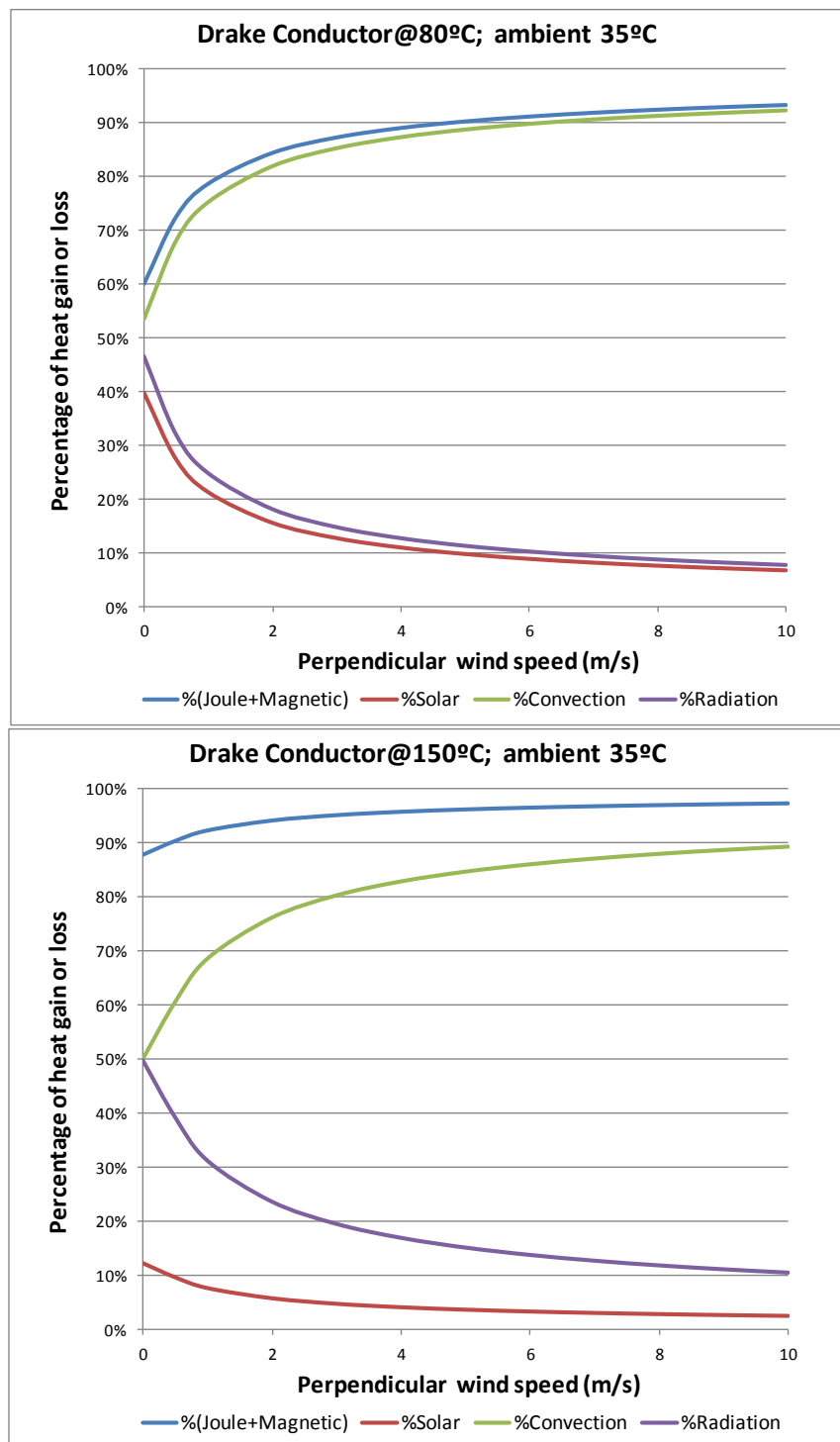


Figure 13: Examples of the percentage variation of heat gain and loss with the wind speed for a “Drake” ACSR conductor at 80 °C and 150°C.

In the vast majority of the cases, the errors introduced by some of the approximate calculations mentioned in this guide have less importance than, for example, the errors that can produce a bad estimation of the wind speed and direction along the line. For example, the error introduced when estimating the ac resistance by linear interpolation compared to measured values of an ACSR “Drake” conductor at 100°C can be in the order of 1%. This can give a difference in rating of around 0.5%, which is much less than other approximations. However, it has to be noted that extrapolating resistance values for high temperatures based on measurements at low temperatures can introduce greater errors which may have an impact on the rating calculations.

The magnetic heating effect is usually negligible. It can only have a relevant impact on the ac resistance when considering steel-cored conductors with one or three aluminum layers and high current densities. For example, a 3 Al-layer ACSR “Grackle” conductor (considered in the example of Annex B), running at 1500 A and 80°C produces a magnetic heating of approximately 10 W/m. The Joule heating in this case is around 130 W/m.

References

- [1] CIGRE, Paris, “Thermal behaviour of overhead conductors”, Technical Brochure 207, August 2002.
- [2] CIGRE, Paris, “Sag-Tension calculation methods for overhead lines”, Technical Brochure 324, June 2007.
- [3] CIGRE, Paris, “Conductors for the uprating of overhead lines”, Technical Brochure 244, April 2004.
- [4] IEEE Std 738–2012, “IEEE Standard for Calculating the Current–Temperature Relationship of Bare Overhead Conductors”. October 2012.
- [5] CIGRE, Paris, “Guide for the selection of weather parameters for bare overhead conductor ratings”, Technical Brochure 299, August 2006.
- [6] N.P. Schmidt, “Comparison between IEEE and CIGRE ampacity standards”, IEEE Trans. on Power Delivery, Vol. 14, No. 4, pp. 1555–1559, October 1999.
- [7] H.B. Dwight, “Electrical Coils and Conductors”, McGraw–Hill, New York 1945.
- [8] J. Zaborszky, “Skin and spiralling effect in stranded conductors”, AIEE Trans., Vol. 72, pp. 599–603, 1953.
- [9] M. Abramowitz and L.A. Stegun, “Handbook of Mathematical Functions”, Dover, New York, 1964.
- [10] A.W. Ewan, “A set of curves for skin effect in isolated tubular conductors”, General Electric Review, Vol. 33, pp.249–251, 1930.
- [11] V.T. Morgan, B. Zhang and R.D. Findlay, “Effects of temperature and tensile stress on the magnetic properties of a steel core from an ACSR conductor”, IEEE Trans. on Power Delivery, Vol. 11, No. 4, pp. 1907–1913, October 1996.
- [12] J.S. Barrett, O. Nigol, C.J. Fehervari and R.D. Findlay, “A new model of AC resistance in ACSR conductors”, IEEE Trans. on Power Delivery, Vol. 1, No. , pp. 198–208, April 1986.
- [13] V.T. Morgan, B. Zhang and R.D. Findlay, “Effect of magnetic induction in steel-cored conductors on current distribution and power loss”, IEEE Trans. on Power Delivery, Vol. 12, No. 3, pp. 1299–1308, July 1997.

- [14] L. Varga, "Determination of the current distribution and current load of overhead line conductors", *Acta Technica Acad. Sci. Hung.*, Vol. 105, No. 1–2, pp. 117–128, 1993.
- [15] O. Guntner and Danyek, "Computer-aided design of optimized stranded conductors", *Acta Technica Acad. Sci. Hung.*, Vol. 105, No. 1–2, pp. 19–40, 1993.
- [16] CIGRE, Paris, "Alternating current resistance of helically stranded conductors", Technical Brochure 345, April 2008.
- [17] W.S. Rigdon, H.E. House, R.J. Grosh and W.B. Cottingham, "Emissivity of weathered conductors in service in rural and industrial environments", *Trans. AIEE*, Vol. 82, pp. 891–896, 1963.
- [18] V.T. Morgan, "The radial temperature distribution and effective radial thermal conductivity in bare solid and stranded conductors", *IEEE Trans. on Power Delivery*, Vol. 5, pp. 1443–1452, July 1990.
- [19] V.T. Morgan, "The thermal rating of overhead line conductors, Part 1– the steady state thermal model", *Electric Power Systems Research*, pp. 119–139, 1982.
- [20] D.A. Douglass, "Radial and axial temperature gradients in bare stranded conductor", *IEEE Trans. on Power Delivery*, Vol. 1, No. 2, pp. 7–15, April 1986.
- [21] L. Varga, "Measurement of the radial thermal conductivity of overhead line conductors", *Elektrotechnika*, Vol. 33, No. 2, pp. 68–71, 1990.
- [22] V.T. Morgan and R.D. Findlay, "The effects of axial tension and reduced air pressure on the radial temperature gradient in stranded conductors", *IEEE Trans. on Power Delivery*, Vol. 8, No. 2, pp. 553–558, April 1993.
- [23] V. T. Morgan, "Rating of bare overhead conductors for continuous currents", *Proc. IEE (Lond)*, Vol. 114, pp. 1473–1482, 1967.
- [24] G. Brunello, "Nombre de Prandtl de l'air humide", *J. Rech. CNRS*, No. 55, pp. 179–181, 1961.
- [25] V.T. Morgan, "The heat transfer from bare stranded conductors by natural and forced convection in air", *Inter. J. Heat Mass Transfer*, Vol. 16, pp. 2022–2034, 1973.
- [26] W.H. McAdams, "Heat Transmission", McGraw-Hill, New York, 1954.

- [27] R.M. Fand and K.K. Keswani, "A continuous correlation equation for heat transfer from cylinders to air in crossflow for Reynolds numbers from 10^{-2} to 2×10^5 ", *Inter. J. Heat Mass Transfer*, Vol. 15, No. 3, pp. 559–562, 1972.
- [28] A.B.Wang and Z. Travnicek. "The linear heat transfer correlation of a heated circular cylinder in laminar crossflow using a new representative temperature concept", *Inter. J. Heat Mass Transfer*, Vol. 44, pp. 4635–4647, 2001.
- [29] V.T. Morgan, "Thermal Behaviour of Electrical Conductors, Steady, Dynamic and Fault-Current Ratings", Research Studies Press, John Wiley & Sons, New York, 1991.
- [30] M.W. Davis, "A new thermal rating approach: the real-time thermal rating system. Part 2, steady-state thermal rating system", *Trans. IEEE Power Apparatus and Systems*, Vol. 96, pp. 810–825, 1977.
- [31] F.P. Kazakevich, "Effect of the angle of incidence of a gas stream on the heat transfer from a circular cylinder", *Zhur. Tekh. Fiz.*, Vol. 24, pp. 1341–1347, 1954.
- [32] V.T. Morgan, "The current-carrying capacity of bare overhead conductors", *Institution of Engineers, Australia, Electrical Engineering Trans.*, Vol. EE4, pp. 63–72, 1968.
- [33] M. Isozaki, H. Haji, K. Nagano and N. Iwama, "Verification of forced convective cooling from overhead conductors in low velocity by wind tunnel testing", *Trans. Institute Electrical Engineers of Japan B*, Vol. 121B, No. 6, pp. 782–788, 2001.
- [34] N. Hattori and J. Kimura, "Forced-convection heat transfer from yawed circular cylinder to air", *Heat Transfer-Japanese Research*, Vol. 22, No. 8, pp. 828–837, 1993.
- [35] S.B. Clemes, K.G.T. Hollands and A.P. Brunger, "Natural convection heat transfer from long isothermal cylinders", *ASME J. Heat Transfer*, Vol. 116, pp. 96–104, 1994.
- [36] S.W. Churchill and H.H.S. Chu, "Correlating equations for laminar and turbulent free convection from a horizontal cylinder", *Inter. J. Heat Mass Transfer*, Vol. 18, pp. 1049–1053, 1975.
- [37] T.H. Kuehn and R.J. Goldstein, "Correlating equations for natural convection heat transfer between horizontal circular cylinders", *Inter. J. Heat Mass Transfer*, Vol. 19, pp. 1127–1134, 1976.
- [38] V.T. Morgan, "The overall convective heat transfer from smooth circular cylinders", *Advances in Heat Transfer*, Vol. 11, pp. 199–264, Academic Press, New York, 1975.

- [39] V.T. Morgan, "Rating of bare overhead conductors for intermittent and cyclic currents", Proc. IEE (Lond), Vol. 116, No. 8, pp. 1361–1376, August 1969.
- [40] V.T. Morgan, "Rating of conductors for short-duration currents", Proc. IEE (Lond), Vol. 118, No. 3–4, pp. 555–570, March/April 1971.
- [41] J. Reichmann, M.Vainberg and J.Kuffel, "Short-circuit capacity of temporary grounding cables", IEEE Trans. on Power Delivery, Vol. 4, No. 1, pp. 269–271, January 1989.
- [42] International Standard IEC 60865, "Short-circuit currents–calculation of effects", 1993.
- [43] International Standard IEC 60889, "Hard-drawn aluminum wire for overhead lines", 1987.
- [44] International Standard IEC 60104, "Aluminum–magnesium–silicon alloy wire for overhead line conductors", 1987.
- [45] International Standard IEC 60888, "Zinc-coated steel wires for stranded conductors", 1987.
- [46] International Standard IEC 61232, "Aluminium-clad steel wires for electrical purposes", 1993.
- [47] F. Jakl and A. Jakl, "Investigation of temperature rise of ACSR conductors and OPGW under short-circuit conditions", CIGRE SC 22 WG 12, Meeting No. 15, Nice, 22–23 August 1996.
- [48] V.T. Morgan, "The thermal rating of overhead–line conductors, Part 2", Electric Power Systems Research, Vol. 6, pp. 287–300, 1983.
- [49] Southwire Company, "Overhead Conductor Manual, 2nd Edition", Carrollton GA (Ed. Ridley Thrash), 2007.
- [50] J. Iglesias, S. Fernandez de Sevilla "Analysis of Convection Models for Overhead Lines. Application to Dynamic Thermal Rating Systems for Integrating Renewable Energy", Cigré Paper 346, International Symposium Auckland, September 2013.
- [51] O. Güntner, "The effect of the uneven current distribution within the aluminum layers on the energy losses of ACSR OHL conductors". Dissertation, Technical University of Vienna. 1989.
- [52] F. Jakl, M. Zunec, A. Jakl, M. Krasna, "Adiabatic Heating of Bare Conductors of Overhead Transmission Lines with Consideration of Temperature Dependent Physical Magnitudes",

10th International Symposium Short-Circuit Currents in Power Systems, Lodz/Poland, October 28–29, 2002.

- [53] M. Zunec, I. Ticar, F. Jakl, “Determination of Current and Temperature Distribution in Overhead Conductors by Using Electromagnetic-Field Analysis Tools”. IEEE Trans. on Power Delivery, Vol. 21, NO. 3, July 2006.
- [54] Shelley L. Chen, W.Z. Black and H.W. Loard, “High-Temperature Ampacity Model for Overhead Conductors”, IEEE Trans. on Power Delivery, Vol. 17, No. 4, pp. 1136–1141, October 2002.
- [55] R.Hilpert, “Warmeabgabe von geheizten Drahten und Rohren im Luftstrom”, Forsch. Ing. Wes. Vol. 4, p. 215, 1933.
- [56] Alcoa Aluminum Overhead Conductor Engineering Data, “Resistance and Reactance of Aluminum Conductors”, 1960.
- [57] D.A. Douglass, B. Clairmont, J. Iglesias, Z. Peter. “Radial and Longitudinal Temperature Gradients in Bare Stranded Conductors with High Current Densities”, Cigré Paper B2–108, Paris, August 2012.
- [58] F.W. Grover, “Inductance calculations”, Dover Publications, 2004.
- [59] R.G. Wylie and T. Lalas, “Confirmation and interpretation of a kink in the Nu (Re) plot for a cylinder in a transverse stream”, Proc. Second Australasian Conf. on Heat and Mass Transfer, Sydney, pp. 273–278, 1977.
- [60] V.T. Morgan and C.F. Price, “Magnetic properties in axial 50 Hz fields of steel core wire for overhead conductors”, Proc. IEE, Vol. 116, No. 10, pp. 1681–1694, 1969.
- [61] W.A. Chisholm, J.S. Barrett. “Ampacity Studies on 49°C-Rated Transmission Line”, IEEE Trans. on Power Delivery, Vol. 4, No. 2, April 1989.
- [62] CIGRE, Paris, “Guide for Qualifying High Temperature Conductors for Use on Overhead Transmission Lines”, Technical Brochure 426, August 2010.
- [63] S. Kitamura, K. Nagano, Y. Terao “Wind Tunnel Equipment for Inspection of Conductor Radiation in Breeze”, Trans. Institute Electrical Engineers of Japan, 2001.
- [64] CIGRE, Paris, “Guide for Application of Direct Real-Time Monitoring Systems”, Technical Brochure 498, June 2012.

- [65] CIGRE, Paris, "Systems for Prediction and Monitoring of Ice Shedding, Anti-Icing and De-Icing for Overhead Power Line Conductors and Groundwires", Technical Brochure 438, December 2010.
- [66] M.R. Sharma and R.S. Paul, "Total, direct and diffuse solar radiation in the tropics", Solar Energy, Vol. 9, pp. 183–192, 1965.
- [67] A.B. Meinel and M.P. Meinel, "Applied Solar Energy. An Introduction", Addison Wesley, New York, 1976.
- [68] J.W. Spencer, "Calculation of solar position for building purposes", CSIRO Australia Division of Building Research, Technical Paper No. 14, 1965.
- [69] V.T. Morgan, "Statistical distribution of diffuse, beam and global solar irradiances in Sydney, Australia", Renewable Energy, Vol. 2, No. 6, pp. 607–610, 1992.
- [70] V.T. Morgan, "Statistical distributions of wind parameters at Sydney, Australia", Renewable Energy, Vol. 6, No. 1, pp. 39–47.
- [71] F. Jakl, A. Jakl, "Effect of Elevated Temperatures on Mechanical Properties of Overhead Conductors Under Steady State and Short-Circuit Conditions", IEEE Transactions on Power Delivery, Vol. 15, No. 1, pp. 242–246, January 2000.
- [72] H.E. House, P.D. Tuttle, "Current Carrying Capacity of ACSR". AIEE Winter General Meeting, Paper 58–41. New York, 1958.
- [73] S. Hoffmann, "The use of weather predictions to enhance overhead line ratings". Cigré Paper B2–5, Edinburgh, September 2003.
- [74] M.W. Davis, "Nomographic computation of the ampacity rating of aerial conductors". Trans. IEEE on Power Apparatus and Systems, Vol. 89, no. 3, March 1970.
- [75] J.H. Lienhard IV and V, "Heat transfer textbook" 3rd ed. Phlogiston press, Cambridge, Massachusetts, 2008.
- [76] M. Kang, M. Strobach and C. M. Franck, "Radial temperature distribution of AAAC overhead line in stationary and transient conditions". 18th International Symposium on High Voltage Engineering, Seoul, August 2013
- [77] M. Strobach, U. Straumann and C. M. Franck, "Smart Energy Transmission: Dynamic Thermal Rating". Institute for Electric Power Systems and High Voltage Technology of ETH Zürich, 2013.

Annex A. Analytical calculation of conductor resistance

The resistance values of overhead conductors, both for ac and dc operation, are usually available in the literature and can be provided with enough accuracy for rating purposes by manufacturers. This annex provides analytical tools to calculate these values if they cannot be obtained by other means. A more detailed explanation can be followed in TB 345 [16].

A.1. DC resistance

The dc resistance per unit length R_{dc} of a conductor depends on the resistivity of the materials ρ ($\Omega \cdot m$) at the temperature considered, the cross-sectional area A (m^2) and the mean temperature of the conductor T_{av} ($^{\circ}C$). The resistivity of a material at any temperature T_{av} can be expressed as follows:

$$\rho = \rho_{20} \cdot [1 + \alpha_{20} \cdot (T_{av} - 20) + \zeta_{20} \cdot (T_{av} - 20)^2] \quad (34)$$

where ρ_{20} , α_{20} and ζ_{20} are the resistivity and its linear and quadratic temperature coefficients ($1/K$ and $1/K^2$) at $20^{\circ}C$. The quadratic term only becomes significant at temperatures higher than about $130^{\circ}C$. See Table 6.

a) For a solid cylindrical non-ferrous conductor,

$$R_{dc} = \frac{\rho}{A} = \frac{4 \cdot \rho}{\pi \cdot D^2} \quad (35)$$

where D is the overall diameter of the conductor (m) and ρ the resistivity of the material at the temperature considered ($\Omega \cdot m$).

b) For a solid tubular non-ferrous conductor,

$$R_{dc} = \frac{4 \cdot \rho}{\pi \cdot (D^2 - D_1^2)} \quad (36)$$

where D_1 is the inner diameter, D is the outer diameter (m) and ρ the resistivity of the material at the temperature considered ($\Omega \cdot m$).

c) For a stranded homogeneous conductor (like AAC and AAAC conductors), the conductance per unit length of each layer is given by:

$$\frac{1}{R_{z(dc)}} = \frac{\pi \cdot d_z \cdot n_z}{4 \cdot \rho_z \cdot K_z} \quad (37)$$

where d_z is the diameter of each wire (m), n_z is the number of wires in layer z , and K_z is found from:

$$K_z = \sqrt{1 + \left(\frac{\pi \cdot D_z}{l_z}\right)^2} \quad (38)$$

where D_z is the mean diameter of layer z (m) and l_z is the lay length of the wires in layer z (m). Hence, the conductance of the whole conductor is found from:

$$\frac{1}{R_{dc}} = \frac{\pi \cdot d_z^2}{4 \cdot \rho} \left(1 + \sum_1^m \frac{6 \cdot z}{K_z}\right) \quad (39)$$

where m is the number of layers and ρ the resistivity of the material at the temperature considered ($\Omega \cdot \text{m}$).

d) For a stranded steel-cored conductor having the same strand diameter in all its layers, the total conductance per unit length is given by:

$$\frac{1}{R_{dc}} = \frac{1}{R_s} + \frac{1}{R_a} = \frac{\pi \cdot d_s^2}{4 \cdot \rho_s} \left(1 + \sum_1^{m_s} \frac{6 \cdot z_s}{K_{zs}}\right) + \frac{\pi \cdot d_a^2}{4 \cdot \rho_a} \left(\sum_{m_s+1}^{m_a} \frac{6 \cdot z_a}{K_{za}}\right) \quad (40)$$

where m_a is the number of layers of non-ferrous wires, m_s is the number of layers of ferrous wires; ρ_a is the resistivity of the non-ferrous material at the temperature considered ($\Omega \cdot \text{m}$), ρ_s is the resistivity of the ferrous material at the temperature considered ($\Omega \cdot \text{m}$). Note this eq. is only valid when the aluminum and steel strands have the same diameter (for example, it does not work for 30/19 or 26/7 ACSR).

In a similar way, the analytical values of dc resistance per unit length for other constructions (gapped conductors, trapezoidal wires, etc.) can be obtained.

Material	γ kg/m ³	c J/kg·K	β 1/K	ρ_{dc} nΩ·m	α 1/K	ζ 1/K ²	λ_a W/m·K
Aluminium	2703	897	3.8×10^{-4}	28.264	4.03×10^{-3}	8×10^{-7}	240
Aluminium alloy	2703	909	4.5×10^{-4}	32.7	3.6×10^{-3}	8×10^{-7}	210
Copper	8890	383	3.35×10^{-4}	17.241	3.9×10^{-3}	5×10^{-8}	400
Galvanized Steel	7780	481	1.0×10^{-4}	287.36 (*) 191.57 (**) 215.5 (***)	4.5×10^{-3}	6×10^{-6}	24
Aluminium-clad steel	(1)	(2)					

20 SA	6590	518	1.4×10^{-4}	84.80	3.6×10^{-3}		80
27 SA	5910	551	1.4×10^{-4}	63.86	3.6×10^{-3}		110
30 SA	5610	566	1.4×10^{-4}	57.47	3.8×10^{-3}		120
40 SA	4640	630	1.4×10^{-4}	43.10	4.0×10^{-3}		160
Thermal-resistant Aluminium alloy							
AT1 (TAL)	2703			28.735	4.0×10^{-3}		
AT2 (KTAL)	2703			31.347	3.6×10^{-3}		
AT3 (ZTAL)	2703			28.735	4.0×10^{-3}		
AT4	2703			29.726	3.8×10^{-3}		
HACIN							
14SA	6935			123.153			
17SA	6715			102.160			
24SA	6055			72.029			
CFCC	1900	638	4.08×10^{-3}	–	–	–	–

Table 6: Typical data for conductor materials at 20 °C [43–46].

(*) Based on 6 % IACS conductivity; (**) Based on 9 % IACS conductivity; (***) Based on 8 % IACS conductivity.

$$(1): \gamma = \frac{\gamma_a \cdot A_a + \gamma_s \cdot A_s}{A_a + A_s}$$

$$(2): c = \frac{c_a \cdot \gamma_a \cdot A_a + c_s \cdot \gamma_s \cdot A_s}{\gamma_a \cdot A_a + \gamma_s \cdot A_s}$$

Resistivity versus temperature relationships up to 400° C for several conductor materials are given in [54].

A.2. AC resistance (skin effect)

The skin effect factor k_{sk} is defined as the ratio between the ac and dc resistances. According to the model used in the TB 345 [16], for a homogeneous conductor, or stranded non-ferrous conductor, or conductors with ferromagnetic material in their core and uneven number of strands, the equations to obtain the skin effect factor are described below.

The electric field per unit value of current E/I is a complex number, whose real part can be written as:

$$(E/I)_R = \text{Real} \left[\frac{\rho \cdot (1 - i)}{D \cdot \pi \cdot \delta} \cdot \left(\frac{J_0}{J_1} \right) \right] \quad (41)$$

where,

D is the diameter of a homogeneous conductor, or the outer diameter of a tubular conductor (m).

δ is the skin depth (m)

J_0 is the Bessel function first kind and 0 order.

J_1 is the Bessel function first kind and 1 order.

ρ is the resistivity of the material ($\Omega \cdot \text{m}$)

The skin depth, δ , or depth of propagation, is defined as a depth at which the current density has fallen to $1/e$ or $\approx 37\%$ of its value at the surface. It is given by:

$$\delta = \sqrt{\frac{\rho}{4 \cdot f \cdot \pi^2 \cdot \mu_r \cdot 10^{-7}}} = 503.3 \cdot \sqrt{\frac{\rho}{f \cdot \mu_r}} \quad (42)$$

where,

f is the frequency

μ_r is the relative permeability of the conductor material (≈ 1 for aluminium). Calculation with relative permeability $\mu_r > 1.0$ is necessary only when the skin effect of the steel core is being calculated separately, and then ac resistance of an ACSR conductor is found as a result of parallel $R_{ac(Al)}$ and $R_{ac(St)}$.

A general expression of Bessel function of any order is:

$$J_n = x^n \cdot \sum \left[\frac{(-1)^m \cdot x^{2m}}{2^{2m+n} \cdot m! \cdot (m+n)!} \right] \quad (43)$$

where,

$m = 0 \dots \infty$

n is the order of the Bessel function; here 0 for J_0 and 1 for J_1 .

x is the variable of the Bessel function; here:

$$x = \frac{(1-i) \cdot D}{2 \cdot \delta} \quad (44)$$

In our case, for power frequency range and for the range of conductors used for overhead lines, the expression can be simplified with sufficient accuracy as:

$$J_0(x) = \left[1 - \left(\frac{x}{2}\right)^2 + \frac{1}{4} \cdot \left(\frac{x}{2}\right)^4 - \frac{1}{36} \cdot \left(\frac{x}{2}\right)^6 \right] \quad (45)$$

and:

$$J_1(x) = \left[\frac{x}{2} - \frac{1}{2} \cdot \left(\frac{x}{2}\right)^3 + \frac{1}{12} \cdot \left(\frac{x}{2}\right)^5 - \frac{1}{144} \cdot \left(\frac{x}{2}\right)^7 \right] \quad (46)$$

Using the expressions as above, the calculation seems to be simple enough and straightforward for any application. The only apparent difficulty might be having to deal with complex numbers. However, ignoring it in a model like this, the calculation of ac resistance values will give wrong results.

The skin effect factor can be written as follows [16]:

$$k_{sk} = \frac{D^2 \cdot \pi \cdot (E/I)_R}{4 \cdot \rho} \quad (47)$$

In calculation of skin effect of tubular conductor or tube which represents a conductive part of ACSR and similar conductor, the skin effect will be the result of the ratio between calculations of electric field for outer and inner diameter of tube and can be calculated as follows:

$$k_{sk(tube)} \approx 1 + (k_{sk(D)} - 1) \cdot \left(1 - \frac{D_1}{D}\right) \quad (48)$$

where D_1 is the inner diameter of a tubular conductor or the outer diameter of the steel core in ACSR and similar conductors.

A graphical expression of skin effect as a function of the outer conductor radius and the ratio between inner and outer diameter of the tube ($D_1/D = r_{in}/r_{ou}$) can be seen in fig. 3 of Section 3. This graphical presentation, similar to those found in the literature ([49], for example), has its advantage for checking that the results are in the expected range, but it is not recommended to use for calculation of the skin effect, because of unavoidable errors. For any calculation of the ampacity, it is much more appropriate to use formulae, as described above.

The results as presented above, suggest, amongst other things, that the best solution to calculating the skin effect for any conductor, including ACSR type, is to assume a solid conductor, with diameter equivalent to the diameter of outer layer and with the total resistance of conductor, including steel core, if applied. The next step, for stranded conductors, is to calculate the same, but for the assumption that the radius of the conductor is equivalent to the Geometric Mean Radius (GMR).

The Geometric Mean Radius represents the radius of a homogeneous conductor with equivalent inductance. Values, in relationship to outer radius of (stranded) conductor are regularly given in catalogues or handbooks, for specific conductor. In absence of that, it can be calculated using a general formula:

$$GMR = \sqrt[N^2]{\sum_{n=1}^N \left(\sum_{m=1}^N d_{k,m} \right)} \quad (49)$$

where:

$d_{k,m}$ is the distance between strands/wires, for $k \neq m$ or r' for $k = m$.

$$r' = e^{-1/4} \cdot r$$

r is the radius of the conductor

The maximum possible deviation from what might be considered as accurate result, is in the region of 1 to 2 % of the resistance of the conductor, and is governed mostly by neglecting the skin effect in the steel core.

Some example values are shown in the following table:

Code Name	Conductor Construction	Max. dc resistance at 20°C (Ω/km)	Conductor Radius (mm)	Skin Effect at 50Hz	GMR (mm)	Skin Effect at 50Hz, using GMR
"Iris"	AAC 7x2.47	0.8577	3.7084	1.0002	2.6914	1.0001
"Laurel"	AAC 19x3.01	0.2133	7.5311	1.0033	5.6998	1.0011
"Goldentuft"	AAC 19x3.91	0.1264	9.7663	1.0092	7.4188	1.0031
"Lilac"	AAC 61x2.90	0.0715	13.0556	1.0287	10.089	1.0104
"Camellia"	AAC 61x3.25	0.0569	14.6304	1.0445	11.308	1.0163
"Coreopsis"	AAC 61x4.10	0.0358	18.4658	1.106	14.265	1.0404
"Lupine"	AAC 91x4.21	0.0230	23.1140	1.2292	16.551	1.0709
"BlueBonnet"	AAC 127x4.22	0.0166	27.4066	1.3904	21.245	1.1732

Table 7: Examples of skin effect for some conductors.

Annex B. Analytical calculation of magnetic heating

For the majority of the cases, the magnetic effects in overhead conductors are negligible. In general, they are included in the published ac resistance values. If these values are not available, the present annex describe a simplified analytical method for calculating the magnetic heating, which is required only for high current densities in steel-cored conductors with an uneven number of conductive layers, in practice only one or three. A detailed method of calculation is described in the TB 345 [16].

The magnetic heating, as presented here, has two components. One is related to the heat gain in the steel core due to the effects of the magnetic field in ferromagnetic material (P_{core}), and another is related to the heat gain due to the redistribution of the current densities in the non-ferrous layers (P_{redis}). In that regard, the magnetic heating, P_M , is a sum of P_{core} and P_{redis} .

B.1. Heat gain in the steel core

The magnetic heat gain of a steel-cored conductor per unit length, P_{core} (W/m), is caused by the alternating currents in the layers of non-ferrous wires spiraling around the core, producing an alternating axial magnetic flux in the core. This flux results in power being dissipated in the steel as a result of eddy currents, magnetic hysteresis and magnetic viscosity.

The heat gain by the core due to magnetic viscosity is usually negligible. The heat gain due to eddy currents and magnetic hysteresis depends on the magnetic induction B (T) of the steel, which is determined by the peak value of the magnetic field strength H_{max} (A/m) and the modulus of the relative permeability μ_r of the steel, which depends on the temperature and the tensile stress in the steel [11].

An experimentally determined equation for the core loss (W/m) in a steel core removed from a “Grackle” ACSR conductor [11] is given in eq. 50:

$$P_{core} = C \cdot A \cdot \gamma \cdot B_{max}^{1.83} \quad (50)$$

where A is the cross-sectional area (m²), B is the magnetic induction (T), γ is the mass density (kg/m³) of the steel core (see Table 6) and C is a constant, having the value of 45 at 25 °C, 290 MPa and 60 Hz. The value of C increases with increasing core temperature, and is equal to 61 at 120 °C, 290 MPa and 60 Hz. The core loss also reduces by about 10 % as the tensile stress increases from 0 MPa to 290 MPa at constant temperature and frequency. For a frequency f other than 60 Hz, the value of P_{core} in eq. 50 should be multiplied by $f/60$.

An alternative equation for the heat gain in the core, based on the heating in individual unstranded wires, is given by [60]:

$$P_{core}(W/kg) = 12.5 \cdot d^{1/2} \cdot f \cdot e^{(-2.5 \cdot 10^{-3} \cdot T_c)} \cdot B_{max}^{1.83} \quad (51)$$

or

$$P_{core}(W/m) = 12.5 \cdot d^{1/2} \cdot f \cdot A_s \cdot \gamma_s \cdot e^{(-2.5 \cdot 10^{-3} \cdot T_c)} \cdot B_{max}^{1.83} \quad (52)$$

where d is the diameter of the steel wire (m), f is the frequency (Hz), A_s is the cross-sectional area of the wire (m²), γ_s is the density of the wire (kg/m³) and T_c is the temperature of the wire (°C). The preforming of steel wires prior to stranding causes a reduction in the magnetic induction, and up to 30% reduction in the relative permeability and the loss tangent at high induction, due to the cold work in bending and twisting of the wires.

The magnetic induction is found from the following equation:

$$B_{max} = \mu_r \cdot \mu_0 \cdot H_{max} \quad (53)$$

where μ_r is the modulus of the relative permeability of the steel wires, $\mu_0 = 4 \cdot \pi \cdot 10^{-7}$ is the permeability of free space (H/m), and H_{max} (A/m) is given by:

$$H_{max} = \sum_{n=1}^p (-1)^{n+1} \frac{I_{n,max}}{l_n} \quad (54)$$

where n is the number of the non-ferrous layer ($n = 1$ for the innermost layer), p is the total number of non-ferrous layers, $I_{n,max}$ is the peak value of the current in layer n and l_n is the lay length (m) of the wires in layer n .

Applied numerical method

For 1 or 3 aluminum-layer conductors, the magnetic field strength can be calculated as follows:

$$H_{max} = \frac{I_{n,max}}{l_n} \quad (55)$$

where $I_{n,max}$ is the peak value of current equivalent to dc current, calculated for the appropriate layer (1 or 3).

For strands not adjacent to the steel core, as in the outer layer of a three-layer conductor, H_{max} has to be replaced by H_x :

$$H_x = H_{max} \cdot e^{\left(1 - \frac{x}{\delta}\right)} \quad (56)$$

where x is the distance between the steel core and the 3rd layer, and δ is the skin depth.

A relative permeability of steel core can be either calculated from interpolated curves, based on measurements of Barrett et al., as given in [12], or using results of measurements by Varga et al. [16], which led to polynomial approximation:

$$\mu_r = -9 \cdot 10^{-8} \cdot H_x^3 + 3 \cdot 10^{-4} \cdot H_x^2 - 11.05 \cdot 10^{-2} \cdot H_x + 6.2951 + i \cdot (-6 \cdot 10^{-8} \cdot H_x^3 + 2 \cdot 10^{-4} \cdot H_x^2 - 3.51 \cdot 10^{-2} \cdot H_x + 75.644) \quad (57)$$

The availability of different measurements of relative permeability gives the opportunity to update either the spreadsheet in [16] or the formula given above.

The relative permeability, μ_r , is a complex quantity with the real part given by $\text{Real}(\mu_r) = |\mu_r| \cdot \sin\theta$, and the imaginary part by $\text{Im}(\mu_r) = |\mu_r| \cdot \cos\theta$, where θ is the angle between the magnetizing current and the search coil voltage. Typical values of the peak-modulus $|\mu_r|$ for a steel core of a “Grackle” conductor are shown in fig. 14 as a function of temperature and tensile stress [11].

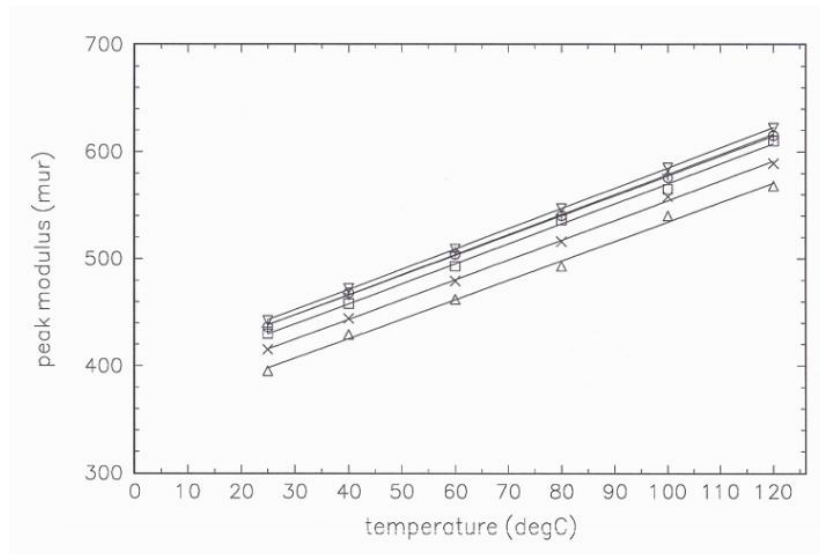


Figure 14: Variation of the peak modulus of the relative permeability of the steel core from a “Grackle” ACSR conductor with temperature and tensile stress [11]. 60 Hz, + 0 MPa, ▽ 58 MPa, o 116 MPa, □ 174 MPa, x 232 MPa, △ 290 MPa.

The simplest way of incorporating these findings is to introduce a temperature correction for relative permeability, which according to fig. 14 can approximately be:

$$\Delta\mu_r = 1.9 \cdot \Delta T \quad (58)$$

where ΔT is the difference between the temperature at which a peak value of permeability is recorded in laboratory measurement and the temperature of conductor at which a peak value is calculated, if this information is available. Otherwise, the result of μ_r should stay the same as calculated in eq. 57.

B.2. Heat gain due to redistribution of the current densities

In addition to magnetic hysteresis and eddy currents, the alternating magnetic field in a steel-cored conductor causes redistribution of the current densities in the non-ferrous layers, P_{redis} (W/m), also known as the transformer effect [12–15, 53]. This redistribution results in increased resistance and decreased internal inductance of the conductor, and depends on the frequency, the total current through the conductor, the temperature and tensile stress of the steel core, and the number of layers and the lay lengths and directions of the layers of the non-ferrous wires [16].

This component of magnetic heating is result of circular and longitudinal flux and its impact on the impedance of the conductor (fig. 15). While circular flux (of the non-ferrous layers) does not depend on the steel core properties, and is expressed here as skin effect, longitudinal flux and related reactance will depend on magnetic properties of steel core and is expressed here as transformer effect.

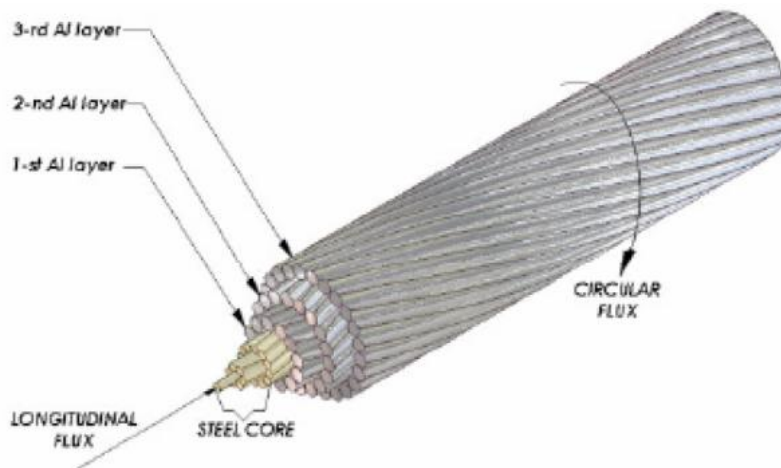


Figure 15: Longitudinal and flux of the non-ferrous layers in a steel-cored conductor.

A theoretical background of both and a simplification for single-layer assumption are presented below.

Note that in the Cigré Technical Brouchure 345 [16], the skin effect is included in the magnetic heating calculation. However, the skin effect, as presented in Annex A, does not have a direct relationship to the magnetic properties of the steel core, and the related increase in resistance of conductor should not be treated as component of magnetic heating. The same calculation described in Annex A applies for conductors with uneven number of non-ferrous layers.

The complex self-inductive reactance of the layer of aluminium wires, due to the longitudinal magnetic flux in the core, is calculated from:

$$X_{nn} = 2 \cdot \pi \cdot f \cdot \mu_0 \cdot \frac{\left(\frac{\pi}{4} \cdot D_n^2 - A_s\right) + \mu_r \cdot A_s}{l_n^2} \quad (59)$$

where:

f is the frequency

D_n is the mean diameter of layer n

l_n is the lay length of layer n

A_s is the cross-sectional area of the steel core

μ_r is the complex relative permeability of the core, and

μ_0 is the permeability of free space.

When the self inductance is calculated for a single-wire core, or with the assumption of replacing a stranded core with homogenous wire, then the following formula by FW Grover [58] can be used:

$$L = 200 \cdot \left[\ln \left(\frac{1}{k_D} \cdot \left(1 + \sqrt{1 + k_D^2} \right) \right) - \sqrt{1 + k_D^2} + \frac{|\mu_0 \cdot \mu_r|}{4} + k_D \right] \quad (60)$$

where

L is the self inductance (H/m)

$$k_D = 5 \cdot 10^{-4} \cdot D_1$$

D_1 is the steel core diameter

From eq. 59, the equivalent lay-length can be written:

$$l_s = \sqrt{\frac{\left[\mu_0 \cdot \left[\left(\frac{\pi}{4} \cdot D_s^2 - A_s \right) + \mu_r \cdot A_s \right] \right]}{L}} \quad (61)$$

The complex mutual inductive reactance due to the longitudinal magnetic flux is calculated from:

$$X_{pq} = X_{qp} = 2 \cdot \pi \cdot f \cdot \mu_0 \cdot \frac{\left(\frac{\pi}{4} \cdot D_p^2 - A_s \right) + \mu_r \cdot A_s}{l_p \cdot l_q} \quad (62)$$

where D_p is the mean diameter of layer p , and l_p and l_q are the lay lengths of layers p and q , respectively. In our case, these formulae will apply for one layer only, which is leading to a simple equation of impedance for one layer of conductor and assumption that the steel core is just one homogeneous wire:

$Z_{ss} = R_s + X_s$ is the self impedance of steel core

$Z_{s1} = Z_{1s} = X_{s1}$ is the mutual impedance of steel core and aluminum layer

$Z_{11} = R_1 + X_1$ is the self impedance of aluminum layer, or non-ferrous material layer

R_{s1} is the dc resistance of steel core and aluminum layer (1 or 3)

$$R_{s1} = \frac{R_s \cdot R_1}{R_s + R_1} \quad (63)$$

A total impedance of one-layer conductor can be expressed as follows:

$$Z_{tot} = \frac{(Z_{ss} + Z_{s1}) \cdot (Z_{11} + Z_{s1})}{(Z_{ss} + 2 \cdot Z_{s1} + Z_{11})} \quad (64)$$

and, finally, the increase in resistance is expressed as:

$$R_{ac} = R_{dc} \cdot \frac{|Z_{tot}|}{R_{s1}} \quad (65)$$

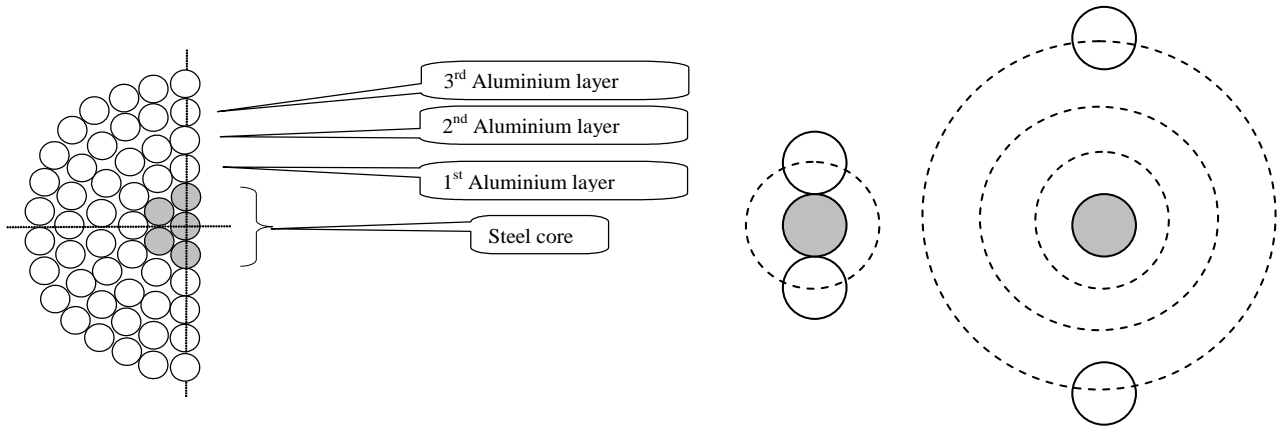
B.3. Example

The conductor selected for the following example of the simplified method described here is ACSR “Grackle”. This conductor is used in the Cigré TB 345 [16] for a more accurate and complex calculation of ac resistance, and is extensively used in the literature.

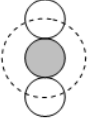
ACSR “Grackle”	A (mm ²)	R_{dc} (Ω /m)	I (A)	Lay length, l (mm)	H_{max} (A/m)
Steel core	47.9	2.9×10^{-3}	29.4	185.7	-158
1st Al layer	134.7	2.629×10^{-4}	328.1	289.1	1125
2nd Al layer	202.0	1.761×10^{-4}	490.1	366.8	-1336
3rd Al layer	269.3	1.324×10^{-4}	652.4	468.2	1393
TOTAL:	652.4	5.755×10^{-5}	1500.0	–	–

Table 8: Example. Characteristics of ACSR “Grackle” conductor.

The values of the current per layer in the table above are obtained from calculation in [16] and will be used as inputs in calculation for single layer and three layers example here.



One layer example:

	Steel strands diameter = 2.24 mm Steel core diameter = 11.2 mm Aluminum strands diameter = 3.78 mm Aluminum layer diameter = 18.76 mm
---	--

a) Calculation of P_{core}

For the magnetic losses, eq. 53 is used to obtain B_{max} . In this, case $H_{max} = 1125$ A/m.

The relative permeability, μ_r , is obtained from eq. 57, giving a value of:

$$\mu_r = 133.53 + 203.85 \cdot i$$

Now, using eq. 52, the value of P_{core} is obtained:

$$P_{core}(W/m) = 12.5 \cdot d^{1/2} \cdot f \cdot A_s \cdot \gamma_s \cdot e^{(-2.5 \cdot 10^{-3} \cdot T_c)} \cdot B_{max}^{1.83} = 0.80 W/m$$

Calculation in the example in [16] is based on the evaluation of a equivalent increase of ac resistance. For a total current of 357.5 A, the increase is 2.6% giving the same value of 0.8 W/m.

b) Calculation of P_{redis}

The dc resistance of a conductor with steel core and 1st layer of aluminum is given by eq. 63, in this case:

$$R_{tot} = \frac{R_s \cdot R_1}{R_s + R} = 2.62 \cdot 10^{-4}$$

The self-reactance of a steel core is obtained from:

$$X_{ss} = i \cdot \left| 2 \cdot \pi \cdot f \cdot \mu_0 \cdot \frac{\left(\frac{\pi}{4} \cdot D_s^2 - A_s \right) + \mu_r \cdot A_s}{l_s^2} \right| = 2.11 \cdot 10^{-4} \cdot i$$

For the mutual reactance it is used the formula:

$$X_{ns} = i \cdot \left| 2 \cdot \pi \cdot f \cdot \mu_0 \cdot \frac{\left(\frac{\pi}{4} \cdot D_n^2 - A_s \right) + \mu_r \cdot A_s}{l_n \cdot l_s} \right| = 1.35 \cdot 10^{-4} \cdot i$$

Here, $l_n = 291.7$ mm and $l_s = 185.7$ mm. D_n is the diameter of the n -th Al-layer, in this case the first Al-layer = 18.76 mm.

For the self reactance of the first Al-layer it is used the formula:

$$X_{nn} = i \cdot \left| 2 \cdot \pi \cdot f \cdot \mu_0 \cdot \frac{\left(\frac{\pi}{4} \cdot D_n^2 - A_s \right) + \mu_r \cdot A_s}{l_n^2} \right| = 8.61 \cdot 10^{-5} \cdot i$$

All the inputs are defined above.

The impedances, as defined and calculated above are:

$$Z_{ss} = 2.95 \cdot 10^{-3} + 2.11 \cdot 10^{-4} \cdot i$$

$$Z_{1s} = 1.35 \cdot 10^{-4} \cdot i$$

$$Z_{11} = 2.63 \cdot 10^{-4} + 8.61 \cdot 10^{-5} \cdot i$$

$$Z_{tot} = \frac{(Z_{ss} + Z_{s1}) \cdot (Z_{11} + Z_{s1})}{(Z_{ss} + 2 \cdot Z_{s1} + Z_{11})} = 2.51 \cdot 10^{-4} + 1.87 \cdot 10^{-4} \cdot i$$

and the modulus:

$$|Z_{tot}| = 3.13 \cdot 10^{-4}$$

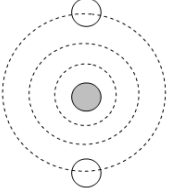
The ac/dc ratio (current re-distribution factor) will be as follows:

$$k_{red} = \frac{|Z_{tot}|}{R_{tot}} = 1.195$$

For this increase of 19.5% of the resistance, the equivalent P_{redis} will be:

$$P_{redis} = I^2 \cdot \Delta R = 357.5^2 \cdot 0.195 \cdot 2.62 \cdot 10^{-4} = 6.53 \text{ W/m}$$

Three layer example:

	<p>Steel strands diameter = 2.24mm Steel core diameter $D_s = 11.2$ mm Aluminium strand diameter $d_n = 3.78$ mm Aluminium layer diameter $D_n = 33.88$ mm</p>
---	--

a) Calculation of P_{core}

For the magnetic losses, it is used the eq. 53 for B_{max} , where, from Table 8 for the 3rd layer, $H_{max} = 1393$ A/m, and from eq. 56, $H_x = 991.5$ A/m.

Then, using eq. 57:

$$\mu = 67.63 + 148.12 \cdot i$$

And from eq. 59:

$$P_{core} = 0.314 \text{ W/m}$$

For the same case, a more complex calculation in [16] has given the value of 0.373 W/m. Anticipating the fact that the influence of 1st and 2nd layer are neglected here completely, an accuracy within 10% is considered acceptable.

b) Calculation of P_{redis}

The dc resistance of a conductor with steel core and 1st layer of aluminum is in this case:

$$R_{tot} = \frac{R_s \cdot R_1}{R_s + R} = 1.27 \cdot 10^{-4}$$

$$X_{ss} = 7.92 \cdot 10^{-5} \cdot i$$

For the mutual reactance it is used the eq. 62. Here, $l_p = 468.2$ mm and $l_q = 185.7$ mm:

$$X_{pq} = i \cdot \left| 2 \cdot \pi \cdot f \cdot \mu_0 \cdot \frac{\left(\frac{\pi}{4} \cdot D_p^2 - A_s \right) + \mu_r \cdot A_s}{l_p \cdot l_q} \right| = 3.14 \cdot 10^{-5} \cdot i$$

For the self-reactance of 1st Al-layer it is used the formula:

$$X_{nn} = i \cdot \left| 2 \cdot \pi \cdot f \cdot \mu_0 \cdot \frac{\left(\frac{\pi}{4} \cdot D_n^2 - A_s \right) + \mu_r \cdot A_s}{l_n^2} \right| = 2.16 \cdot 10^{-5} \cdot i$$

All the inputs are defined above.

The impedances, as defined and calculated above, are:

$$Z_{ss} = 2.95 \cdot 10^{-3} + 7.92 \cdot 10^{-5} \cdot i$$

$$Z_{3s} = 3.14 \cdot 10^{-5} \cdot i$$

$$Z_{33} = 1.32 \cdot 10^{-4} + 1.26 \cdot 10^{-5} \cdot i$$

$$Z_{tot} = \frac{(Z_{ss} + Z_{s1}) \cdot (Z_{11} + Z_{s1})}{(Z_{ss} + 2 \cdot Z_{s1} + Z_{11})} = 1.27 \cdot 10^{-4} + 4.05 \cdot 10^{-5} \cdot i$$

and the modulus:

$$|Z_{tot}| = 1.33 \cdot 10^{-4}$$

The ac/dc ratio (current re-distribution factor) will be:

$$k_{red} = \frac{|Z_{tot}|}{R_{tot}} = 1.047$$

For this increase of 4.7% of the resistance, the equivalent P_{redis} will be:

$$P_{redis} = I^2 \cdot \Delta R = 652^2 \cdot 0.047 \cdot 1.27 \cdot 10^{-4} = 2.53 \text{ W/m}$$

Annex C. Models of convective cooling

The present annex compares different convective models proposed for thermal rating of overhead lines. The local effect of wind on overhead conductors is determined by the Nusselt number, Nu , (see Section 3.5), so the different approaches to obtain Nu are described here.

C.1. Perpendicular flow

Different correlations between Nusselt and Reynolds numbers to evaluate the local convective cooling of a conductor inside a perpendicular air flow are studied and compared in [50]. The following figure compares the most relevant of these correlations, by Hilpert [55], McAdams [26], Davis [30], Morgan [29] and Isozaki et al. [33].

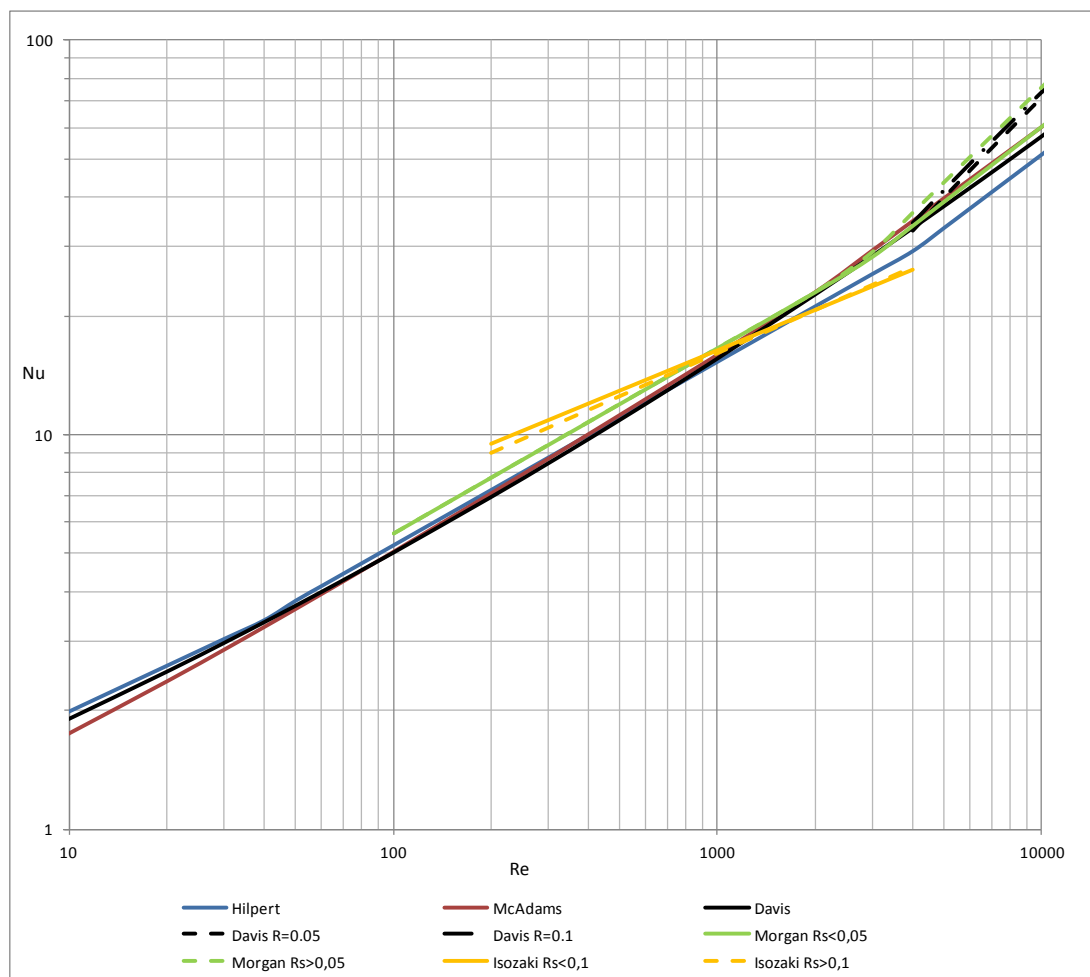


Figure 16 Comparison of different $Nu-Re$ correlations for Forced Convection [26, 29, 30, 33, 55].

It can be seen from fig. 16 that in general there is a good agreement among most of the correlations, which have been obtained from different test data and are used by many authors.

But some differences seem to arise with the correlations proposed by Isozaki et al. [33], which have been derived from tests performed in a wind tunnel facility specially designed for low winds [63], achieving values as low as 0.1 m/s of laminar wind flow and conductor diameters used for transmission lines. However, as indicated in Section 3, it is complicated to contrast and translate the test results to real outdoor conditions, due to the great variability of the wind, both in time and space.

It can be seen from this comparison that the roughness of the conductor is not relevant in general for low Reynolds numbers, but it can increment considerably the cooling at higher winds, for it has to be taken into account especially for dynamic ratings. It has been observed that there is a critical Reynolds number beyond which the Nusselt number increases with the roughness of the conductor [29, 30].

The wind regime is also critical for the convection cooling. The assessment of the turbulence is very complicated for real installations, and can't be easily replicated in laboratory tests. For the normal conductors used for overhead lines, the Nusselt number increases with the intensity and the scale of turbulence, and can be much higher than that obtained for a laminar flow [30]. These correlations compared in fig. 16 can be considered as the local performance of the conductor with a constant, laminar wind. Therefore, the user has to take care of the values to be used for dynamic ratings of a whole line or section, as the local measurements may not be necessary valid to assess the system.

C.2. Wind direction

There are several proposals for considering the reduction of the Nusselt number with the angle of attack, δ , in forced convection cooling. Some of them are compared in the following fig. 17 [50], which shows the ratio Nu_{δ}/Nu_{90} at different angles of attack. The proposals are by Morgan, for smooth conductors [29] and stranded conductors [32], Davis, based on results from mostly smooth conductors [30], and Isozaki et al. for Reynolds numbers around 4000 and roughness below and higher 0.1 [33].

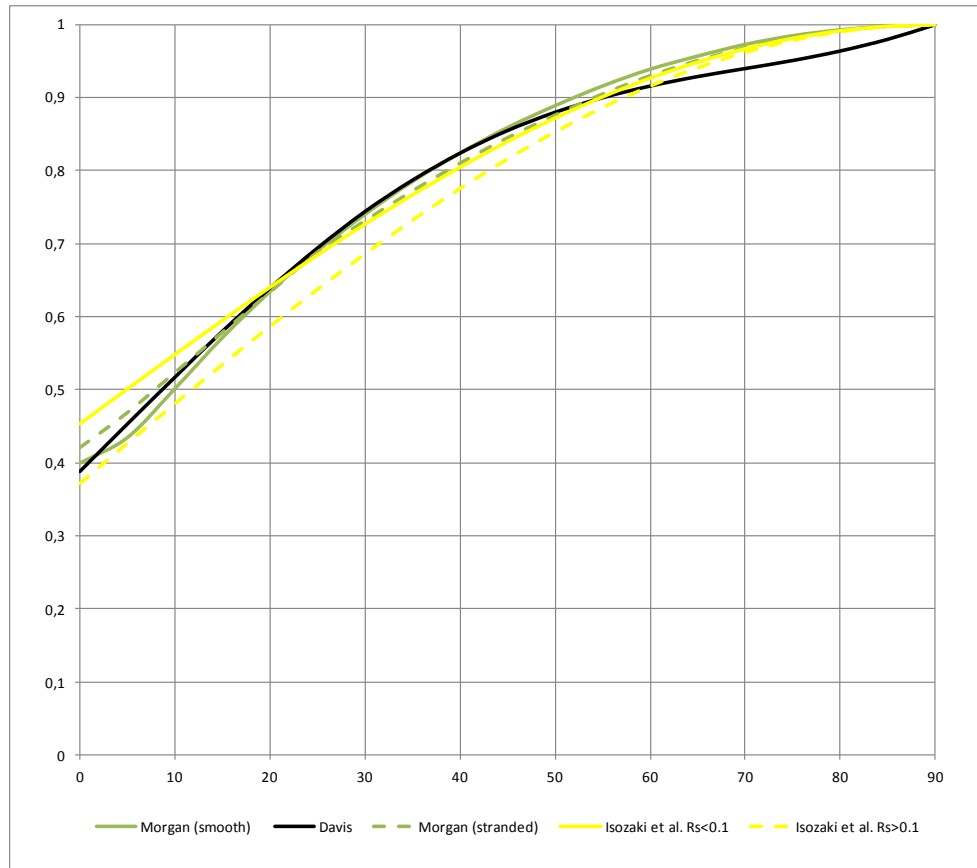


Figure 17 Comparison of different proposals for the Nu_{δ} / Nu_{90} ratio at different angles of attack, δ (deg) [29, 30, 32, 33].

It is observed a good agreement in general for the proposals considered. With parallel flow, the convective cooling is around 40% of the perpendicular, and at an angle of attack of 55 degree the cooling is around 90% of the perpendicular.

The relationships proposed by Morgan and Davis are for Reynolds numbers lower or equal than 4000. The relationship proposed by Isozaki et al. depends on the Reynolds number, being used here 4000. Other proposals [34] make also a distinction for high and low Reynolds numbers, being 4000 the transition.

Although these relationships are derived from different researches and tests, it has to be highlighted again that the wind direction in overhead lines environments is seldom constant, and even it can be considered essentially random at low wind speeds.

C.3. Natural Convection

In the case of zero wind, the most relevant correlations between the Nusselt number and the product $Gr \cdot Pr$ numbers are compared in the following fig. 18 [50]. These proposals are by

House and Tuttle [72] (adapted for the comparison), Davis [30], Morgan [29] and Isozaki et al. [33] for smooth and rough conductors. Other correlations are described in [35–37].

Again, it can be observed a good agreement for a wide range of $Gr \cdot Pr$ numbers for most correlations, except for the correlation proposed by Isozaki et al. for smooth conductors, which has a quite different slope. For $Gr \cdot Pr$ numbers in the order of 100,000 to 1,000,000 the results seem to show a better agreement.

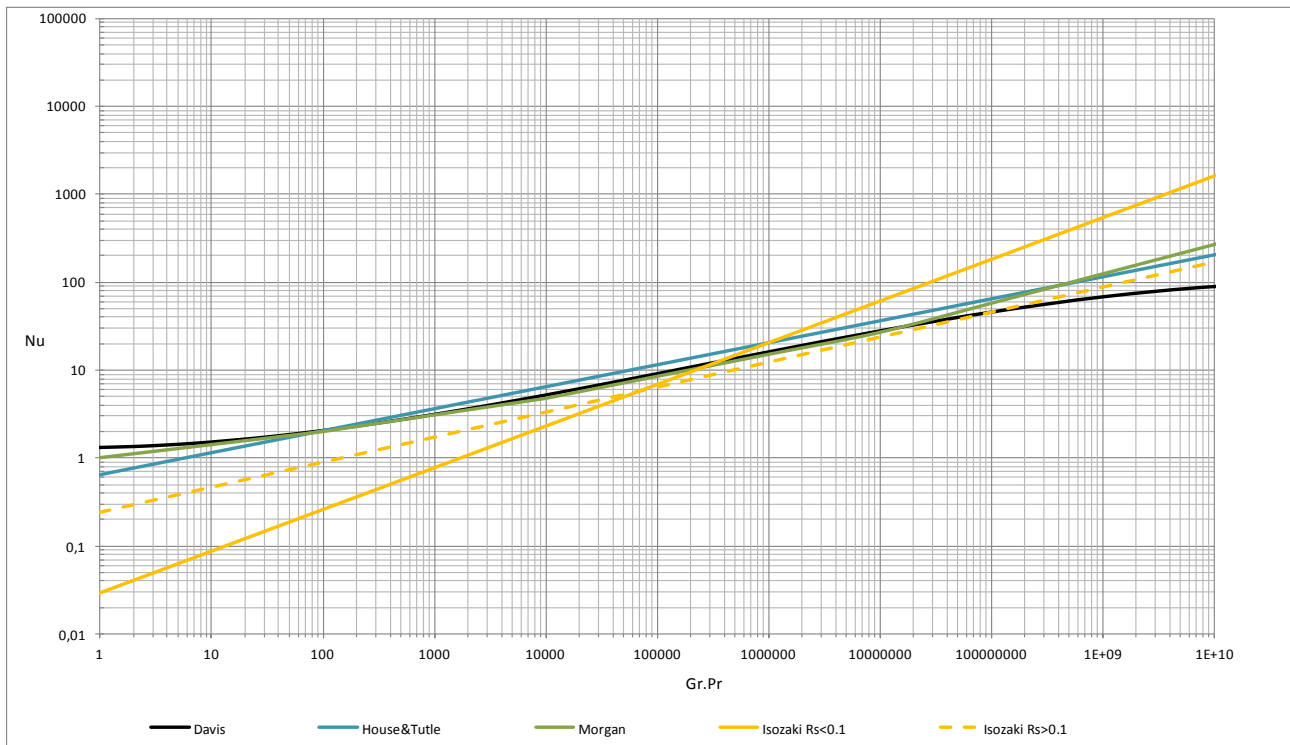


Figure 18. Comparison of different $Nu - Gr \cdot Pr$ correlations for Natural Convection [29, 30, 33, 72].

C.4. Low wind speeds

At low wind speeds, both forced and natural convection may be significant, with natural convection becoming dominant as wind speeds approach zero. Design conditions for conductors usually specify a wind speed of the order of 0.5 m/s. Inconveniently, this is just the region where the transition from forced to natural convection occurs. It is recommended to use the higher of both values as a safe assumption, although there are different proposals to model this wind behaviour.

In the Cigré Technical Brochure 207 [1] the approach to model this transition was:

- a) above 0.5 m/s assume forced convection at a specified attack angle δ with Nu_δ given by eq. 22;
- b) below 0.5 m/s assume either natural convection with Nu_{nat} given by eq. 23 or forced convection Nu_δ with an attack angle δ of 45° , whichever gives the higher Nusselt number. An attack angle of 45° is assumed because there is no preferred wind direction at very low wind speeds.

This has bizarre implications for attack angles δ less than 45° . As wind speed drops below 0.5 m/s, Nu suddenly increases and the predicted conductor temperature therefore suddenly falls. So lower wind speed apparently gives increased cooling and lower predicted conductor temperature, which is unlikely to be true. Such a discontinuity makes any sensitivity analysis in this region difficult.

A simple way to remove this discontinuity has been proposed by Bertinat:

- a) above 0.5m/s assume forced convection at a specified attack angle δ given by eq. 22, as in TB207;
- b) below 0.5 m/s allow Nu to fall linearly with wind speed, from Nu_δ at $V = 0.5$ m/s to Nu_{nat} at $V = 0$, i.e.

$$Nu = Nu_{nat} + \left(\frac{V}{0.5}\right) \cdot (Nu_\delta - Nu_{nat}) \quad (66)$$

Another approach proposed by Morgan is to use a vector summation of the equivalent Reynolds number for natural convection and the Reynolds number for forced convection. To obtain the equivalent Reynolds number for natural convection, Re_{eq} , one can equalize eq. 21 and 23. The effective Reynolds number to be used is then given by:

$$(Re_{eff})^2 = (Re_{eq} \pm Re \cdot \cos\alpha)^2 + (Re \cdot \sin\alpha)^2 \quad (67)$$

where $Re_{eq} = [(A/B) \cdot (Gr \cdot Pr)^m]^{1/n}$ and α is the angle between the vertical natural flow and the forced flow. When the wind aids the direction of the natural convective flow, $Re \cdot \cos\alpha$ is positive, and when it opposes the natural flow $Re \cdot \cos\alpha$ is negative. When the wind flow is horizontal, $\alpha = 90^\circ$ and

$$(Re_{eff})^2 = (Re_{eq})^2 + (Re)^2 \quad (68)$$

A more flexible method for calculating actual temperatures and/or temperature probability distributions as distinct from fixed ratings has been proposed by Hoffmann [73]. In this, one assumes wind speeds above a certain “critical” value exhibit a uniform angle of attack (e.g. the

measured 10-min average of wind direction relative to the span), but that all wind speeds below the “critical” value exhibit a random angle of attack. This means that for low wind speed periods one never gets the same answer twice, but one does get consistent probability distributions of temperature over longer periods of time if the right “critical” wind speed is selected.

Hoffmann found that a “critical” wind speed of 1.5 m/s produces the best fit of calculated and measured temperature distributions over an extended period of time. Using the TB207 equations to calculate the temperature of a conductor from measured weather conditions and a known current was reliable when the wind speed was 1.5 m/s or greater. Below 1.5 m/s, the predictions became increasingly less reliable as wind speeds decreased.

For determining thermal ratings, Hoffmann recommends that the $V = 0.5$ m/s transition be retained, along with an assumed attack angle of $\delta = 45^\circ$ at lower wind speeds, as discussed above. However, when calculating actual temperatures and/or temperature distributions, users may wish to use a different transition wind speed and different or random values of δ .

For dynamic rating purposes, further studies may be needed in real environments in order to ensure that the weather parameters have been correctly adjusted.

Annex D. Analytical calculations for transient state

The present annex describes a mathematical approach to calculate the conductor temperature change with time, considering changes in the ambient parameters and current. The adiabatic heating case is treated separately from the general case of time dependent heating/cooling.

The general heat equation for a homogeneous and isotropic solid can be expressed in polar co-ordinates in the form [39]:

$$\frac{\partial T}{\partial t} = \frac{\lambda}{\gamma \cdot c} \cdot \left(\frac{\partial^2 T}{\partial r^2} + \frac{1}{r} \cdot \frac{\partial T}{\partial r} + \frac{1}{r^2} \cdot \frac{\partial^2 T}{\partial \phi^2} + \frac{\partial^2 T}{\partial z^2} \right) + \frac{Q(T, r, t, \phi, z)}{\gamma \cdot c} \quad (69)$$

where,

c = specific heat capacity (J/kg·K)

Q = power per unit volume (W/m³)

r = radius (m)

t = time (s)

T = temperature (°C)

z = axial length (m)

γ = mass density (kg/m³)

λ = thermal conductivity (W/m·K)

ϕ = azimuthal angle (deg)

$\lambda/(\gamma \cdot c)$ = thermal diffusivity (m²/s)

If it is assumed that the conductor has cylindrical symmetry and semi-infinite length, then the terms in ϕ and z can be neglected, hence eq. 69 reduces to eq. 70:

$$\frac{\partial T}{\partial t} = \frac{\lambda}{\gamma \cdot c} \cdot \left(\frac{\partial^2 T}{\partial r^2} + \frac{1}{r} \cdot \frac{\partial T}{\partial r} \right) + \frac{Q(T, r, t)}{\gamma \cdot c} \quad (70)$$

Eq. 70 requires a numerical solution with appropriate initial and boundary conditions. However, if a specific radial temperature distribution, such as eq. 16 for a full-body mono-metallic conductor or eq. 15 for a hollow core mono-metallic conductor or a steel-cored conductor, is assumed, then there is a fixed relationship between the core temperature T_c and

the surface temperature T_s for a given total power input per unit length. The mean temperature of the conductor can then be calculated, but it is usually sufficiently accurate to assume that the mean temperature of the conductor is given by eq. 71:

$$T_{av} = \frac{T_c + T_s}{2} \quad (71)$$

Since the mass per unit length $m = \gamma \cdot A$ and $Q = P/A$, where A is the cross-sectional area and P is the total power transfer per unit length, eq. 70 can be reduced to the general differential equation showed in Section 4.2:

$$m \cdot c \cdot \frac{dT_{av}}{dt} = P_J + P_M + P_S - P_c - P_r \quad (72)$$

where the terms on the right-hand side of eq. 72 are described in Section 3. In most of the cases, the magnetic heat gain, P_M , can be neglected, and in general it can be included in the Joule heat gain, P_J (see Section 3.1). So the time dependent heating or cooling can be divided into four distinct components: Joule and magnetic heat gain, change in solar radiation gain, change in radiative heat loss and change in convective heat loss.

D.1. Time dependent heating or cooling

The calculation of the conductor temperature variation with time depends on the four components described above, Joule and magnetic heat gain, change in solar radiation gain, change in radiative heat loss and change in convective heat loss. These components depend at the same time on the ambient parameters (solar radiation, ambient temperature, wind speed and wind direction) as well as the current through the conductor.

The variation of the ambient parameters and conductor current with time can be represented in different ways, obtaining different results. It is important to understand the model used to represent these variations, as it can be a major source of errors. The simplest way to model the variations of all the parameters is a step change: the parameters are considered constant during a period of time. The shorter the interval of time, the more realistic will be the solution. It can also be considered a linear change between two values, which leads to a different conductor temperature, as explained below, because the total energy supplied or lost within the interval is different.

The following paragraphs describe a method to calculate the conductor temperature change under transient conditions, i.e. after a variation of the different weather parameters and the current. The variations produced by the different parameters are calculated separately, and the

final result for the conductor temperature is presented at the end. For this method, it will be considered a step change in current I (A), as main contributing factor. The other parameters will be represented here by a linear change: global solar radiation I_T (W/m²), ambient temperature T_a (°C), wind speed V (m/s) and direction (deg). Similar process can be followed to represent a step change for these parameters.

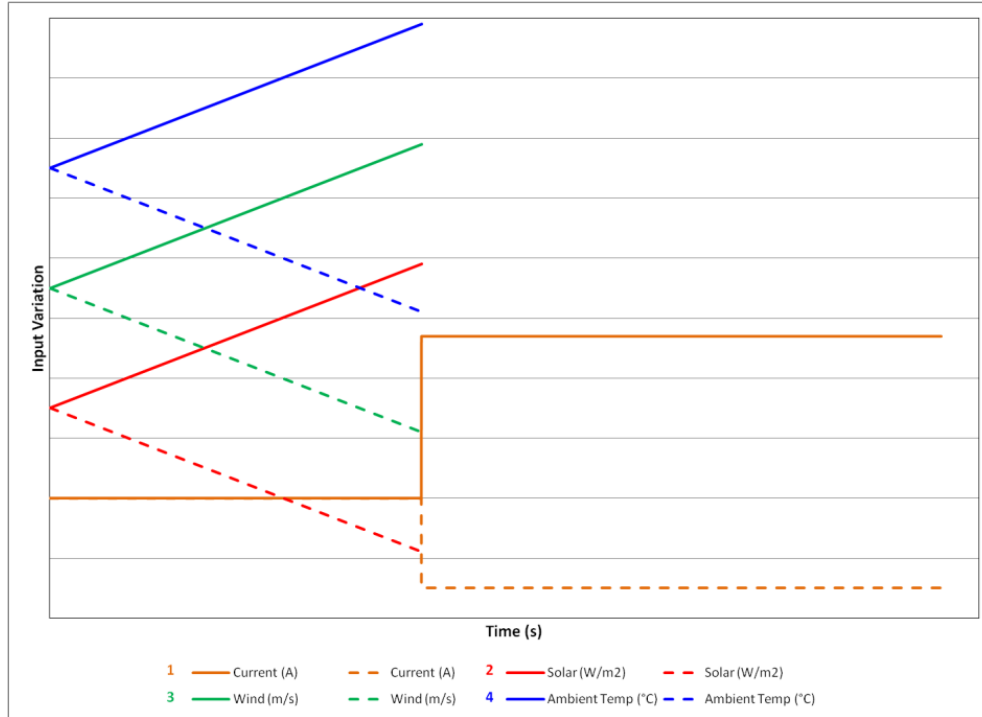


Figure 19. Change of different parameters: step change in current and linear change in ambient parameters

a) Step change in current

The differential heat balance eq. 72 can be solved by numerical integration. However, by using a degree of approximation, it is possible to solve by anticipating a total change in heat balance as a result of conductor step-change. Then, the solution is given in the following equation (see fig. 19):

$$t = \frac{-m \cdot c \cdot (\theta_m - \theta_1)}{P_T} \cdot \left[\beta \cdot (\theta - \theta_1) + (1 - \beta \cdot \theta_m) \cdot \ln \left(\frac{\theta_m - \theta}{\theta_m - \theta_1} \right) \right] \quad (73)$$

where P_T is a difference in the heat gain for step change in current I (A), while other parameters (I_T , T_a , V) are constant for incremental period of time Δt ; c and β are calculated at the ambient temperature. Since it can be seen from Table 6 in Annex A that β is small, and for moderate temperature rise (≤ 130 K), and first approximation of $P_T \approx \Delta(P_J + P_M)$:

$$t \cong \frac{-m \cdot c \cdot (\theta_m - \theta_1)}{\Delta(P_J + P_M)} \cdot \ln \left(\frac{\theta_m - \theta}{\theta_m - \theta_1} \right) \quad (74)$$

where,

$m \cdot c$ = product of the mass per unit length and the specific heat capacity of the conductor

$\theta = T_{av} - T_a$ = rise of conductor average temperature above ambient temperature at time t

$\theta_1 = T_{av1} - T_a$ = initial rise of the conductor average temperature above ambient at $t = 0$

$\theta_m = T_{avm} - T_a$ = asymptotic rise of the conductor average temperature above ambient

The thermal time constant during heating of the conductor τ is the time interval for the temperature change of the conductor above ambient to reach $(1 - 1/e)$, that is 63.2% of its asymptotic (steady state) value θ_m . The thermal time constant for the current change is given by:

$$\tau_I \cong \frac{\pm m \cdot c \cdot (\theta_m - \theta_1)}{\Delta(P_J + P_M)} \quad (75)$$

The sign + or - depends on the trend of the step-change in current; + for increase and - for decrease.

Hence, from eqs. 74 and 75:

$$t \cong -\tau_I \cdot \ln \left(\frac{\theta_m - \theta}{\theta_m - \theta_1} \right) \quad (76)$$

and:

$$\theta \cong \theta_m - (\theta_m - \theta_1) \cdot e^{-t/\tau_I} \quad (77)$$

The heating thermal time constant for current in a steel-cored conductor is found from [39]:

$$\tau_I \cong \frac{(m_a \cdot c_a + m_s \cdot c_s) \cdot (\theta_m - \theta_1)}{\Delta(P_J + P_M)} + \frac{m_s \cdot c_s \cdot \ln \left(\frac{D}{D_1} \right)}{2 \cdot \pi \cdot \lambda_a} \quad (78)$$

where λ_a is the thermal conductivity of the non-ferrous section of the conductor (W/mK), D is the overall diameter of the conductor (m) and D_1 is the diameter of the core. The value of the second term on the right-hand side of eq. 78 varies from 2 % to 7 % of the first term, so can be usually neglected.

If a steady current I_1 has produced a maximum temperature rise θ_{m1} in the conductor, and the current is then increased in a step to a higher value I_2 , which results in a new maximum temperature rise θ_{m2} , then the time interval t_{12} for the temperature rise to increase from θ_{m1} to a prescribed value θ_2 is given by:

$$t_{12} \cong \tau_I \cdot \ln \left(\frac{\theta_{m2} - \theta_2}{\theta_{m2} - \theta_{m1}} \right) \quad (79)$$

where the current I in eqs. 75 and 76 is now the current I_2 , and θ_{m1} and θ_{m2} are calculated according to the steady state methods.

b) Linear change in solar radiation

In a similar way, it can be obtained the thermal time constant for the change in the solar radiation gain:

$$\tau_S \cong \frac{\pm 2 \cdot m \cdot c \cdot (\theta_m - \theta_1)}{\Delta(P_S)} \quad (80)$$

The factor 2 comes from the assumption that the change in solar radiation from step 1 to step 2 is linear; as shown in fig. 19. It is a result of integration of thermal function for the given time interval.

Hence, from eq. 80:

$$t \cong -\tau_S \cdot \ln \left(\frac{\theta_m - \theta}{\theta_m - \theta_1} \right) \quad (81)$$

and:

$$\theta \cong \theta_m - (\theta_m - \theta_1) \cdot e^{-t/\tau_S} \quad (82)$$

The heating thermal time constant for solar radiation in a steel-cored conductor is:

$$\tau_S \cong \frac{2 \cdot (m_a \cdot c_a + m_s \cdot c_s) \cdot (\theta_m - \theta_1)}{\Delta(P_S)} + \frac{m_s \cdot c_s \cdot \ln \left(\frac{D}{D_1} \right)}{2 \cdot \pi \cdot \lambda_a} \quad (83)$$

c) Linear change in air temperature

Again, for a linear change in air temperature, the thermal time constant for the conductor radiation change can be obtained from:

$$\tau_T \cong \frac{\pm 2 \cdot m \cdot c \cdot (\theta_m - \theta_1)}{\Delta(P_r)} \quad (84)$$

The factor 2 comes from the assumption of linear change. Hence, from eq. 84:

$$t \cong -\tau_T \cdot \ln\left(\frac{\theta_m - \theta}{\theta_m - \theta_1}\right) \quad (85)$$

and:

$$\theta \cong \theta_m - (\theta_m - \theta_1) \cdot e^{-t/\tau_T} \quad (86)$$

The heating thermal time constant for the conductor radiation change in a steel-cored conductor is:

$$\tau_{hT} \cong \frac{2 \cdot (m_a \cdot c_a + m_s \cdot c_s) \cdot (\theta_m - \theta_1)}{\Delta(P_r)} + \frac{m_s \cdot c_s \cdot \ln\left(\frac{D}{D_1}\right)}{2 \cdot \pi \cdot \lambda_a} \quad (87)$$

d) Linear change in windspeed

The thermal time constant for a change in windspeed is again given by:

$$\tau_V \cong \frac{\mp 2 \cdot m \cdot c \cdot (\theta_m - \theta_1)}{\Delta(P_c)} \quad (88)$$

note the change in sign: the conductor temperature decreases with increasing windspeed. The factor 2 comes from the assumption of linear change in windspeed.

Hence, from eq. 88:

$$t \cong -\tau_V \cdot \ln\left(\frac{\theta_m - \theta}{\theta_m - \theta_1}\right) \quad (89)$$

and:

$$\theta \cong \theta_m - (\theta_m - \theta_1) \cdot e^{-t/\tau_V} \quad (90)$$

The heating thermal time constant for windspeed change in a steel-cored conductor is:

$$\tau_V \cong \frac{-2 \cdot (m_a \cdot c_a + m_s \cdot c_s) \cdot (\theta_m - \theta_1)}{\Delta(P_c)} + \frac{m_s \cdot c_s \cdot \ln\left(\frac{D}{D_1}\right)}{2 \cdot \pi \cdot \lambda_a} \quad (91)$$

Summary of time dependent heating or cooling

As a result of the different changes produced for each component, the total, simultaneous change can be represented in the following equation:

$$\theta \cong \theta_m - (\theta_m - \theta_1) \cdot e^{-t/\tau_I} \cdot e^{-t/\tau_S} \cdot e^{-t/\tau_T} \cdot e^{-t/\tau_V} \quad (92)$$

An example of calculation can be followed in Annex E.3, where the results are compared with the numerical method described in Section 4 for tracking the conductor temperature taking weather and current measurements every 10 minutes.

Similar results can be obtained calculating the global power increment, $\Delta(P_T)$, and obtaining with it a global thermal time constant τ like in eq. 75. The global rise of conductor temperature above ambient θ can be obtained like in eq. 77.

D.2. Adiabatic heating

A mathematical solution to the adiabatic heating of a mono-metallic conductor with all the parameters assumed to vary quadratically with temperature is given in [40]. This solution has been shown to be accurate to within 0.5 % with both symmetrical alternating current and with alternating current with a dc offset [41]. The calculation of the adiabatic heating of a steel-cored conductor is more difficult. IEC Publication 60865 [42] states that the steel core should not be taken into account in the calculation. However, this assumption can lead to significant errors in calculating the temperature rise of a conductor during a short-circuit, particularly where there is a high steel content. The following assumptions have been made in the IEC publication and in this annex:

- Skin effect (magnetic influence of the conductor itself) and proximity effect (magnetic influence of other conductors) are disregarded, i.e. the current density is assumed to be evenly distributed over the conducting cross-sectional area of the conductor.
- The resistance of the conductor is assumed to vary linearly with temperature.
- The steel core, where present, is considered to be saturated by the fault current, ($P_M=0$).
- The specific heat capacity of the conductor is assumed to be constant.
- The heating of the conductor is assumed to be adiabatic, i.e. heat gains and losses at the surface of the conductor are neglected, due to the very short time span, i.e. $P_S = P_C = P_r = 0$.
- Taking the above assumptions into account, eq. 72 reduces, under short-circuit conditions, to:

$$m \cdot c \cdot \frac{dT}{dt} = P_J \quad (93)$$

Hence,

$$\frac{dT}{dt} = \frac{I^2 \cdot R_{dc} \cdot [1 + \alpha \cdot (T - 20)]}{m \cdot c} = \frac{I^2 \cdot \rho_{dc} \cdot [1 + \alpha \cdot (T - 20)]}{\frac{A}{A_1 \cdot \gamma_1 \cdot c_1 + A_2 \cdot \gamma_2 \cdot c_2}} \quad (94)$$

where ρ_{dc} and α are taken at 20 °C, see Table 6, and A is the area of the conducting section. Separating the variables and integrating we get:

$$\int_{T_1}^{T_2} \frac{dT}{1 + \alpha \cdot (T - 20)} = \int_0^t \frac{I^2 \cdot \rho_{dc}}{A \cdot (A_1 \cdot \gamma_1 \cdot c_1 + A_2 \cdot \gamma_2 \cdot c_2)} dt \quad (95)$$

which gives:

$$\frac{1}{\alpha} \cdot \ln \left[\frac{1 + \alpha \cdot (T_2 - 20)}{1 + \alpha \cdot (T_1 - 20)} \right] = \frac{I^2 \cdot \rho_{dc}}{A \cdot (A_1 \cdot \gamma_1 \cdot c_1 + A_2 \cdot \gamma_2 \cdot c_2)} \cdot t \quad (96)$$

The final temperature of the conductor for a given thermal equivalent short-time withstand current I_{ad} (see clause 3.2.2 of IEC 60865) is then given by:

$$T_2 = \frac{[1 + \alpha \cdot (T_1 - 20)] \cdot e^{\frac{I_{ad}^2 \cdot \rho_{dc} \cdot \alpha \cdot t}{A \cdot (A_1 \cdot \gamma_1 \cdot c_1 + A_2 \cdot \gamma_2 \cdot c_2)}} - 1}{\alpha} + 20 \quad (97)$$

The following three cases are considered, where the subscripts a and s refer to aluminum and steel (or aluminum clad steel), respectively:

(1) Homogeneous non-ferrous conductor:	(2) Homogeneous ferrous conductor	(3) Steel-cored aluminium conductor or aluminium-clad-steel-cored aluminium conductor
$\rho_{dc} = \rho_a$	$\rho_{dc} = \rho_s$	$\rho_{dc} = \rho_a$
$\alpha = \alpha_a$	$\alpha = \alpha_s$	$\alpha = \alpha_a$
$A = A_1 = A_a$	$A_1 = 0$	$A = A_1 = A_a$
$A_2 = 0$	$A = A_2 = A_s$	$A_2 = A_s$
$\gamma_1 = \gamma_a$	$\gamma_1 = 0$	$\gamma_1 = \gamma_a$
$c_1 = c_a$	$c_1 = 0$	$c_1 = c_a$
$\gamma_2 = 0$	$\gamma_2 = \gamma_s$	$\gamma_2 = \gamma_s$
$c_2 = 0$	$c_2 = c_s$	$c_2 = c_s$

Table 9: Conductors considered for adiabatic state.

The thermal equivalent short-time withstand current I_{ad} for a given final temperature T_2 can be found from eq. 98:

$$I_{ad} = \sqrt{\frac{A \cdot (A_1 \cdot \gamma_1 \cdot c_1 + A_2 \cdot \gamma_2 \cdot c_2)}{\rho_{dc} \cdot \alpha \cdot t} \cdot \ln \left[\frac{1 + \alpha \cdot (T_2 - 20)}{1 + \alpha \cdot (T_1 - 20)} \right]} \quad (98)$$

The material data for the calculation of the short-time conductor temperature or withstand current are given in Table 6, Annex A. When calculating with steel wires, the known value for the resistivity should be used. If the resistivity is not known, the relatively high value corresponding to a conductivity of 6 % IACS should be used.

Table 6 of IEC Publication 60865 [42] gives the highest recommended temperatures for various types of conductors. If the temperature does not exceed the value given in the table, there will be a negligible decrease in tensile strength, and safety will not be jeopardised. However, the strength of a conductor depends on its whole operational history, which may mean specifying a lower limiting temperature than that given in [42]. It should be noted that there are several types of new high-temperature conductors now available [3, 62].

Calculated and measured values of the maximum temperature rise of various types of conductor under short-circuit are compared in Table 10.

Type and construction of conductor	T ₁ (°C)	Current (kA rms)	Duration (s)	T ₂ (°C) Measured	T ₂ (°C)	
					Calculated (A)	Calculated (B)
500 mm ² AAC 61 wires	20	30.1	1.0	64.8	65.3	N/A
120/70 ACSR 12/7	40	5.4	0.35	45.0	45.7	45.1
		10.8		62.6	63.6	61.0
		15.5		92.7	90.9	85.1
		19.8		126.4	128.2	117.7
490/65 ACSR 54/7	20	4.8	1.0	22.2	21.1	21.0
		10.0		25.5	24.8	24.7
		15.1		30.7	31.1	30.8
		20.2		39.1	36.2	35.8
120/70 AACSR 12/7	20	5.4	0.35	24.9	25.9	25.9
		10.8		49.0	44.5	44.2
		13.3		60.5	58.0	57.5
		15.7		74.4	74.0	73.5
		20.8		121.6	122.1	120.6
		24.9		181.0	179.5	175.6
240/55 AACSR	25	7.4	1.0	35.7	36.8	36.2

30/7		15.1		68.8	77.5	74.7
		21.6		108.9	142.8	135.8
		25.5		167.3	201.4	190.4

(A): calculated with total current in aluminum or alloy section and with heat capacity of total conductor.

(B): calculated with distributed current in aluminum or alloy section and with total heat capacity of conductor

**Table 10: Comparison between calculated (eq. 97) and measured [47]
final temperatures of various conductors during symmetrical 50 Hz
short-circuit.**

The measured values of T_2 refer to the outer layer, whereas the calculated values of T_2 refer to the average temperature of the conducting section.

Research on the mechanical properties of various conductors at elevated temperatures under transient conditions, with change in sag and remaining strength after a short circuit is discussed in [71].

Annex E. Examples of calculation

E.1. Steady state thermal rating

The following calculation example determines the steady state ampacity rating for a “Drake” 26/7 ACSR conductor at a temperature of 100°C (deterministic calculation for given conditions). Examples A and B vary in different ambient and solar conditions.

Conductor characteristics	Example A	Example B
Conductor outside diameter (mm)	28.1	28.1
Core diameter (mm)	10.4	10.4
Outer strand diameter (mm)	4.44	4.44
Maximum allowable conductor temp. (°C)	100	100
Emissivity	0.8	0.9
Solar absorptivity	0.8	0.9
Conductor ac resistance at 25°C (Ω/m)	$7.283 \cdot 10^{-5}$	$7.283 \cdot 10^{-5}$
Conductor ac resistance at 75°C (Ω/m)	$8.688 \cdot 10^{-5}$	$8.688 \cdot 10^{-5}$
Ambient conditions		
Ambient air temperature (°C)	40	20
Wind speed (m/s)	0.61	1.66
Wind angle of attack (°)	60	80
Inclination β to the horizontal (°)	0	10
Height above sea level y (m)	0	500
Solar conditions		
Azimuth of line (°)	90 (east–west direction)	0 (north–south direction)
Latitude (°)	30	50
Clearness of Atmosphere	clear ($N_s = 1$)	industrial ($N_s = 0.5$)
Date	11 a.m. 10th June	2 p.m. 3rd October
Reflectance of the ground (albedo)	forest ($F = 0.1$)	urban ($F = 0.15$)

Table 11: Example. Conductor characteristics and ambient conditions

The following table shows a step by step calculation including all required auxiliary variables:

Convective heat loss	Example A	Example B	Units
$T_f = 0.5 \cdot (T_s + T_a)$	70	60	°C
$\lambda_f = 2.368 \cdot 10^{-2} + 7.23 \cdot 10^{-5} \cdot T_f - 2.763 \cdot 10^{-8} \cdot T_f^2$	0.0286	0.0279	W/K · m
ρ_0 (density of the air at sea level)	1.2041	1.2041	kg/m ³
$\gamma = \frac{1.293 - 1.525 \cdot 10^{-4} \cdot y + 6.379 \cdot 10^{-9} \cdot y^2}{1 + 0.00367 \cdot T_f}$	1.0287	0.9985	kg/m ³
$\mu_f = (17.239 + 4.635 \cdot 10^{-2} \cdot T_f - 2.03 \cdot 10^{-5} \cdot T_f^2) \cdot 10^{-6}$	$20.384 \cdot 10^{-6}$	$1.9947 \cdot 10^{-5}$	kg/m · s
$\nu_f = \mu_f / \gamma$	$19.815 \cdot 10^{-6}$	$1.9977 \cdot 10^{-5}$	m ² /s

$R_s = d/2 \cdot (D - d)$	$\frac{4.44}{2 \cdot (28.1 - 4.44)} = 0.0938$	0.0938	–
$Re = V \cdot D / \nu_f$	$\frac{0.61 \cdot 28.1 \cdot 10^{-3}}{19.815 \cdot 10^{-6}} = 865$	2335	–
$B; n$ (Table 4)	$R_s > 0.05$ and $Re < 2650$ $B = 0.641; n = 0.471$	$B = 0.641;$ $n = 0.471$	–
$Nu_{90} = B \cdot Re^n$	15.495	24.73	–
$Nu_{\delta} = Nu_{90} \cdot (0.42 + 0.58 \cdot \sin(\delta)^{0.90})$	14.40	24.53	–
$P_{c,forced} = \pi \cdot \lambda_f \cdot (T_s - T_a) \cdot Nu_{\delta}$	$\pi \cdot 0.0286 \cdot 60 \cdot 14.40 = 77.6$	172.1	W/m
$Gr = \frac{D^3 \cdot (T_s - T_a) \cdot g}{(T_f + 273) \cdot \nu_f^2}$	$96.95 \cdot 10^3$	$131 \cdot 10^3$	–
$Pr = c_f \cdot \mu_f / \lambda_f$	$\frac{1005 \cdot 20.384 \cdot 10^{-6}}{0.0286} = 0.716$	0.718	–
$A; m$ (Table 5)	$Gr \cdot Pr = 69.43 \cdot 10^3$ $A = 0.48; m = 0.25$	$A = 0.48;$ $m = 0.25$	–
$Nu_{nat} = A \cdot (Gr \cdot Pr)^m$	7.7916	8.41	–
$Nu_{\beta} = Nu_{nat} \cdot (1 - 6.76 \cdot 10^{-6} \cdot \beta^{2.5})$	7.7916	8.39	–
$P_{c,nat} = \pi \cdot \lambda_f \cdot (T_s - T_a) \cdot Nu_{\beta}$	42.0	58.9	W/m
$P_c = \max(P_{c,forced}; P_{c,nat})$	77.6	172.1	W/m
Radiative heat loss			
$P_r = \pi \cdot D \cdot \sigma_B \cdot \varepsilon_s \cdot [(T_s + 273)^4 - (T_a + 273)^4]$	$4.004 \cdot 10^{-9} \cdot [(373)^4 - (313)^4] = 39.1$	54	W/m
Solar heat gain			
$\delta_s = 23.4 \cdot \sin[2 \cdot \pi \cdot (284 + N^*)/365]$	$23.4 \cdot \sin(7.66) = 23$	–5	deg
$H_s = \arcsin(\sin(\varphi) \sin(\delta_s) + \cos(\varphi) \cos(\delta_s) \cos(Z))$	$\arcsin(\sin(30) \sin(23) - \cos(30) \cos(23) \cos(-15)) = 74.8$	29.2	deg
$\gamma_s = \arcsin(\cos(\delta_s) \cdot \sin(Z) / \cos(H_s))$	$\arcsin(\cos(23) \cdot \sin(-15) / \cos(74.8)) = 65.85$	34.8	deg
$\eta = \arccos[\cos(H_s) \cdot \cos(\gamma_s - \gamma_c)]$	$\arccos[\cos(74.8) \cdot \cos(65.85 - 90)] = 76.2$	44.2	deg
$I_{B(0)} = N_s \cdot \frac{1280 \cdot \sin(H_s)}{\sin(H_s) + 0.314}$	$1 \cdot \frac{1280 \cdot \sin(74.8)}{\sin(74.8) + 0.314} = 965.8$	389.4	W/m ²
$I_{B(y)} = I_{B(0)} \cdot \left[1 + 1.4 \cdot 10^{-4} \cdot y \left(\frac{1367}{I_{B(0)}} - 1 \right) \right]$	$965.8 \cdot [1 + 0] = 965.8$	457.8	W/m ²
$I_d = (430.5 - 0.3288 \cdot I_{B(y)}) \cdot \sin(H_s)$	$(430.5 - 0.3288 \cdot 965.8) \sin(74.8) = 109$	136.6	W/m ²
$I_T = I_{B(y)} \cdot \left(\sin(\eta) + \frac{\pi}{2} \cdot F \cdot \sin(H_s) \right) + I_d \cdot \left(1 + \frac{\pi}{2} \cdot F \right)$	$\left(965.8 \left(\sin(76.2) + \frac{\pi}{2} \cdot 0.1 \sin(74.8) \right) + 109 \left(1 + \frac{\pi}{2} \cdot 0.1 \right) \right) = 1210$	540.6	W/m ²
$P_s = \alpha_s \cdot I_T \cdot D$	$0.8 \cdot 1210 \cdot 0.0281 = 27.2$	13.7	W/m

Electrical resistance			
$R_{ac}(T) = R_{ac}(T_1) + (T - T_1) \cdot \frac{R_{ac}(T_2) - R_{ac}(T_1)}{T_2 - T_1}$	$7.283 \cdot 10^{-5} + (100 - 25) \cdot \frac{(8.688 \cdot 10^{-5} - 7.283 \cdot 10^{-5})}{75 - 25}$ $= 9.3905 \cdot 10^{-5}$	$9.3905 \cdot 10^{-5}$	Ω/m
Current calculation			
$I = \sqrt{\frac{P_r + P_c - P_s}{R_{ac}}}$	$\sqrt{\frac{39.1 + 77.6 - 27.2}{9.3905 \cdot 10^{-5}}} = 976$	1054	A
Radial temperature difference			
$T_c - T_s = \frac{I^2 \cdot R}{2 \cdot \pi \cdot \lambda} \cdot \left[\frac{1}{2} - \frac{D_1^2}{D^2 - D_1^2} \cdot \left(\ln \frac{D}{D_1} \right) \right]$	$\frac{976^2 \cdot 9.3905 \cdot 10^{-5}}{2 \pi \cdot 0.7}$ $\cdot \left[\frac{1}{2} - \frac{10.4^2}{28.1^2 - 10.4^2} \ln \left(\frac{28.1}{10.4} \right) \right]$ $= 7$	16.5	$^{\circ}\text{C}$

Table 12: Example. Equations for steady state thermal rating calculation

In the equations above, it is considered that the conductor is operating above its knee-point temperature, and a value for the effective radial thermal conductivity, λ , of 0.7 W/m·K is used as a conservative approach. It can be seen that for the example B, it could be necessary to reduce the rating, and thus the core temperature, in order to avoid problems with clearances and/or material damages.

In this case, the interpolated value of ac resistance differs in less than 1% with the measured value given by the manufacturer, so the error can be considered negligible. Also, the conductor has two aluminum layers, so the magnetic heating doesn't have to be considered in the calculation for being irrelevant.

E.2. Steady state conductor temperature

The following calculation example determines the steady state temperature for a “Drake” 26/7 ACSR conductor. Conductor characteristics and ambient conditions are as given in Examples A and B of the steady state thermal rating Annex E.1 (deterministic approach). The calculation is done in an iterative way to solve the equations and find the adequate conductor temperature for a fixed current. A flow chart for the routine is given in fig. 10, Section 4. For each step, the calculation shown in the example E.1 is performed, showing only the results. In this example the iteration starts with an assumed conductor temperature of 85°C. This conductor temperature has to be estimated by the user. If the heat balance ($P_s + I^2 \cdot R_{ac} - P_c - P_r$) results in a value above zero, the assumed temperature has to be increased for the next step and vice-versa. The iteration can be stopped if the result of the heat balance is close to zero.

Conductor characteristics	Example A	Example B
Conductor outside diameter (mm)	28.1	28.1
Core diameter (mm)	10.4	10.4
Outer strand diameter (mm)	4.44	4.44
Maximum allowable conductor temp. (°C)	100	100
Emissivity	0.8	0.9
Solar absorptivity	0.8	0.9
Conductor ac resistance at 25°C (Ω/m)	$7.283 \cdot 10^{-5}$	$7.283 \cdot 10^{-5}$
Conductor ac resistance at 75°C (Ω/m)	$8.688 \cdot 10^{-5}$	$8.688 \cdot 10^{-5}$
Ambient conditions		
Ambient air temperature (°C)	40	20
Wind speed (m/s)	0.61	1.66
Wind angle of attack (°)	60	80
Inclination β to the horizontal (°)	0	10
Height above sea level y (m)	0	500
Solar conditions		
Azimuth of line (°)	90 (east-west direction)	0 (north-south direction)
Latitude (°)	30	50
Clearness of Atmosphere	clear ($N_s = 1$)	industrial ($N_s = 0.5$)
Date	11 a.m. 10th June	2 p.m. 3rd October
Reflectance of the ground (albedo)	forest ($F = 0.1$)	urban ($F = 0.15$)

Table 13: Example. Conductor characteristics and ambient conditions

Step	Description	Example A	Example B	Units
	Fixed current	976	1504	A
	First assumed conductor temperature	85	85	°C
	$P_s = \text{constant}$ (independent of temperature)	27.2	13.67	W/m

Step	Description	Example A	Example B	Units
1	$P_c(T); P_r(T)$	58.8; 27.34;	141.3; 40.8;	W/m
$T = 85\text{ }^{\circ}\text{C}$	$R_{ac}(T); I^2 \cdot R_{ac}(T)$	$8.969 \cdot 10^{-5}; 85.43$	$8.969 \cdot 10^{-5}; 202.9$	$\Omega/\text{m}; \text{W}/\text{m}$
	$P_S + I^2 \cdot R_{ac} - P_c - P_r$	26.51 (>0)	34.45 (>0)	W/m
	$T = T + 10\text{ }^{\circ}\text{C}$	95	95	$^{\circ}\text{C}$
2	$P_c(T); P_r(T)$	71.4; 35	161.9; 49.4	W/m
$T = 95\text{ }^{\circ}\text{C}$	$R_{ac}(T); I^2 \cdot R_{ac}(T)$	$9.25 \cdot 10^{-5}; 88.1$	$9.25 \cdot 10^{-5}; 209.3$	$\Omega/\text{m}; \text{W}/\text{m}$
	$P_S + I^2 \cdot R_{ac} - P_c - P_r$	8.96 (>0)	11.6 (>0)	W/m
	$T = T + 10\text{ }^{\circ}\text{C}$	105	105	$^{\circ}\text{C}$
3	$P_c(T); P_r(T)$	83.8; 43.3	182.2; 58.8	W/m
$T = 105\text{ }^{\circ}\text{C}$	$R_{ac}(T); I^2 \cdot R_{ac}(T)$	$9.531 \cdot 10^{-5}; 90.78$	$9.531 \cdot 10^{-5}; 215.6$	$\Omega/\text{m}; \text{W}/\text{m}$
	$P_S + I^2 \cdot R_{ac} - P_c - P_r$	-9.08 (<0)	-11.7 (<0)	W/m
	$T = T - 1\text{ }^{\circ}\text{C}$	104	104	$^{\circ}\text{C}$
4	$P_c(T); P_r(T)$	82.5; 42.5	180.2; 57.8	W/m
$T = 104\text{ }^{\circ}\text{C}$	$R_{ac}(T); I^2 \cdot R_{ac}(T)$	$9.503 \cdot 10^{-5}; 90.5$	$9.503 \cdot 10^{-5}; 215$	$\Omega/\text{m}; \text{W}/\text{m}$
	$P_S + I^2 \cdot R_{ac} - P_c - P_r$	-7.26 (<0)	-9.36 (<0)	W/m
	$T = T - 1\text{ }^{\circ}\text{C}$	103	103	$^{\circ}\text{C}$
5	$P_c(T); P_r(T)$	81.3; 41.6	178.2; 56.8	W/m
$T = 103\text{ }^{\circ}\text{C}$	$R_{ac}(T); I^2 \cdot R_{ac}(T)$	$9.48 \cdot 10^{-5}; 90.25$	$9.48 \cdot 10^{-5}; 214.3$	$\Omega/\text{m}; \text{W}/\text{m}$
	$P_S + I^2 \cdot R_{ac} - P_c - P_r$	-5.44 (<0)	-7 (<0)	W/m
	$T = T - 1\text{ }^{\circ}\text{C}$	102	102	$^{\circ}\text{C}$
6	$P_c(T); P_r(T)$	80.1; 40.8	176.2; 55.9	W/m
$T = 102\text{ }^{\circ}\text{C}$	$R_{ac}(T); I^2 \cdot R_{ac}(T)$	$9.45 \cdot 10^{-5}; 89.98$	$9.45 \cdot 10^{-5}; 213.7$	$\Omega/\text{m}; \text{W}/\text{m}$
	$P_S + I^2 \cdot R_{ac} - P_c - P_r$	-3.62 (<0)	-4.67 (<0)	W/m
	$T = T - 1\text{ }^{\circ}\text{C}$	101	101	$^{\circ}\text{C}$
7	$P_c(T); P_r(T)$	78.8; 39.9	174.1; 55	W/m
$T = 101\text{ }^{\circ}\text{C}$	$R_{ac}(T); I^2 \cdot R_{ac}(T)$	$9.419 \cdot 10^{-5}; 89.71$	$9.419 \cdot 10^{-5}; 213.1$	$\Omega/\text{m}; \text{W}/\text{m}$
	$P_S + I^2 \cdot R_{ac} - P_c - P_r$	-1.8 (<0)	-2.33 (<0)	W/m
	$T = T - 1\text{ }^{\circ}\text{C}$	100	100	$^{\circ}\text{C}$
8	$P_c(T); P_r(T)$	77.6; 39	172.1; 54	W/m
$T = 100\text{ }^{\circ}\text{C}$	$R_{ac}(T); I^2 \cdot R_{ac}(T)$	$9.3905 \cdot 10^{-5}; 89.4$	$9.3905 \cdot 10^{-5}; 212.4$	$\Omega/\text{m}; \text{W}/\text{m}$
	$P_S + I^2 \cdot R_{ac} - P_c - P_r$	$1.42 \cdot 10^{-14} (\approx 0)$	$2.8 \cdot 10^{-14} (\approx 0)$	W/m
	Power flow is in balance	100	100	$^{\circ}\text{C}$

Table 14: Example. Equations for steady state conductor temperature

E.3. Temperature tracking calculation

The following example describes a method to continuously calculate the conductor temperature, considering that the weather and current data are provided in 10 minutes time intervals. The conductor temperature can be plotted against time with the aid of computer tools. It will be shown here the calculation method for the first two intervals, from 00:00 h to 00:20 h. It has to be noted that the meteorological data provided may vary significantly along the line, so the calculation provided is valid for the location considered. The results are compared with the analytical calculation described in Annex D.

The conductor considered is the same “Drake” 26/7 ACSR conductor as used in examples in Annex E.1 and E.2.

Conductor characteristics	“Drake” 26/7 ACSR
Conductor outside diameter (mm)	28.143
Core diameter (mm)	10.4
Outer strand diameter (mm)	4.44
Total area (mm ²)	486.6
Emissivity	0.8
Solar absorptivity	0.8
Conductor ac resistance at 25°C (Ω/km)	0.0727
Conductor ac resistance at 75°C (Ω/km)	0.0872
Specific heat capacity of steel at 20°C, c_s (J/kg·K)	481
Specific heat capacity of aluminum at 20°C, c_a (J/kg·K)	897
Temperature coefficient of steel specific heat capacity, β_s (1/K)	$1.00 \cdot 10^{-4}$
Temperature coefficient of aluminum specific heat capacity, β_a (1/K)	$3.80 \cdot 10^{-4}$
Steel mass per unit length, m_s (kg/m)	0.5119
Aluminum mass per unit length, m_a (kg/m)	1.116
Total mass per unit length, m (kg/m)	1.6279

Table 15: Example. Conductor characteristics.

Initial situation: it is assumed that the conductor is in thermal equilibrium before monitoring the parameters (before 00:00 h):

- Ambient Temperature: 24.0°C
- Wind Speed: 1.9 m/s
- Wind direction, δ : 55 deg
- Solar Radiation: 0 W/m²
- Current: 802 A

The line is located at sea level. Under this situation, the initial conductor temperature for the example is 42.01°C (Steady State calculation).

Input parameters: for this example, all the parameters are monitored every 10 minutes. The effective values considered for the 10-min. interval are the average values in these 10 minutes, obtained from real-time monitoring systems and from the control center. The first interval starts at 00:00 h and ends at 00:10 h. The second one starts at 00:10 h and ends at 00:20 h.

Measured Values (10 min. average)					
Interval (hh:mm)	Ambient Temp (°C)	Wind Speed (m/s)	Wind direction, δ (deg)	Solar Radiation (W/m ²)	Current (A)
00:00 - 00:10	23.7	1.7	62	0	819
00:10 - 00:20	23.5	0.8	37	0	856

Table 16: Example. Ambient conditions

Note that the determination of the time interval is a major source of error when calculating the conductor temperature continuously. Particularly the wind speed and direction varies greatly with time at low speeds, so it is needed a sufficiently small interval to obtain good results.

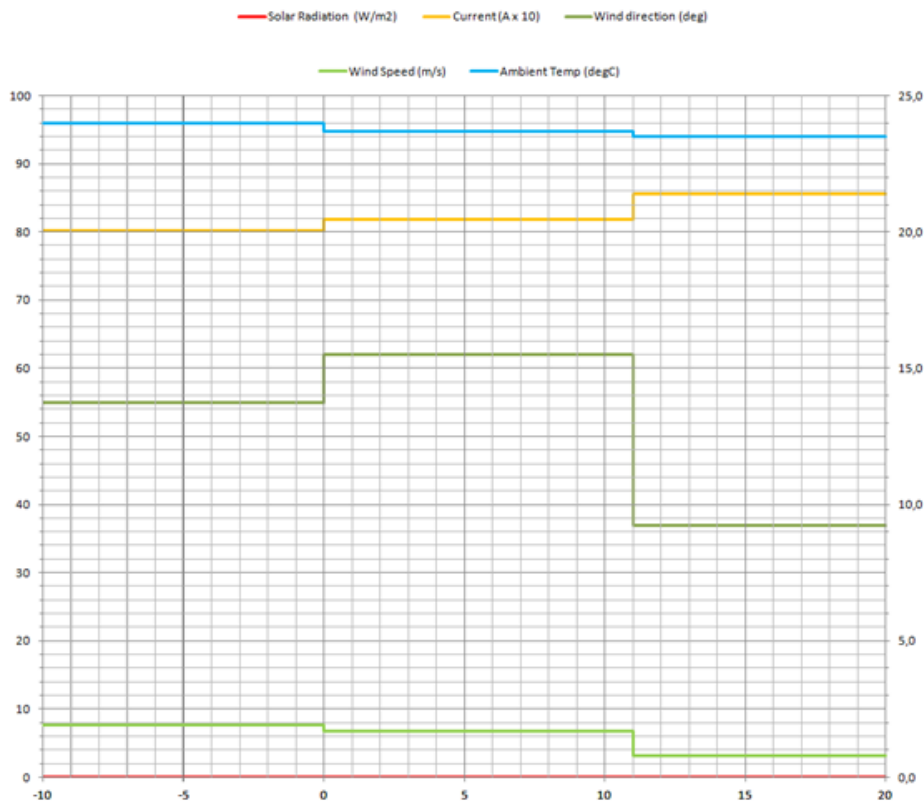


Figure 20. Example of variation of ambient parameters and current for dynamic rating calculation from 00:00h to 00:20h.

It is assumed that for each 10-minute interval the weather parameters and current remain constant. In order to apply the method described in Section 4, each interval is at the same time divided into 1-minute steps, Δt . These steps are smaller than the thermal time constant, but the calculation process can be easily repeated considering smaller steps to check the results. The eq. 30 applied to each 1-minute step can be written as:

$$\Delta T = \frac{P_J + P_S - P_r - P_c}{m \cdot c} \cdot \Delta t$$

The final temperature for each step is the initial temperature for the next one.

The total heat capacity of the conductor at each step is given by the eq. 31:

$$m \cdot c = m_a \cdot c_a + m_s \cdot c_s$$

where the heat capacity of the aluminum wires and steel core are temperature dependent. According to eq. 32, for each step, the heat capacities can be written as:

$$m_a \cdot c_a = 1.116 \cdot 897 \cdot (1 + 3.8 \cdot 10^{-4} \cdot (T - 20))$$

$$m_s \cdot c_s = 0.5119 \cdot 481 \cdot (1 + 1.0 \cdot 10^{-4} \cdot (T - 20))$$

The ac resistance is also temperature dependent. In this case, if a linear interpolation is applied, for each step it can be written, in Ω/km :

$$R_{ac} = 0.0727 + \left[\frac{0.0872 - 0.0727}{75 - 25} \right] \cdot (T - 25)$$

The magnetic heating is negligible for this conductor. The Joule heating, in W/m, can be obtained from the ac resistance value for each step, considering that the current is constant for the 10-minute interval:

$$P_J = \frac{R_{ac}}{1000} \cdot I^2$$

The solar heating is obtained from eq. 8, and is constant for each 10-minute interval, considering the global radiation intensity I_T is constant within the interval. For these time intervals (00:00 h to 00:20 h), the global radiation measurements are zero.

The radiative cooling for each step is calculated from eq. 27, considering that the ambient temperature is constant for the 10-minute interval.

The convective cooling is calculated according to the equations in Section 3.5. The wind speed, wind direction and ambient temperature are considered constant for the 10-minute interval.

Therefore, these calculations can be performed for every 1-minute step to obtain a final temperature, taking the final temperature of the previous step as the initial temperature. The results are showed in the following table:

	$T_{initial}$	$m \cdot c$	R_{ac}	P_J	P_S	P_r	P_c	Δt	ΔT	T_{final}
Units	°C	J/(K · m)	Ω/km	W/m	W/m	W/m	W/m	s	°C	°C
	Initial Situation (Steady State)									
	42.010	1256.19	0.0776	49.934	0	8.286	41.658	–	–	42.010
Steps	First 10-min Interval									
1 (00:00 – 00:01)	42.010	1256.19	0.0776	52.073	0	8.412	40.206	60	0.165	42.175
2 (00:01 – 00:02)	42.175	1256.26	0.0777	52.105	0	8.494	40.563	60	0.146	42.321
3 (00:02 – 00:03)	42.321	1256.32	0.0777	52.134	0	8.568	40.878	60	0.128	42.449
4 (00:03 – 00:04)	42.449	1256.37	0.0778	52.159	0	8.632	41.154	60	0.113	42.562
5 (00:04 – 00:05)	42.562	1256.41	0.0778	52.181	0	8.689	41.398	60	0.100	42.662
6 (00:05 – 00:06)	42.662	1256.45	0.0778	52.200	0	8.739	41.613	60	0.088	42.750
7 (00:06 – 00:07)	42.750	1256.49	0.0778	52.217	0	8.784	41.803	60	0.078	42.828
8 (00:07 – 00:08)	42.828	1256.52	0.0779	52.232	0	8.823	41.971	60	0.069	42.897
9 (00:08 – 00:09)	42.897	1256.55	0.0779	52.246	0	8.858	42.119	60	0.061	42.958
10 (00:09 – 00:10)	42.958	1256.57	0.0779	52.257	0	8.889	42.251	60	0.053	43.011
Steps	Second 10-min Interval									
1 (00:10 – 00:11)	43.011	1256.60	0.0779	57.097	0	8.999	24.300	60	1.136	44.147
2 (00:11 – 00:12)	44.147	1257.06	0.0783	57.339	0	9.578	25.716	60	1.052	45.199
3 (00:12 – 00:13)	45.199	1257.48	0.0786	57.562	0	10.119	27.026	60	0.974	46.174
4 (00:13 – 00:14)	46.174	1257.88	0.0788	57.769	0	10.625	28.241	60	0.902	47.075
5 (00:14 – 00:15)	47.075	1258.24	0.0791	57.961	0	11.097	29.364	60	0.834	47.910
6 (00:15 – 00:16)	47.910	1258.58	0.0793	58.138	0	11.538	30.404	60	0.772	48.682
7 (00:16 – 00:17)	48.682	1258.89	0.0796	58.302	0	11.949	31.366	60	0.714	49.396
8 (00:17 – 00:18)	49.396	1259.18	0.0798	58.454	0	12.331	32.256	60	0.661	50.057
9 (00:18 – 00:19)	50.057	1259.45	0.0800	58.594	0	12.688	33.079	60	0.611	50.668
10 (00:19 – 00:20)	50.668	1259.70	0.0801	58.724	0	13.019	33.841	60	0.565	51.233

Table 17: Example. Results for temperature-tracking calculation

These results are plotted in the following figure.

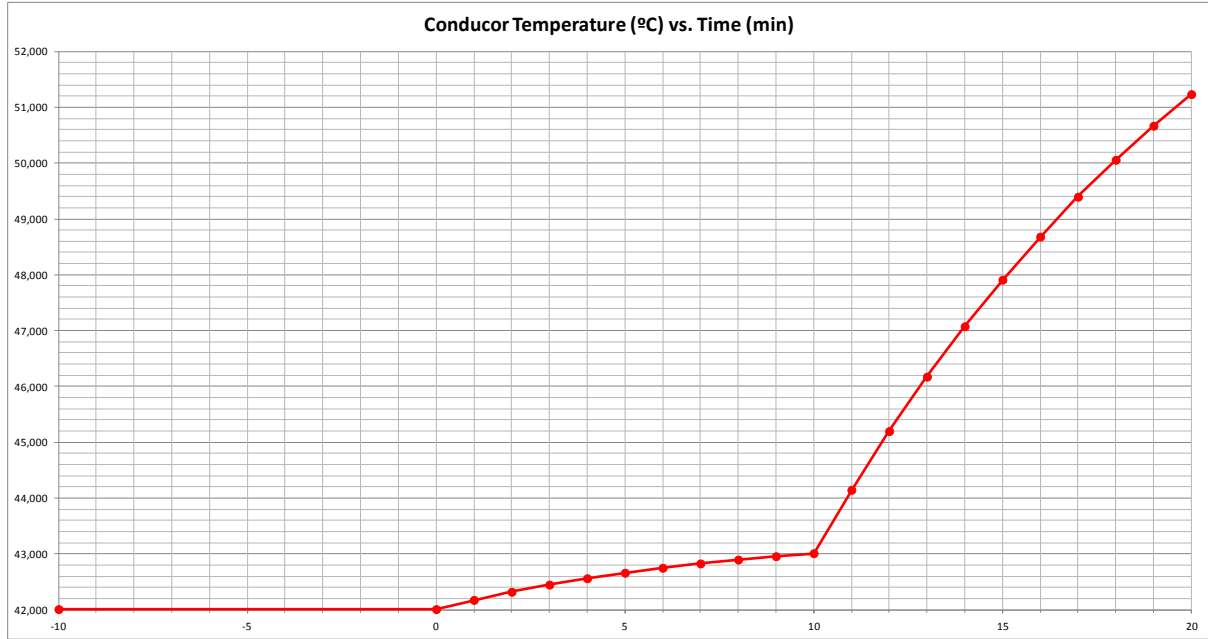


Figure 21. Example of conductor temperature variation from 00:00h to 00:20h considering a step change of ambient parameters and current.

Comparison with the analytical equations of time dependent heating or cooling

The results obtained for the conductor temperature in this example can be compared with the results obtained from the analytical equations developed in Annex D. The following paragraphs detail these calculations.

00:00 h – 00:10 h

For the first 10-minute interval we start from the initial situation at 00:00 h (thermal equilibrium with the conductor at $T_1 = 42.01^\circ\text{C}$, therefore $\theta_1 = T_1 - T_a = 18.310^\circ\text{C}$). It is necessary first to calculate the steady state temperature (asymptotic temperature) for the first 10-minute interval. The process is detailed in Annex E.2.

$$T_m = 43.42^\circ\text{C} \text{ (steady - state)}$$

$$\theta_m = T_m - T_a = 19.715^\circ\text{C}$$

The total heat capacity of the conductor is calculated as explained above. This time it is considered constant for the whole 10-minute interval:

$$m_a \cdot c_a = 1.116 \cdot 897 \cdot (1 + 3.8 \cdot 10^{-4} \cdot (T_1 - 20)) = 1009.42 \text{ J/(K} \cdot \text{m)}$$

$$m_s \cdot c_s = 0.5119 \cdot 481 \cdot (1 + 1.0 \cdot 10^{-4} \cdot (T_1 - 20)) = 246.77 \text{ J/(K} \cdot \text{m)}$$

$$m \cdot c = m_a \cdot c_a + m_s \cdot c_s = 1256.19 \text{ J/(K} \cdot \text{m)}$$

In the same way, the ac resistance is considered constant for the whole 10-minute interval:

$$R_{ac} = 0.0727 + \left[\frac{0.0872 - 0.0727}{75 - 25} \right] \cdot (T_1 - 25) = 0.0776 \, \Omega/\text{km}$$

$$P_J = \frac{R_{ac}}{1000} \cdot I^2 = 52.073 \, \text{W/m}$$

The magnetic heating is negligible for this conductor. The increment of the Joule heating for this 10-minute interval is the difference with the Joule heating in the previous interval (initial situation):

$$\Delta P_J = 52.073 - 49.934 = 2.139 \, \text{W/m}$$

The thermal time constant for the current change can be calculated from eq. 75. The radial difference is neglected here:

$$\tau_I = \frac{m \cdot c \cdot (\theta_m - \theta_1)}{\Delta P_J} = 825 \, \text{s}$$

The solar heating is zero for the whole interval, and there is no difference with the previous interval.

The radiative cooling is calculated from eq. 27, and considered constant for the 10-minute interval, resulting in 8.411 W/m. The increment with respect to the previous interval is:

$$\Delta P_r = 8.411 - 8.286 = 0.125 \, \text{W/m}$$

The thermal time constant for the conductor radiation change is calculated from eq. 84. Note that the factor 2 does not apply here because we are considering a step change function instead of a linear change. Also the radial difference is neglected:

$$\tau_T = \frac{m \cdot c \cdot (\theta_m - \theta_1)}{\Delta P_r} = 14119 \, \text{s}$$

The convective cooling is also considered constant in the whole interval. It is calculated according to the equations in Section 3.5, obtaining 40.206 W/m. The increment with respect to the previous interval is:

$$\Delta P_c = 40.206 - 41.658 = -1.452 \, \text{W/m}$$

The convection decreases (negative) with respect to the initial situation. The thermal time constant for the convection change is calculated from eq. 88. Again, the factor 2 does not apply because it is a step change function instead of a linear change. Also the radial difference is neglected:

$$\tau_V = \frac{-m \cdot c \cdot (\theta_m - \theta_1)}{\Delta P_c} = +1215 \, \text{s}$$

Applying eq. 92 for the final of the first 10-minute interval ($t = 10 \text{ min} = 600 \text{ s}$):

$$\theta = 19.715 - (19.715 - 18.310) \cdot e^{-600/825} \cdot e^{-600/14119} \cdot e^{-600/1215} = 19.318 \text{ }^{\circ}\text{C}$$

Therefore, the final temperature for the first 10-minute interval is:

$$T_{final} = \theta + T_a = 19.318 + 23.70 = 43.018^{\circ}\text{C}$$

00:10 h – 00:20 h

For the second 10-minutes interval, the initial temperature considered is $T_1 = 43.018^{\circ}\text{C}$. The same procedure as in the first interval is followed. The values obtained are:

$$\theta_1 = 43.018 - 23.50 = 19.518 \text{ }^{\circ}\text{C}$$

$$T_m = 58.11 \text{ }^{\circ}\text{C (steady-state)}$$

$$\theta_m = T_m - T_a = 34.61 \text{ }^{\circ}\text{C}$$

$$m_a \cdot c_a = 1.116 \cdot 897 \cdot (1 + 3.8 \cdot 10^{-4} \cdot (T_1 - 20)) = 1009.81 \text{ J/(K} \cdot \text{m)}$$

$$m_s \cdot c_s = 0.5119 \cdot 481 \cdot (1 + 1.0 \cdot 10^{-4} \cdot (T_1 - 20)) = 246.79 \text{ J/(K} \cdot \text{m)}$$

$$m \cdot c = m_a \cdot c_a + m_s \cdot c_s = 1256.60 \text{ J/(K} \cdot \text{m)}$$

$$R_{ac} = 0.0727 + \left[\frac{0.0872 - 0.0727}{75 - 25} \right] \cdot (T_1 - 25) = 0.0779 \text{ } \Omega/\text{km}$$

$$P_J = \frac{R_{ac}}{1000} \cdot I^2 = 57.099 \text{ W/m}$$

$$\Delta P_J = 57.099 - 52.073 = 5.025 \text{ W/m}$$

$$\tau_I = \frac{m \cdot c \cdot (\theta_m - \theta_1)}{\Delta P_J} = 3774 \text{ s}$$

$$P_r = 9.003 \text{ W/m}$$

$$\Delta P_r = 9.003 - 8.411 = 0.591 \text{ W/m}$$

$$\tau_T = \frac{m \cdot c \cdot (\theta_m - \theta_1)}{\Delta P_r} = 32062 \text{ s}$$

$$P_c = 24.30 \text{ W/m}$$

$$\Delta P_c = 24.30 - 40.206 = -15.906 \text{ W/m}$$

$$\tau_V = \frac{-m \cdot c \cdot (\theta_m - \theta_1)}{\Delta P_c} = +1192 \text{ s}$$

$$\theta = 34.61 - (34.61 - 19.518) \cdot e^{-600/3774} \cdot e^{-600/32062} \cdot e^{-600/1192} = 26.971 \text{ }^{\circ}\text{C}$$

$$T_{final} = \theta + T_a = 26.971 + 23.50 = 50.471^{\circ}\text{C}$$

E.4. Temperature tracking calculation. Comparison with steady state

The following example shows the impact of the heat capacity of a conductor on the time dependent temperature calculation. A change in weather conditions or line current requires a recalculation of the heat balance.

Typically the weather and current data are given in discrete time intervals and there is an update of the parameters every time interval. In the following figure the weather and current data from 8 a.m. to 10 a.m. of an exemplary day in spring are shown. The current data is updated every 15 minutes and the global-radiation, ambient temperature and wind speed are updated every 2 minutes. Between the update intervals the values are assumed to be constant. The current carrying conductor is the same “Drake” 26/7 ACSR conductor as used in the previous examples in Annex E. The ambient parameters are different.

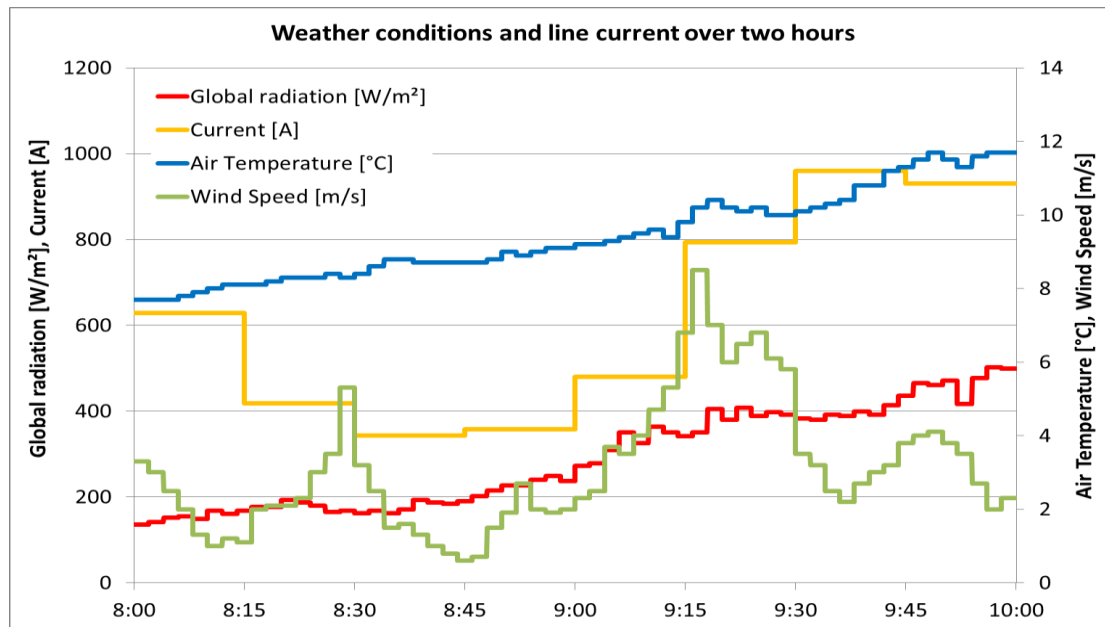


Figure 22. Example of variation of ambient parameters and current for dynamic rating calculation.

The eq. 30 has to be applied. Because of the temperature dependency of most of the summands, it is easier to solve this equation by calculating small increments of the time, as explained in Section 4.2.

$$\frac{dT}{dt} = \frac{P_J(T) + P_S + P_M(T) - P_r(T) - P_C(T)}{m \cdot c(T)} = \frac{\Delta T}{\Delta t}$$

These time increments Δt should be smaller than the thermal time constant of the conductor. In the next step the conductor temperature T can be adjusted by adding ΔT and all parts of the power flow can be recalculated with the adjusted temperature ($T + \Delta T$) in the next time step.

The heat capacity of the conductor is temperature dependent itself (Section 4.2). The calculation for the “Drake” conductor is done as follows:

$$m \cdot c(T) = m_a \cdot c_{a,20} \cdot [1 + \beta_{a,20} \cdot (T - 20)] + m_s \cdot c_{s,20} [1 + \beta_{s,20} \cdot (T - 20)]$$

Values for calculation can be taken from Table 6, Annex A.

With the given weather and current values from the figure above it is possible to calculate the steady state temperature for every interval during the operation by solving the heat balance, shown in Section 4.1. Results for the first given dataset are listed in the following table:

Time [hh:mm:ss]	Global radiation [W/m ²]	Air temperature [°C]	Wind speed [m/s]	Wind angle [°]	Line current [A]	Steady State temperature [°C]
08:00:00	135,3	7.7	3.3	45	628,8	14.34

Table 18: Example. Ambient parameters and current for the first interval

These values are kept constant for the next 2 minutes, so the calculated steady state temperature is valid and also constant for the same duration.

If the conductor temperature was at 9.3°C before 8 o'clock, the change in steady state temperature to 14.34°C would result in a positive temperature slope. The rate of this slope is dependent on the change of weather and current situation as well as the heat capacity of the conductor. The next table shows calculation steps with temperature tracking method for the first seconds after 8 o'clock with a new estimated steady state temperature of 14.34°C:

Time [hh:mm:ss]	$\Delta T = \frac{P_J + P_S - P_r - P_c}{m \cdot c} \cdot \Delta t$ [°C]	$T + \Delta T$ [°C]
08:00:00 (T=9.3°C)	$\frac{(27.052 + 3.042 - 0.572 - 6.878)}{1242.9} \cdot 1 = +0.0182$	9.3 + 0.0182 = 9.3182
08:00:01 (T=9.3182°C)	$\frac{(27.054 + 3.042 - 0.578 - 6.955)}{1242.9} \cdot 1 = +0.0182$	9.3364
08:00:02 (T=9.3364°C)	$\frac{(27.056 + 3.042 - 0.585 - 7.033)}{1243} \cdot 1 = +0.0181$	9.3545
...
8:01:59 (T=11.0619°C)	$\frac{(27.248 + 3.042 - 1.213 - 14.389)}{1243.7} \cdot 1 = +0.0118$	11.0738

Table 19: Example. Results for temperature-tracking calculation

After 2 minutes under constant conditions the conductor has increased its temperature by approximately 1.8°C . For each step, the difference ΔT is decreasing with time until the conductor reaches its steady state temperature after the conductor time constant and $\Delta T \approx 0$. But if, before that, there is another change in weather or current conditions, then ΔT is adjusted accordingly.

The temperature tracking calculation is repeated for the time intervals shown in fig. 22 from 8 o'clock until 10 o'clock. The temperature changing progress can be seen in the following figure. It is compared with the steady state conductor temperature, which can be calculated for each 2-minutes interval. It can be seen the unrealistic variations of the steady state calculation for not considering the thermal inertia of the conductor.

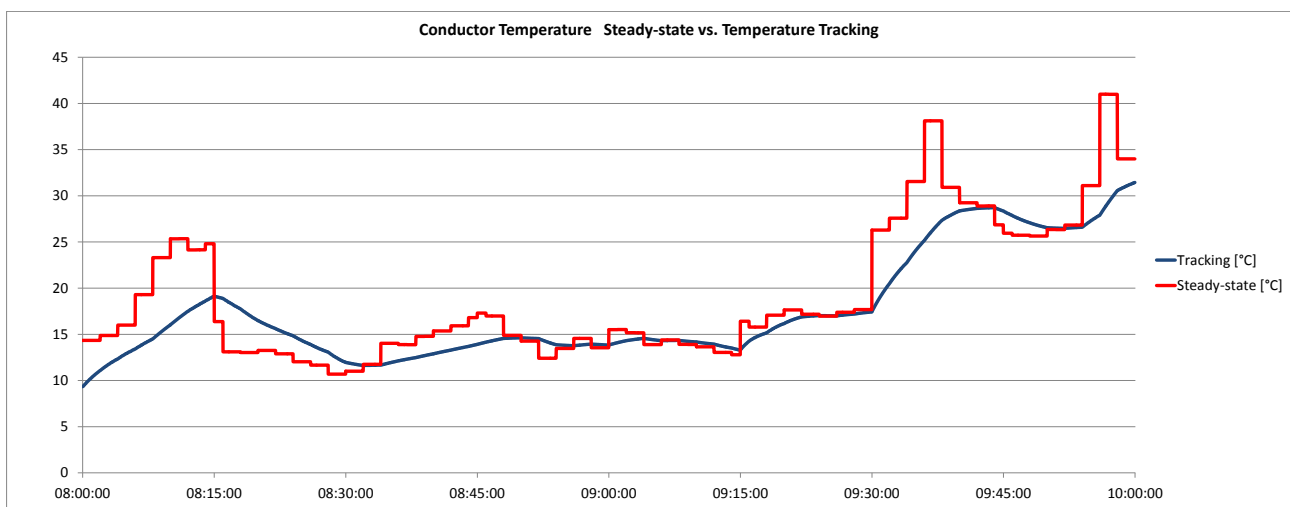


Figure 23. Example of conductor temperature variation. Comparison with the steady state temperature.